Survey of codes relevant to design, engineering and simulation of transmutation of actinide by spallation.
(The cost estimation of accelerator for incinerator and the problem of radiation hazard)

Hiroshi Takahashi
Brookhaven National Laboratory
Upton, New York,11973

1. Introduction

The use of neutron produced by the medium energy proton accelerator (1 Gev-3Gev) has considerable potential in reconstructing the nuclear fuel cycle. About 1.5 -2.5 ton of fissile material can be produced anually by injecting a 450 MW proton beam directly into fertile materials. A source of neutrons, produced by a proton beam, supplying subcritical reactors could alleviate many of the safety problems associated with critical assemblies, such as positive reactivity coefficients due to coolant voiding. The transient power of the target could be safely controlled by controlling the power of the proton beam. Also, the use of a proton beam would allow more flexibility in the choice of fuel and structural materials which otherwise might reduce the reactivity of the reactor.

There is now a plan to permanently store long-lived highly radioactive material in a stable geologic formation such as Yucca Mountain in Death Valley. However, there is concern that geologic formations and the climate might change over millions of years. Therefore, it may be worthwhile to study an alternative approach that would separate the long-lived nuclei from the high-level waste by transmuting such nuclei into short-lived or non-radioactive wastes.
Studies have been made of incinerating actinides in light-water reactors and in liquid metal fast breeders without processing the long-lived nuclei [C1,82]. However, thermal neutrons and fast neutrons, whose spectrum is not sufficiently hard do not incinerate actinide efficiently, because, in these two types of reactors the neutron capture reaction, which creates another higher actinide, predominates over the fission reaction which incinerates the actinide. To incinerate the actinide, a fast neutron spectrum is needed that is hard enough to make the fission reaction dominate the capture reaction.

This requirement may be obtainable by using the Np-237 elements that give a harder neutron spectrum in the target assembly than the spectrum obtained in the conventional LMFBR [MT,88]. However, the life time of neutrons in this hard spectrum is very short and the transient behavior of the reactor becomes more violent as it approaches the supercritical condition. Furthermore, the delayed neutron fraction of Np-237 [Tm,89] fission is smaller than those for uranium isotopes, which makes control somewhat more restricted.

To obtain the hard neutron spectrum, the amount of the coolant in the reactor must be reduced, so that more stringent restrictions must be applied to operate this kind of reactor safely.

To keep a minor actinide fuel reactor running, the choice of the composite materials of fuel, cladding structure, and coolant is very restricted: this restriction makes the problem of safety associated with criticality much more severe.

The accelerator actinide incinerator can resolve the difficulties associated with criticality in reactor safety,because it is a subcritical reactor, assisted by neutrons created by the high energy proton spallation and the high-energy fission reaction. The target assembly is similar that of the accelerator breeder that was studied earlier, except that the fuel assembly is actinide not depleted uranium.

Studies of the incineration of actinide nuclei [BR,87][Ta,85] that have very long half-lives, such as Np-237, suggest that the power from a small beam, in the order of 15 - 30 MW, can incinerate the actinide produced by about ten 1 GWe light water reactors. Furthermore, an incinerator with 900 MW thermal power can produce 270-240 MWe of excess electricity, as well as the 100kg of fissile materials such as U or Pu when its core is surrounded with fertile material such as Th or U, respectively.

In this report we discuss the code system used for this accelerator incinerator and its limitations.

This report is organized as follows, in the second section accelerator actinide incinerator studied so far will be discussed .

In 3-rd section, nuclear cascade process which play important role for designing the accelerator breeder and incinerator will be discussed. The nuclear cascade process is assumed as two step process of intra-nuclear and evaporation and fission process.

In the 4-th and 5-th sections, the intra-nuclear cascade process will be discussed and the high energy fission process which produces about twice of neutron yield in the actinide nuclei than the non-actinide nuclei will be presented.

In the 6-th section, 4 fission models accommodated to the nuclear cascade code NMTC and HETC will be described. In this section, the code systems made for studying the accelerator breeder and incinerator at BNL, JAERI, and LANL will be discussed.

In the 7-th section, to verify these code systems, the comparison of the experimental data and their analysis used by these code systems will be described.

In the next section 8-th, the cost analysis of accelerator incinerator will be presented. Because of infancy of this concept, there is no over-all cost analysis for this accelerator incinerator at present time. It will describe the cost analysis of two types of accelerator: linear accelerator and segmented cyclotron as well as the description of the accelerator.

In the 9-th section, the health physics problem related to the accelerator operation is discussed.

In the final 10-th section, the discussion and the concluding summary are presented.

2. Accelerator Actinide Incinerator

Accelerator technolgy has been extensively developed last few decades and the accelerators have become large, fine tunned ,and more powerful and efficient, with their widespread application, ranging from research of high energy and material physics. The experimental results of medium energy charged particle injecting to target of heavy elements supports theory to make resonably accurate prdiction of transmuting the minor actinide (MA) nuclei.

The process of spallation, medium energy fission, and evapolation of neutron and other particles are illustrated in Fig.1. The estimates of numbers of neutron, fission, and spallated nuclei in several infinite target materials are shown in Figs.2, 3, and 4 as function of incident proton energy.

Fig.2 shows the neutron yields and the number of fissions when a proton is injected into infinite media of Np-237 and U-238. The values are obtained from the NMTC-BNLF code, which calcuates the intra-and-inter-nuclear cascade process, including high-energy fission. This figure shows that Np-237 is more efficient in giving a large neutron yield and more Np-237 than U-238 is incinerated by direct, high-energy proton irradiation.

Present-day light water reactor (LWRs) are based exclusively on the uranium cycle. Neutron capture in U-235, as well as in U-238, leads to the generation of transuranium elements which, except for Pu go into the waste system. The main components of these so-called "by-product actinides" are Np-239 ,Am-241, Am-243, Cm-242, and Cm-244.

In the process of transmuting actindes it would be unwise not to make use of the many fast neutrons generated by the spallation processes. Since these neutrons can induce further fissions in the target area they can contribute substantially to the incineration of actinide.

In quantitative terms the total number of fissions N_{fiss} can be expressed by:

$$N_{fiss} = N_h S_h \frac{K}{(1-k)\nu} \qquad (1)$$

where N_{fiss} = total number of fissions,

N_h = total number of fissions by high-energy proton reactions,

S_h = Number of neutrons produced by high-energy proton reactions (spallation, evaporation, and very high energy fission)

ν = number of neutrons per 'regular' fission

k = multiplication factor for 'regular' fission neutrons.

By increasing the k value of subcritical target, we can reduce the proton current required to incinerate the MAs. If the k value reaches 1, then the target becomes critical and does not require any outside neutron source created by the proton accelerator; but, as indicated before, the safety problem assocaiated with criticality has yet to be addressed. So far, the k value that is most suitable for actinide incineration is unknown. The k value of the incinerator should be considered from many aspects such as safety, the operational procedure, material choice, and the cost of the incinerator. Since this has not been studied we arbitarily choose the value of k = 0.9 - .95. When NP-239 captures a neutron it converts the fertile material to fissile material and the reactivity of the target increases during the incineration operation.

Studies have been made of the incineration of MAs in light-water reactors and liquids metal fast breeders without processing the long-lived nuclei. However, thermal neutrons and fast neutrons, whose spectrum is not sufficiently hard do not incinerate actinides efficiently because in these two types of reactor the neutron capture reaction which creates another higher actinide, predominates over the fission reaction which incinerates the actinide. To incinerate the actinide, a fast reactor is required, which has neutron spectrum hard enough to allow the fission reaction to dominate the capture reaction.

Figure 1 HIGH ENERGY PROTON-INDUCED NUCLEAR SPALLATION REACTION

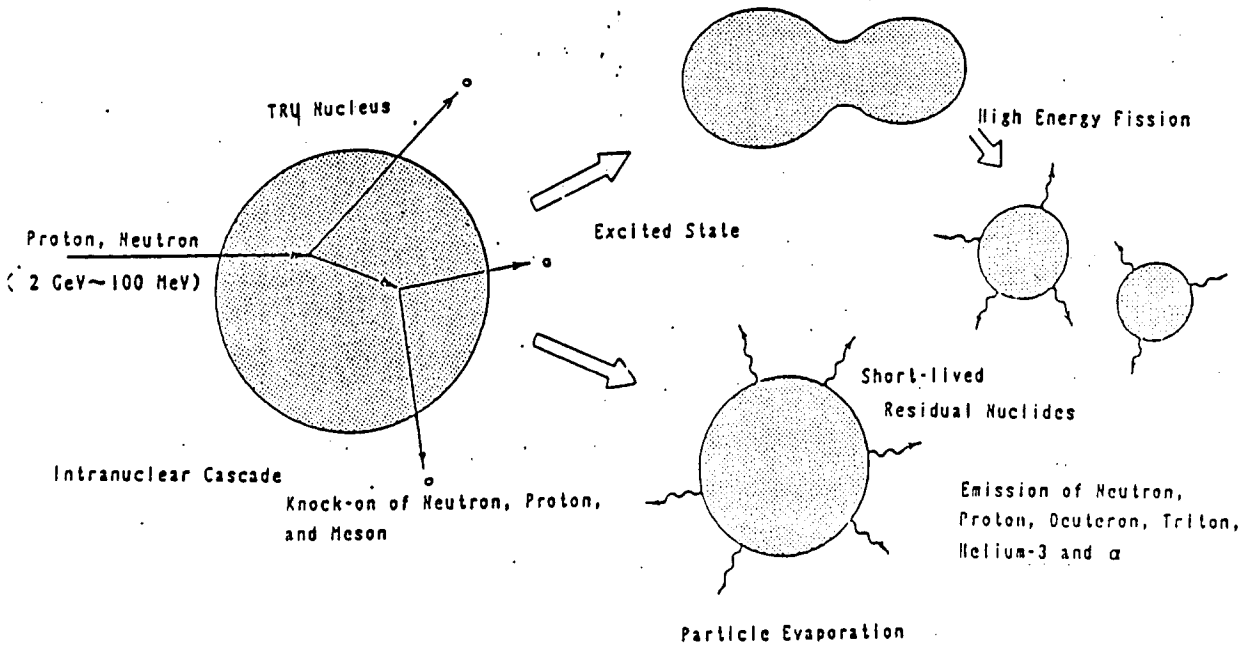

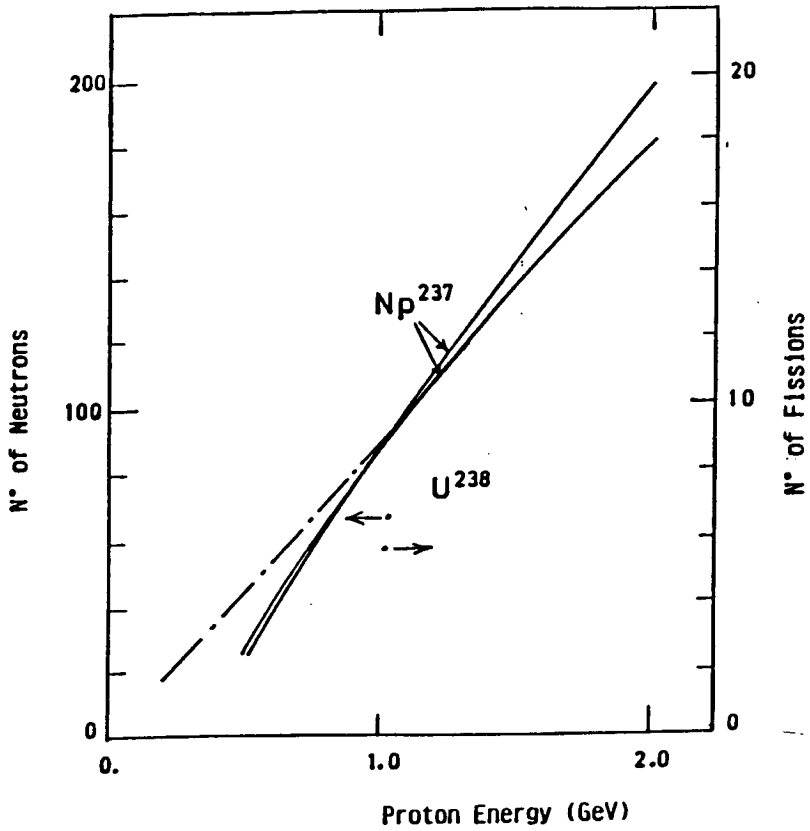

Figure 2 : Number of Neutrons and Number of Fissions produced by High Energy Reactions in an Infinite Np237 + U238 medium

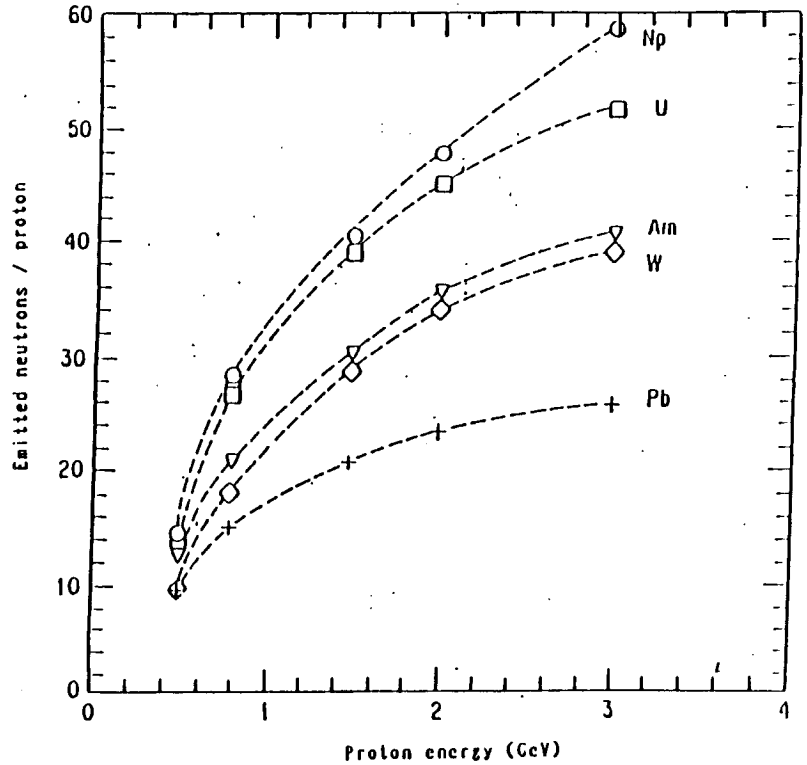

Figure 3 Number of neutrons produced per an incident proton energy

2.1 Study at EURATOM,CERN,and BNL.[BR.87]

Table 1.1shows the actinide waste from a 1000 MWe LWR after a 3300 MWD/ton burnup, which is processed with a 99.5 % removal efficiency. About 246 Kg of minor actinide are produced annually from 10 units of 3000 MW(Th) LWR without uranium isotopes, and the thermal power generated by incinerating this amount of actinides is 900 MW. When this 900MW thermal power is generated with the specific power of 150 W /gr HA, the total amount of actinide becomes 6 tons.

We studied the target lattice system made of actinide oxide fuel pellets cladded by steel can, and cooled by sodium or helium. The design parameters are shown in the Table1.2.

Pellet, outer diameter :	0.510 cm
SS clad , inner diameter:	0.524 cm
SS clad outer diameter :	0.600cm
Fuel Pitch:	0.75-0.85 cm
Active length:	80 cm.

Table 1.2 The design parameters

In our conceptual design, we adopted a V-shaped target region as shown in Fig.1. The target zone was surrounded by a thorium blanket to capture the large fraction of leakage neutrons to produce the fissile material of U-233; the tagret lattice is irradiated directly by a 1-GeV proton beam which is spread by a magnetic field.

Table1.3 shows the beam power requirement, the excess electricity produced, the effective multiplication factor, and the production rate of U233 per year for both sodium- and helium-cooled accelerator incinerators.

Coolant	Keff	Beam Power (MW)	Beam Current 1GeV	3GeV	Reactor Power (MWth)	U-233 prod. in blanket (Kg)
Na	.90	27.9	27.9	9.3	900	85
He	.95	13.0	13.0	4.3	900	103

Table 1.3 Requirements for accelerator-driven sodium- or helium-cooled incinerators.

The first, surprising result is the low beam current required to incinerate the actinides produced by ten units of 1GWe LWRs. Depending on the beam's energy (1 to 3 GEV) and the self multiplication of the target, the required beam currents are between 5 - 15 mA in the He cooled incinerator, while in the Na-cooled incinerator, this requirement would be raised by a factor of 2. A further reduction in proton beam current can be obtained by optimising the fuel composition and the geometry of the target.

As a by-product, the actinide incinerator can produce annually at least 100 Kg of fissionable material when the target is surrounded by a uranium or thorium blanket, and excess electricity of 240-270 MW beyond the 30-60 MW required to operate the proton accelerator. Due to the fact that a rather small power accelerator is required to incinerate the minor actinide from a 10 unit of 1GWe LWR, it might be possible to use a multistage cyclotron as accelerator instead of a linear accelerator from the following reason.

According to present technical know-how, linear accelerators can reach relative high currents of 300 mA. But even at an energy of 1 GeV, a building of several hundred meters in length is required to house such a machine. Also a longitudinal accelerator is relatively fragile, and suffers of the short-coming that if maintenance work is needed, the entire machine has to be stopped.

On the other hand, the multistage-parallel cyclotron does not allow equally high beam currents to be accelerated, but this can partially be compensated for by an easily achievable higher beam power with much less material and space requirements. Furthermore, the multistage cyclotron arrangement permits a more or less continuous operating mode with maintenance carried out separately on each

TABLE 1.1 Actinide Waste from a Typical 1000 MWe LWR Reactor After Reprocessing.

Nuclide	Burn-up 1000 MWD_{th} (g)		Burn-up 3000 MWD_{th} (kg)	
U-235	1.21	144.83	not considered	
236	0.618			
238	143.0			
Np-237	23.1	23.1	18.97	
Pu-238	0.025	1.374	1.13	
-239	0.815			
-240	0.327			
-241	0.154			
-242	0.053			
Am-241	1.61	4.35	3.57	
* 243	2.74			
Cm-242	0.177	0.271	0.22	
-244	0.094			
		Sum	23.83	

1) Reprocessing Plant Efficiency 99.5% for U and Pu

2) Plant factor: 75%

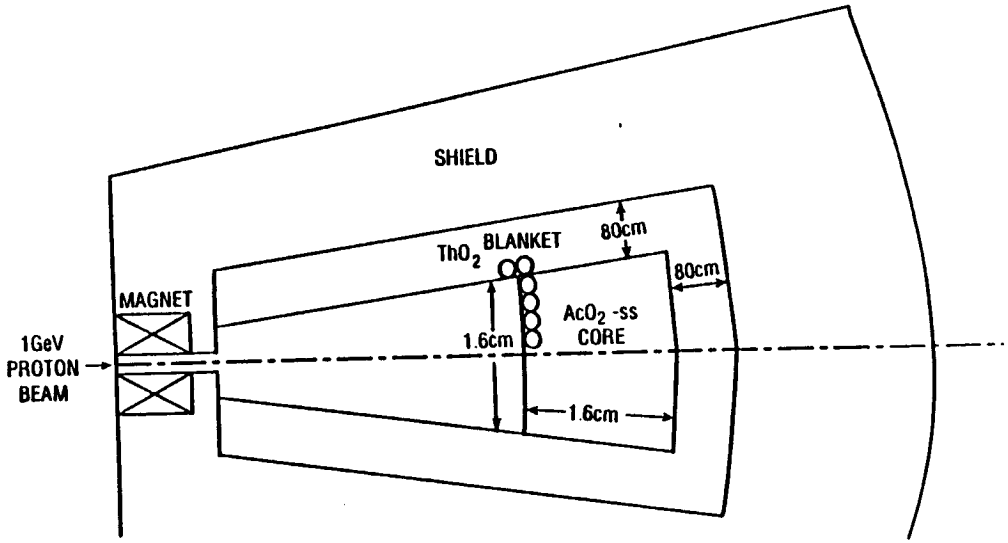

Figure 5 : Horizontal Section of an Actinide Fueled Target

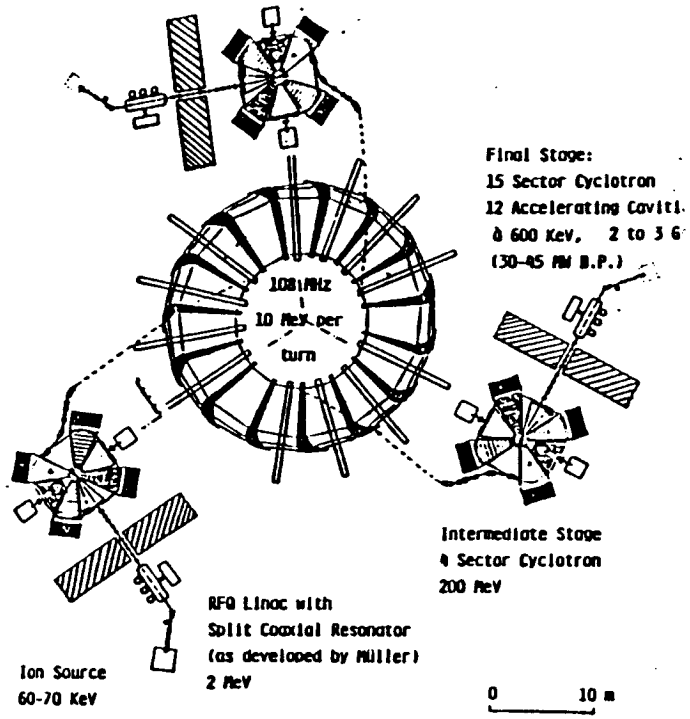

Figure 1.2(a) Arrangement of a multistage cyclotron.

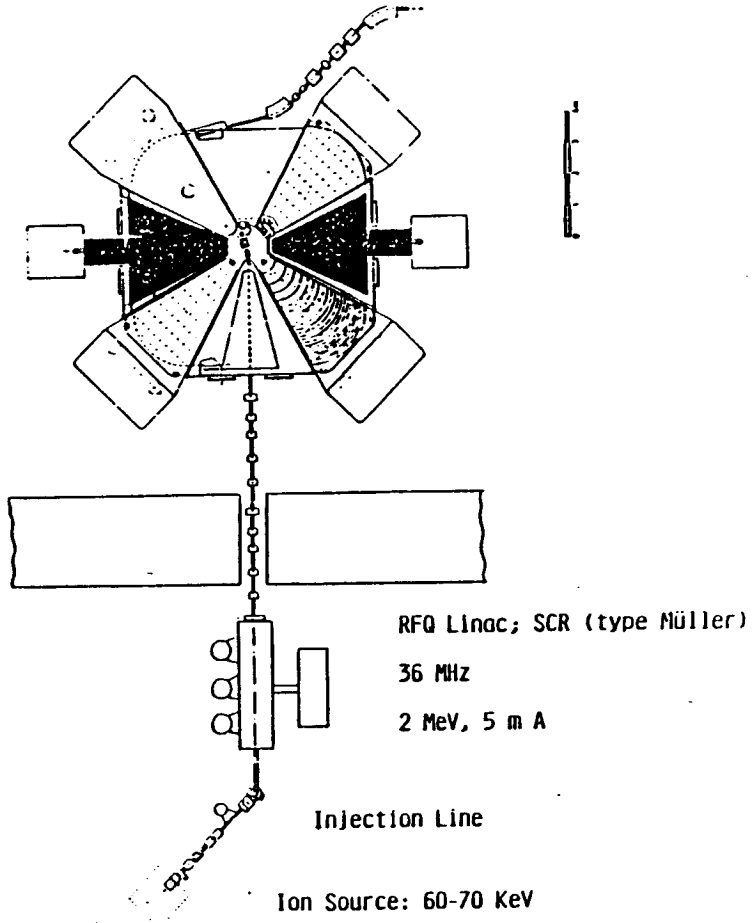

Figure 1.2(b) Intermediate 4 Sector Cyclotron, phase width 36°, F_{Hf}= 36 MHz, 200 MeV, 5 m A (limited by longitudinal space charge problems, flat topping)

accelerator without the need to shut down the whole assembly.

Besides these advantages, during the construction phase of the assembly, at the completion of each stage a valuable research tool becomes available which would provide first, 2 MeV, and then, 200 MeV protons. Fig.1.2 shows a conceptual design of the segmented cyclotron system for such a middle-scale incinerator.

From this study we reached the following conclusions:

Spallation neutron and induced fission generated by a proton of 20 to 30 mA of 1GeV could transmute the minor actinide produced by ten 1GWe LWR in a subcritical assembly cooled by He or Na. As a by product, this transmutor annually could generate at least 100 Kg of fissile material in a U or Th blanket, and excess electric power of 230-260 MWe.

The requirement for a relatively low beam current favors the comparatively inexpensive "Multistage Cyclotron Technique" which provides a mean to transmute actinide by the spallation process at a reasonable cost.

The modular-structure of the multistage concept promises a reliable operation of the system, as required in an industrial environment.

In the first test plant, the modular structure of the accelerator would allow us to make initial experiments verifying the calculated transmutation factor when only a part of the overall configuration was assembled.

2.2 JAERI Incinerator study [TK,89]

Fig.2.1 shows a accelerator-driven MA target system designed at JAERI. This target is operated at a subcritical condition of k= 0.90-0.95. The target core is 2 m long in the direction of the beam with 1.0 m height and 0.85 m width. This core is surrounded by a stainless steel reflector of 0.2 m thickness. The beam window is located at a depth of 0.7 m from the front face. The heat is removed by forced circulation of liquid metal coolant of Na or Pb-Bi. The metallic alloy fuels of Np-Pu-Zr and Am-Cm-Pu-Y give a considerably harder neutron spectrum than the oxide fuel. These alloys are expected to have sufficient high phase stability, and with the addition of 20 wt% of Zr, the melting point of Np is supposed to increase from 640 C to about 900 C. The nuclear cascade above the cutoff energy of 15 MeV was calculated by NMTC/JAERI code: below the cutoff energy, the three-dimensional Monte Carlo neutron transport code, MORSE-DD, was used.

The results are summarized in Table 2.1, and the power distribution for both coolants is shown in Fig.2.2. The Pb-Bi-cooled target has large power peaking at the place where the beam window is located. Thermal hydraulic calculations were made to determined the maximum achievable thermal power within the maximum allowable temperature limits of 900 C and 650 C for the MA and HT-9 cladding tube respectively. Coolant temperature at the target inlet was set to 300 C. The temperature distributions along the hottest fuel pin, cooled by Na and Pb-Bi, are shown in Fig.2.3 (a) and (b). For Na cooling the maximum thermal power is 390 MW and the beam current required is 18.1 mA. For Pb-Bi cooling, the maximum thermal power is 163 MW, requiring 5.4 mA beam current.

Since the direct proton beam irradiation on the minor actinide is not used, the beam current required is higher than when there is direct irradiation. Furthermore the power peaking factor is higher than under direct irradiation; this limits the thermal power of this target system.

2.3 BNL large scale incinerator[VT,90].

We recently studied the large-scale accelerator incinerator concept using state-of-the-art technology. In order to use the present technology , the incinerator target assembly was designed in very conservative way. For the initial design, a sodium-cooled oxide fuel lattice based on the FFTF reactor was chosen as the target. The FFTF system design characteristics were scaled with minor actinide substitutes of uranium & plutonium in the lattice. For the accelerator we chose the large linear accelerator, with a peak current of 250 mA of 1.6 GeV protons to derive a subcritical lattice of K=0.9. (see Fig.3.1) This accelerator was designed for the accelerator tritium producer.

The study showed that after 2 years of operation at a 75 % capacity factor

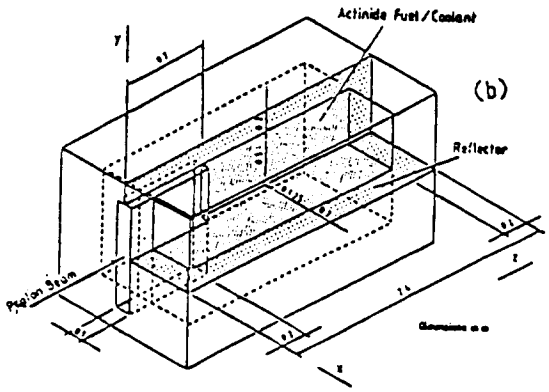

Figure 2.1

Table 2.1 Target Parameters and Operating Conditions

Coolant		Na	Pb-Bi
Proton Beam Energy (GeV)		1.3	1.5
Current (mA)		20	7.8
Target Length (m)		2	
Height (m)		1	
Width (m)		0.85	
Reflector Thickness (m)		0.2	
Fuel		Np-Pu-Zr/AmCm-Pu-Y	
Bond		Na	
Clad		HT-9 Steel	
Fuel Slug Diameter (mm)		4	
Clad Outside Diameter (mm)		5.22	
Thickness (mm)		0.3	
Fuel Pin Length (mm)		1000	
Pitch (mm)		8	10
Number of Fuel Pins		31100	18900
Actinide Inventory (kg)		2550	1550
Thermal Power (MW)		769	226
Power Density (W/cc)	max.	1168	595
	ave.	472	145
Linear Power Rating (W/cm)	max.	647	516
	ave.	262	126
Coolant Temperature (°C)	inlet	300	300
	outlet	451	423
Clad Temperature (°C)	max.	510	589
Fuel Temperature (°C)	max.	900	900
Coolant Velocity (m/s)	max.	3	2.35
Pressure Drop (kPa)		70	37

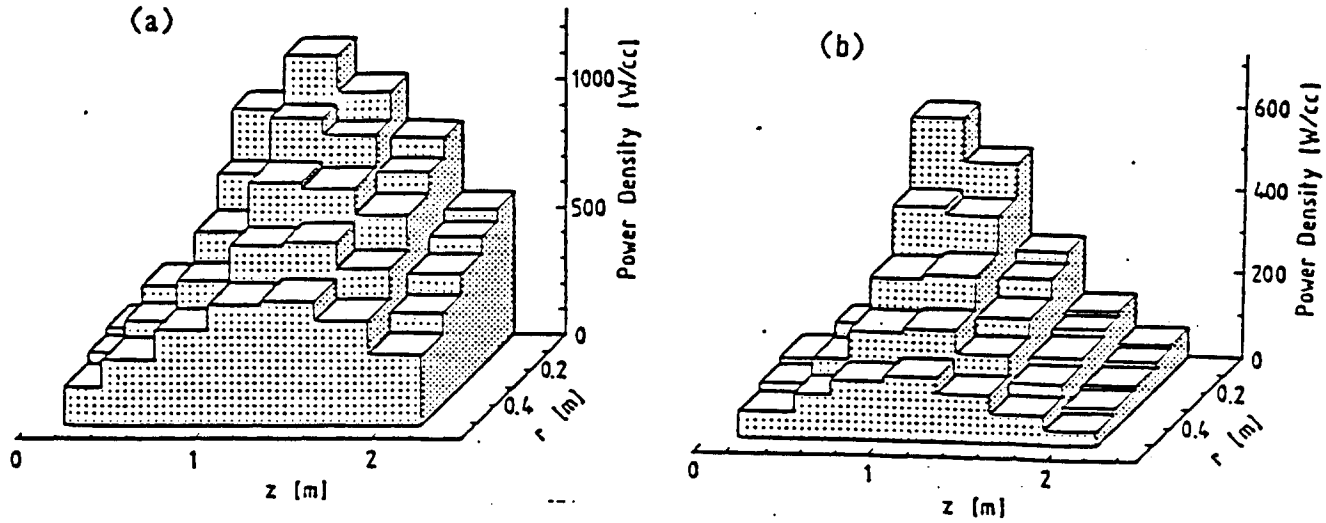

Figure 2.2 Power distributions in (a) Na cooled and (b) Pb-Bi cooled cores

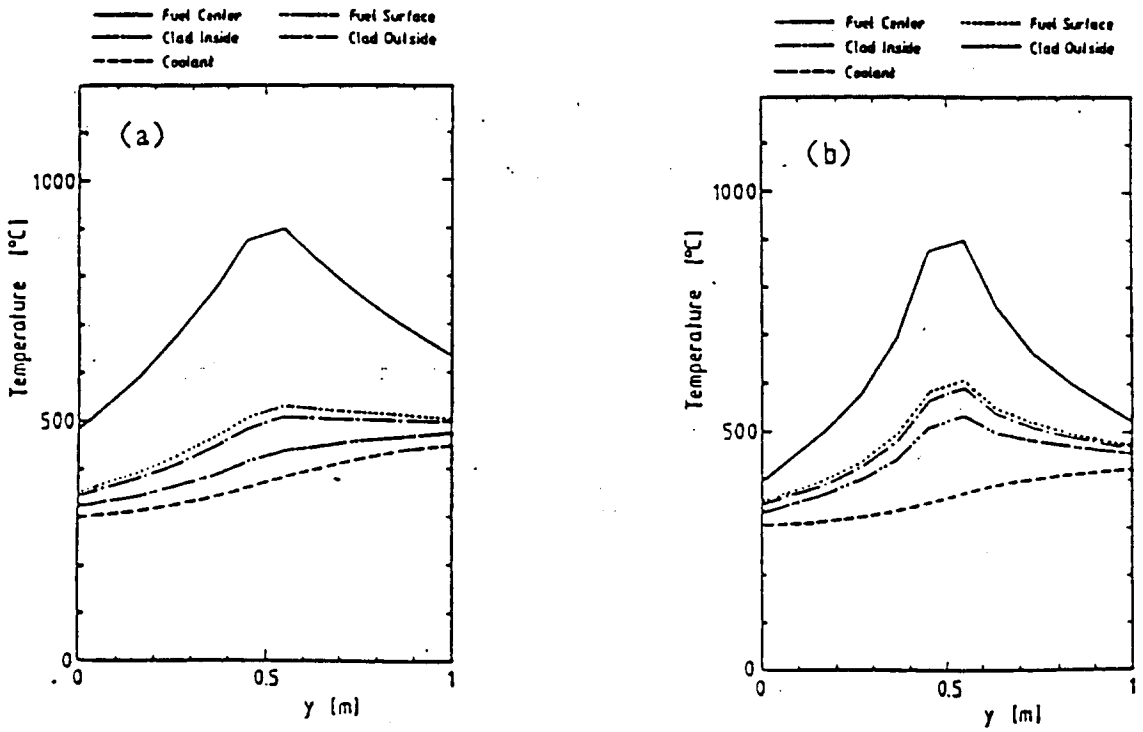

Figure 2.3 Temperature distributions in (a) Na cooled and (b) Pb-Bi cooled cores

, the fuel reaches an average burn-up of 8.6%, with an additional 12.7% converted to plutonium. The use of a 2-year cycle assures that most of the plutonium (> 85%) is Pu-238, which is valuable as a long- term remote power source, and also reduces any concerns about degradation in the fuel or in structural steels. During the 2-year reprocessing step, the plutonium and the fission products are replaced by a new, minor actinide from the LWRs. Plutonium that is not useful for isotropic applications could be blended with the highly fissile plutonium from the LWR waste steam, so that with resulting mixture would contain enough Pu-238 and Pu-236 to make weapon production difficult.

The results of a 12-year burn up calculation by ORIGIN2 codes are shown Fig.3.2. The k infinity starts out quite low , and the effective value would be even lower, so the accelerator would initially operate at near peak current. After the first cycle, k infinity varies between roughly 0.9 and 1.1, so that the current must be adjusted accordingly.

The combined neptunium and americium inventory decreases by about 2.6 Tones/year, with 1.55 Tones/yr being converted to plutonium. Thus, one unit of incinerator would transmute the minor actinide wastes from about 75 1 GWe LWRS.

2.4 LANL Thermal neutron incinerator study [Bo,90]

Another accelerator incinerator of actinide, as well as of fission products such as Cs and Sr, was studied by LANL [Bo,90]. Fig.4.1 shows the elevation view of the flowing Pb-Bi eutectic target for spallation neutron production. Instead of using the fast neutron, the LANL incinerator creates the high-intensity thermal neutron flux, similar to that in our old study of a fission product incinerator using spallation neutrons [TM,80]. The geometry of the target system is different and the high energy proton is injected vertically into the eutectic flowing target. The irradiating material is immersed into the D2O moderator which surrounds the eutectic flow target. Fig.4.2 shows the time averaged thermal neutron isoflux profile for a beam energy of 1.6 GeV and proton current of 25 mA.

Using the 4.8 10^{15} $n/cm^2/sec$ maximum flux, the minor actinide and the fission products will be incinerated. If thermal neutron is used instead of fast neutrons,, the minor actinide of Np-237 will be converted to the fissile material at first by capturing neutrons. The incineration of the actinide will occur by fissioning these resulting nuclei. The process of capture and the following fission is rather complicated; assesment requires detailed calculations using burn- up codes. He estimated that one spallation neutron produced from the 400 MW proton beam accelerator (8.6* 10^{25} neutron /year) theoretically can destroy the minor actinide output of 84 PWRs!

Figure 3.1

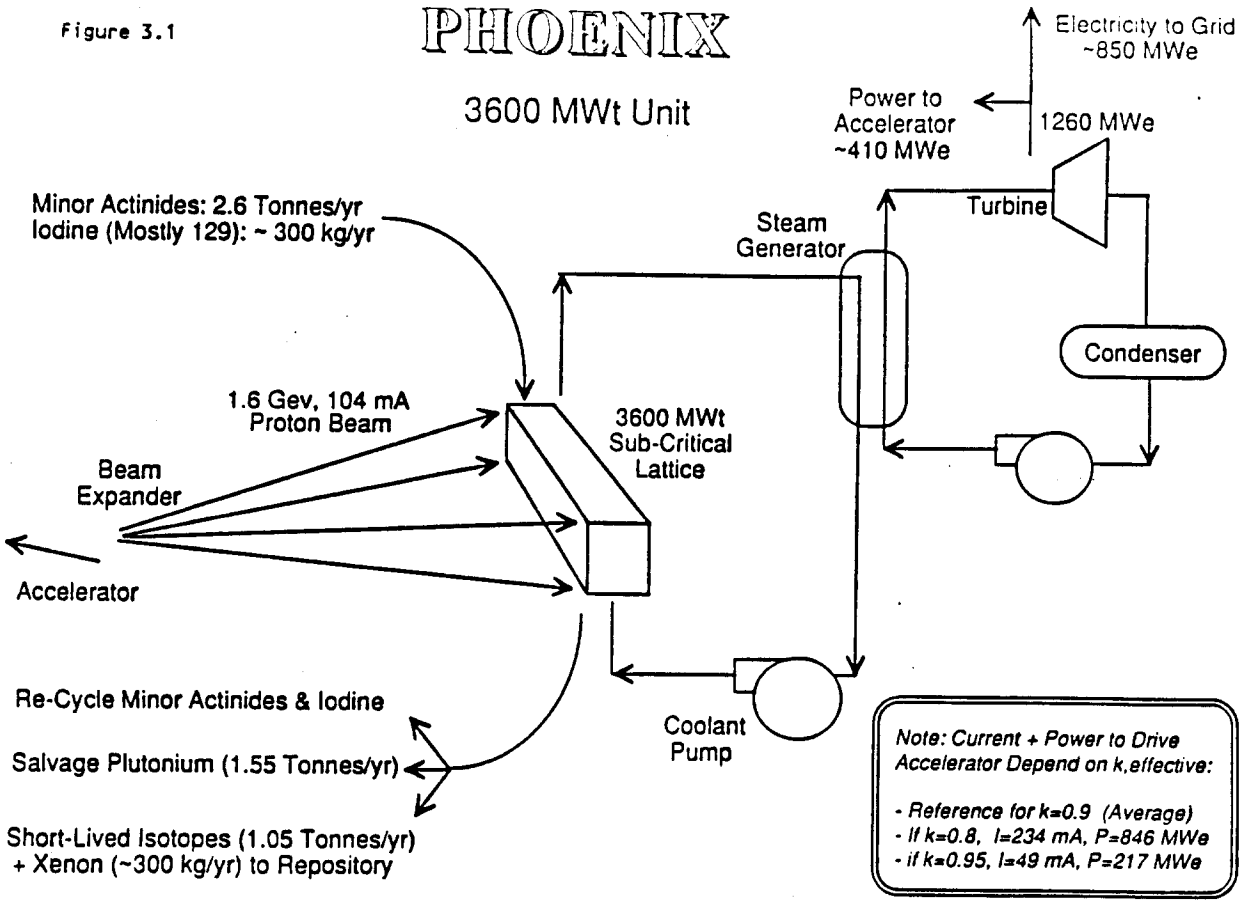

Figure 3.2

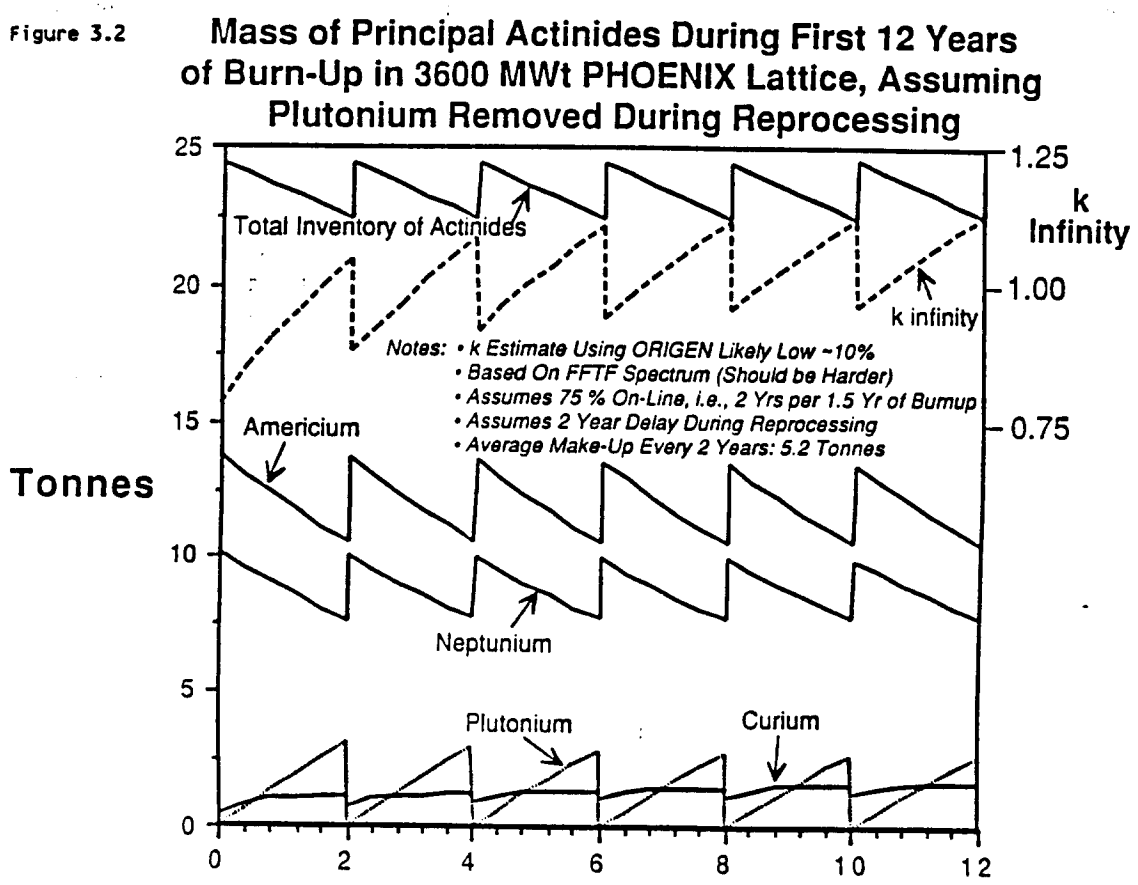

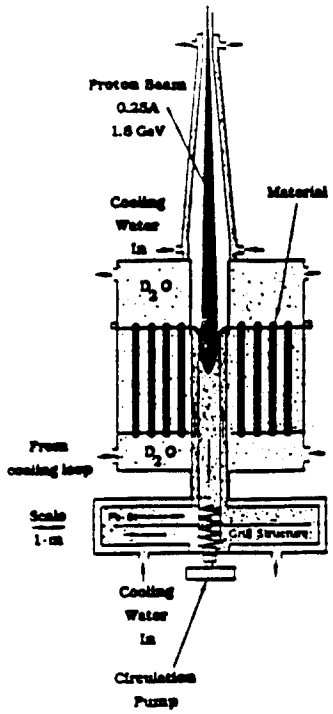

Fig. 4.1 Elevation view of the flowing Pb-Bi eutetic target for spallation neutron production.

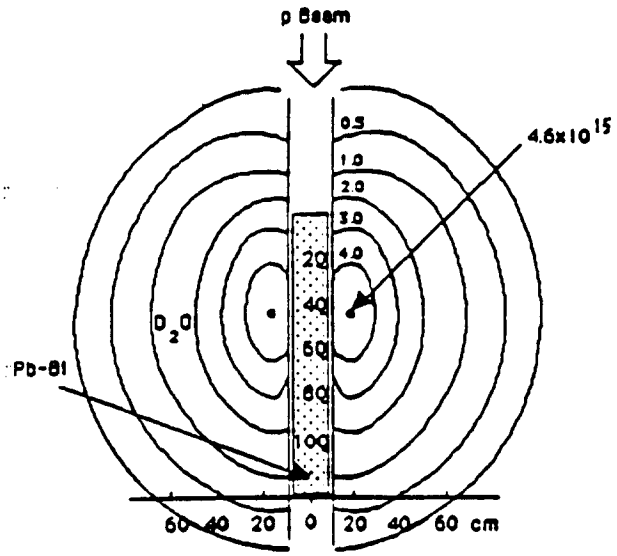

Fig. 4.2 The time average thermal neutron isoflux profiles for a Pb-Bi eutetic flowing target for a beam energy of 1.6 GeV and a proton current of 25 ma. The shaded column in the center is the metal target with dimensions along the vertical in cm with zero marking the top of the liquid metal. The dimension in the horizontal direction is in cm.

3. Nuclear cascade calculation
(Energy nucleon-nucleus interaction)

When medium energy proton collide with the nucleus, the nuclear reaction occurs by a two-step process of spallation and evaporation of the residual nucleus. When the residual nucleus has a large mass and has the moderately high excitation energy then this nucleus might be undergo fission in competition with the evaporation reaction. The third process is emission of the cluster and the emission of the particle [Br,71] before reaching the thermal equilibrium state the so-called the pre-equilibrium emission of the particle. However, knowledge of these processes are still developing, and few codes can handle the pre-equilibrium emission of the particle. Thus, in this report we primarily discuss the process of the spallation, evaporation, and the high energy fission process. We present a brief discussion of the pre-equilibrium model and the fragmentation model.

Neutron and photon transport below the cut-off energy has been accurately calculated in the conventional reactor calculation which are very familiar to the nuclear engineer; thus, we do not discuss these subjects.

When the medium-energy proton collides with the nucleus, the transport of the nucleon in the nucleus can be treated as the classical particle, because the wavelength of the nucleon inside the nucleus is smaller than the nucleon's average distance. The collision of the nucleon and nucleon is treated as a two-body collision . The π meson of π^+ and π^- which are created in the nucleon-nucleon collision also included in the calculation of the cascade process, thus, the basic data for a two-body collision between the pion and nucleon is required to describe the cascade process for the meson. In the nuclear cascade codes NMTC [CA,70,71] and HETC[CA,72],[RS,77], the data for the nucleon-nucleon collision is obtained by Bertini's[Be,63] evaluated data and the production of the meson is treated by using the Isobar model developed by Sternheimer and Lindenbaum. [SL,58,61]

The collision of a nucleon and a nucleon inside the nucleus is treated by a two-body collision which satisfies the relativistic energy momentum conservation law. Since the nucleon is fermion, the nucleon which is scattered below the Fermi energy is not allowed as a real scattering event. These events are discarded and another scattering event is calculated. When the kinetic energy of the scattered nucleon through the nuclear surface is above the binding energy of nucleon, this nucleon escapes from the nucleus with kinetic energy minus its binding energy.

When the nucleon's kinetic energy inside the nucleus is less than the binding energy , the nucleon gives kinetic energy to the nucleus as its excitation energy. This energy thermalises the nucleus, and neutrons, protons or other light nuclei are evaporated as evaporation process. When this energy surpasses the fission barrier in the heavy nucleus fission events will compete with evaporation of light element particles.

The particle emitted from the nucleus collision travel until the next nucleus collision (called an inter-nuclear cascade); after the next collision, a similar process as that described above is repeated until the energy of the particle becomes less than the cut-off energy. When the particle emitted or scattered from the nucleus is a charged particle, their energy is lost by exciting the electron surrounding the their tracking path; we called this process the inter-nuclear cascade process. The cascade process inside the nucleus is called the intra-nuclear process. As the energy of the particle is lowered, then the wave-length of this particle becomes longer than the average distance between the nucleons; then the reaction process cannot be described as a two-body collision of the nucleon or meson, and must be described by the quantum mechanics, using the optical potential model.

Although the nucleon energy reaches as the order comparable to the cut-off energy the wavelength of these particle becomes almost same as the average nucleon distance; consequently the accuracy of this collision model gets worse, However, according to the Bertini's study, the cut-off energy is not as sensitive to the results.

NMTC [CA,70,71] and HETC [CA,72][Rs,77] codes are the system codes which calculate by Monte Carlo mehod the nuclear reaction of protons, neutrons, and pions above the cut-ff energy and the transport of these particle in the heterogeneous media. Fig.1-5 shows the role of NMTC and HETC and that they consist of many subroutines.

The cascade of nucleon in the nucleus is calculated by the code MECC2, which was developed by Bertini; the calculation of the evaporation process from the excited nucleus is calculated by EVAP developed by Dresner[Dr,62]. The transport of particles in the heterogeneous medium is calculated by many subroutines developed in the O5R codes[IR,65]. Furthermore, many subroutines are added to calculating the transporte of the charged particle and the nuclear reaction associated with the pions. The EVAP subroutine has been improved by Guthrie and the present evaporation reaction is treated by subroutine called by DRES; the MECC2 in the NMTC code is named as BERT subroutine. In the HETC code, which can treate more higher energy than the NMTC code, the subroutine called MECC7 is used.

The original NMTC and HETC codes have no capability to calculate the high energy fission which is very important for the target of the high atomic number nucleus, such as the nucleus of uranium and of actinides. To treat this high-energy fission reaction, many authors developed the codes. The detailed model of fission will be discussed in a later section.

By adding their own fission models to the NMTC code, the NMTC/JAERI [NT,82] and NMTC/BNLF [Ta,84] codes have been generated. LAHET code [Pr,89] was made by adding the Ratherford Appleton Laboratory (RAL) [At,79] and ORNL models [Al,81] to HETC code.

The cascade and evaporation models give reasonable results for the high mass number nucleus but they are not as suitable for the light mass nucleus. Thus, the NMTC code is made for targets of nucleus mass number A > 8. However the collision with the proton nucleus can be treated separately by excluding the cascade and evaporation. In order to treat the lithium-6 and 7 in the NMTC/JAERI and NMTC/BNLF codes, the restriction of applicability of A > 8 is relaxed to A > 6. In the LAHET code, the nuclear cascade reaction of a light mass nucleus less than A = 21 is treated by Fermi's break-up model.

Beside of the NMTC and HETC, the ISABEL code [YF,79] was developed from the VEGAS code [CFF,68],[CFM,68] which can treat the refraction process contract to the NMTC and HETC codes. The LAHET code offers the option to use this ISABEL code as well as the HETC code: LAHET treats the light mass nuclei's cascade by Fermi's break-up model.

For the third step of the pre-equilibrium and fragmentation reaction, NMTC/JAERI and LAHET have the capability to handle the pre-equilibrium process based on the Exciton model.

Other nuclear cascade codes such as FLUKA series [Ra,85] and CASIM [VB,71],[VG,71] were developed in the high energy community. However, these codes were for designing the experimental facility and for calculating the shielding necessary, and are not suited for the type of calculation needed for the actinide incinerator, because they do not includeed the high energy fission process. However, for calculating the shielding of accelerator and the target, these codes are very useful and we discuss them in the section on health hazards.

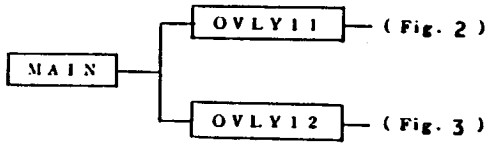

Figure 1 Structure of main routine

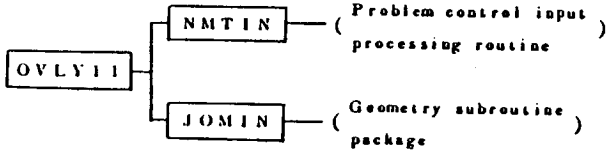

Figure 2 Structure of OVLY11

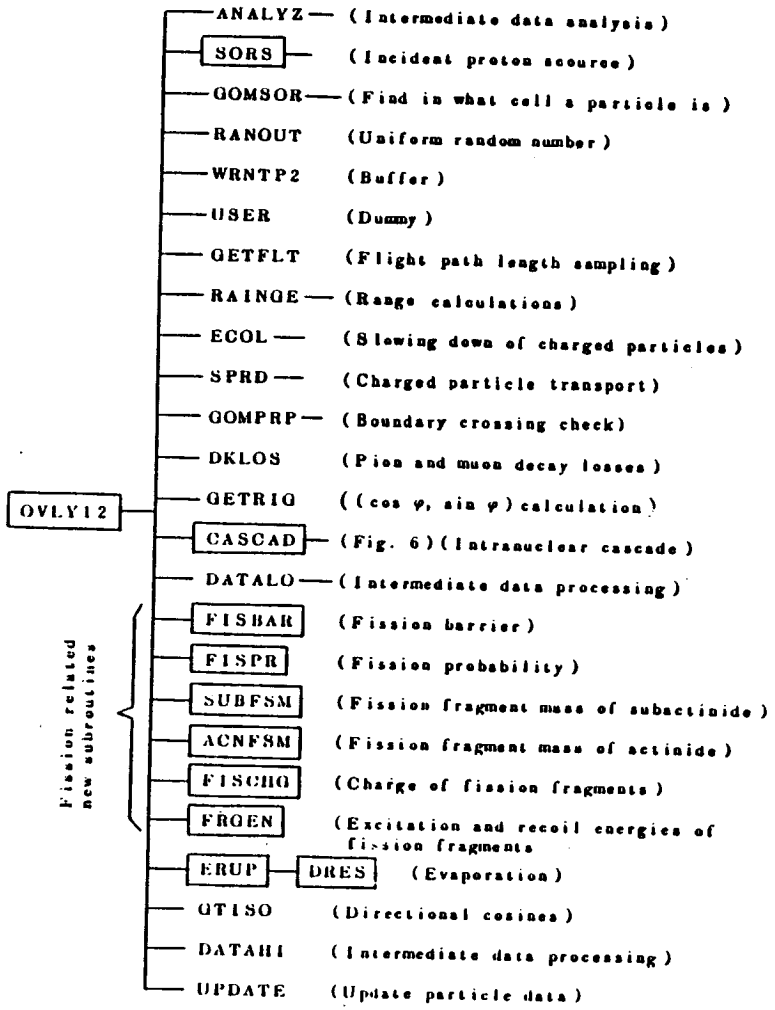

Figure 3 Structure of OVLY12

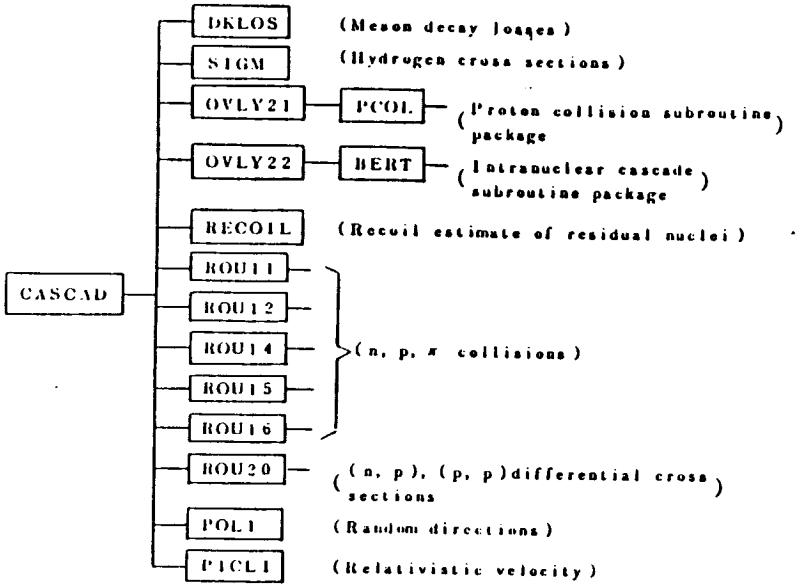

Figure 4 Structure of CASCAD

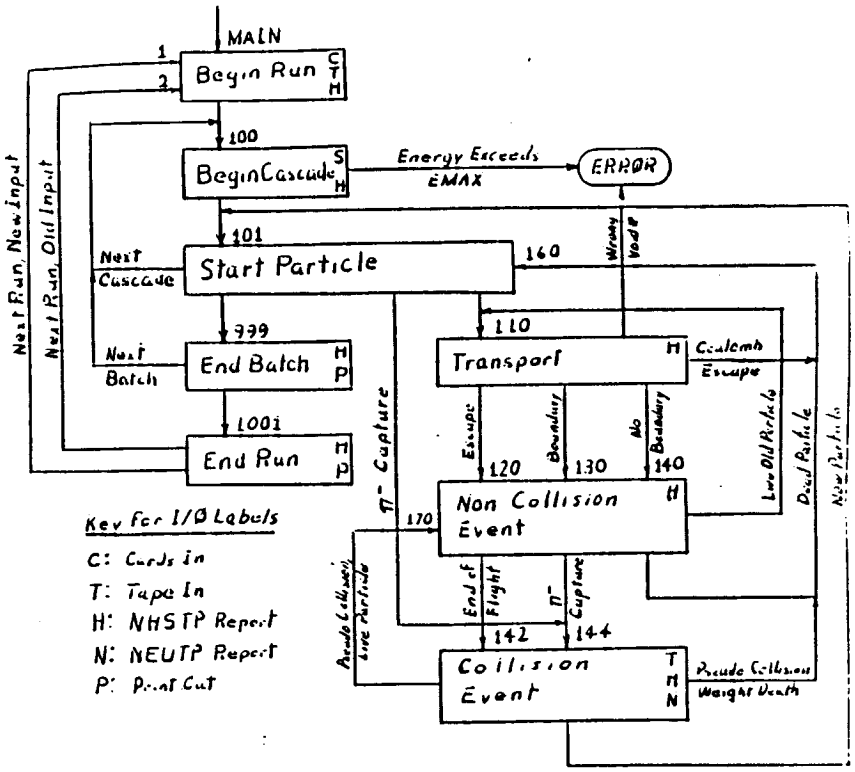

Figure 5 MAIN Flow Chart by Procedures

4. Procedure to calculate the nuclear cascade reaction.

4.1 NMTC [CA,70,71] and HETC [CA,72],[RS,77] codes

In this section, we discuss the details of calculational procedure adopted in the NMTC and HETC codes for the intra-nuclear cascade process.

The information provided by the intra-nuclear cascade calculation consists of the energy and direction of each emitted neutron, proton, d, t, and π-meson, as well as the excitation energy, recoil kinetic energy, charge, and mass of the excited residual nucleus.

To calculate the nucleon's cascade process inside the nucleus, a model is required for the nuclear matter, which is described her as the degenerated nucleons in the Wood-Saxon type potential.

The collision of a nucleon with a nucleon inside the nucleus is treated by a two-body collision which satisfies the relativistic energy momentum conservation law. After collision, when the energy of the particle is less than the Fermi energy, this collision event is discarded and the another collision is performed. When the particles energy after a collision becomes less than the cut-off energy, then this history is terminated. This cut-off energy is different from the 15 or 20 MeV which assigned in the calculation of cut-off energy for neutron transport. The two-body collision used in this cascade calculation is not then sufficiently accurate to describe the collision.

This cut-off energy is set as half the value of the coulomb potential energy, and it is applied all kind of the particles including the neutron: for the neutron, the Coulomb energy must be set at zero. The reason not adopting this procedure is the following. The proton whose energy is less than the Coulomb energy has a chance to collide the neutron, and this neutron will get a large part of the proton's energy ,and continue to cascade down. If the cut-off energy is taken as the whole coulomb energy, this process is terminated prematurely. Therefore, a cut-off energy of a half the value of the coulomb energy is a convenient value.

When the kinetic energy of the scattered nucleon through the nuclear surface is above the binding energy of nucleon, this nucleon escapes from the nucleus with its kinetic energy decreased by the value of its binding energy.

When the nucleon's kinetic energy inside the nucleus is less than the binding energy, the nucleon gives kinetic energy to the nucleus as its excitation energy. This energy thermalizes the residual nucleus, and neutrons, protons, or other light nuclei are evaporated in the evaporation process. When this energy surpasses the fission barrier in the heavy nucleus fission events will be compete with the evaporation of the light elements particles.

In the Bertini's cascade code [Be,63], the binding energy is taken as 7 MeV for all kind of nuclei because of its simplicity in the cascade process. But, in the case of the evaporation process which is occurs in the rather low energy range of nucleus, the binding energy is rather sensitive in calculations of the evaporation process, and an accurate value for binding energy which is included in tabulated form in the codes is used in calculating the evaporation process instead of 7 MeV which used in the cascade calculation.

When the energy and momentum of the particles associated in the collision are determined, these values are recorded temporarily; then, each particle is started from this collision point and the same calculations are repeated. In this way, the cascade calculation is performed.

From the point at which the particle leaves nucleus, records are kept of the kind of the particle, its energy, directional cosine, and the coordinate of the last location of the collision with the nucleus.

In both the NMTC and HETC codes, the nucleon number density, kinetic energy and the distribution of the nuclear potential are described by that assuming the nucleus is composed of three segmented regions.

When nucleon penetrated is inside in the nucleus, the kinetic energy of the nucleon is increased by the nuclear potential energy of about 50 MeV. Although the potential energy of neutron differs from the proton's potential energy, the difference is so small that the same potential is applied for both.

A) Nucleon distribution

Hofslader's formula for the nucleon distribution is used in these codes.

$$\rho(r) = \frac{\rho(0)}{e^{(r-c)/z_1}+1} \qquad (1.1)$$

where c is the r value at which ρ becomes half of

$$\rho(0) = r_1 A^{1/3},\ r_1 = 1.07\ 10^{-13}\text{cm},\ z_1 = 0.545\ 10^{-13}\text{cm}. \qquad (1.2)$$

To simplify the calculation of the nucleon and pion inside the nucleus, Hofstra's formula for the nucleon density ρ is approximated using the three segmented-step function as

$$\rho(r) = \alpha_i \rho(0) \qquad (1.3)$$

the outer radius of each cell is determined in this code as
$\alpha_1 = 0.9 \quad \alpha_2 = 0.2 \quad \alpha_3 = 0.01$

B) Momentum distribution

As described before, the momentum distribution of the proton and neutron are distributed as the degenerated Fermi momentum distribution with absolute zero temperature. That is

$$f(P) = c_i P^2 \qquad (1.4)$$

where c_i is the normalization constant which is determined from the following normalization of Eq.(1.5)

$$\int_0^{P_f} f(p)\,dP = \textit{number of nucleons inside i-th region} \qquad (1.5)$$

as $c_i = 3N/P_f^2$, where P_f is the Fermi momentum of the nucleon.

C) Distribution of potential energy

This distribution is also approximated using the step wise functions. The potential energy in each region is determined as the sum of the Fermi energy and the binding energy of nucleons.

D) Nucleon-nucleon cross section

To calculate the two-body collision inside the nucleus , nucleon-nucleon cross-sections are required. Figs.1.1 and 1.2 show the high-energy proton-proton and neutron-proton cross sections that are used in these codes.

The differential cross-section for p-p scattering was assumed to be isotropic in the center of mass system for proton energies up to 500 MeV. For the energies from 500 to 1000 MeV, semi-empirical fits are made to the p-p cross-section data reported by Hess [He,55]. An expression of the form

$$\frac{d\sigma}{d\Omega}(p\text{-}p) = A + B\mu^3 \qquad (1.6)$$

was used, where μ represents the cosine of the scattering angle in the center of mass system. Representative values of A and B that were used in this code are given in Table 1.1.

Cross-section data are required at energies that are higher than the limiting value already given for the incident particles (350 MeV) because the relative kinetic energy for colliding particles whose momenta are anti-parallel will be larger then the energy of the incident particle alone. This energy can

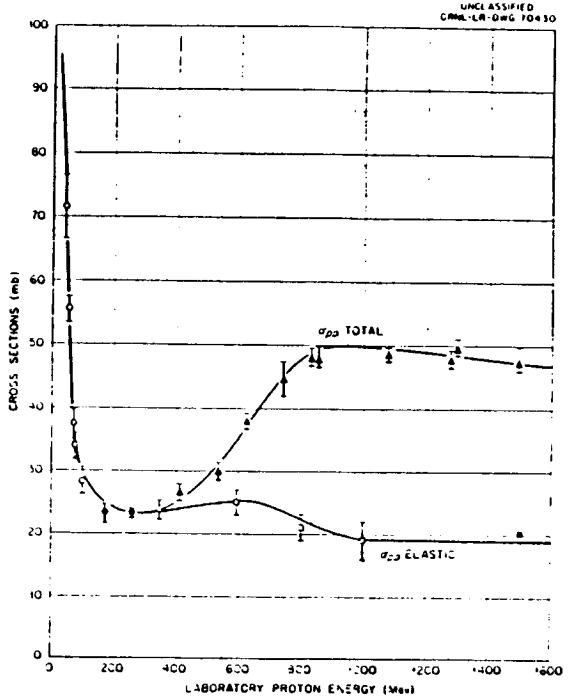

Figure 1.1 Proton-Proton Total and Elastic Cross Sections vs. Energy. ○ U. E. Kruse, J. M. Teem, and N. F. Ramsey, Phys. Rev. 101, 1079 (1956); ●,○ Chamberlain and J. D. Garrison, Phys. Rev. 96, 1349(L) (1954); Δ,○ Chamberlain, E. Segrè', and C. Wiegand, Phys. Rev. 83, 923 (1951); ▲ F. F. Chen, C. P. Leavitt, and A. M. Shapiro, Phys. Rev. 103, 211 (1956); □ L. W. Smith, A. W. McReynolds, and G. Snow, Phys. Rev. 97, 1186 (1955); ■ W. B. Fowler et al., Phys. Rev. 103, 1479 (1956).

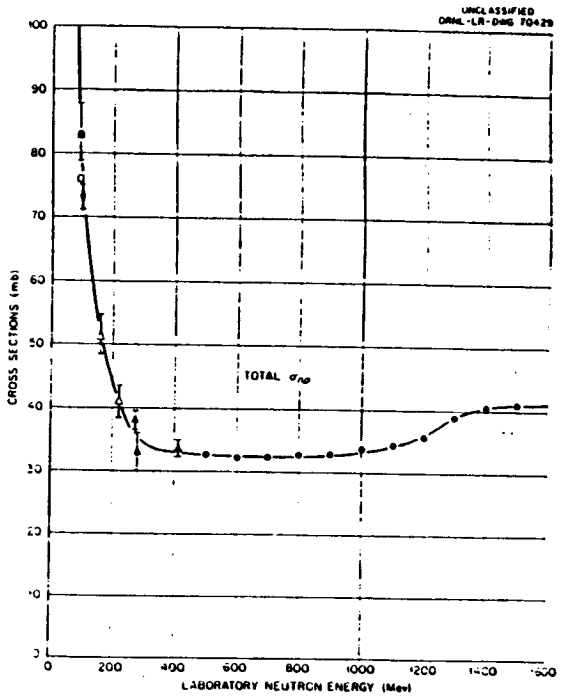

Figure 1.2 Neutron-Proton Total Cross Sections vs. Energy. ■ L. J. Cook et al., Phys. Rev. 75, 7 (1949); □ J. Hadley et al., Phys. Rev. 75, 351 (1949); ◆ J. DeJuren and N. Knable, Phys. Rev. 77, 606 (1950); Δ J. DeJuren and B. J. Moyer, Phys. Rev. 81, 919 (1951); ▲ A. V. Hedzel, Phys. Rev. 95, 174 (1954); ● F. F. Chen, C. P. Leavitt, and A. M. Shapiro, Phys. Rev. 103, 211 (1956).

exceed the threshold for pion production, but the cross section for such production is relatively small, and reactions of this type are infrequent for the energy range to which the incident particles are restricted.

The work of Hess was also used as a source for the n-p differential scattering data. Four parameters were used to fit this data semi-empirically. They are defined by the following:
For $0 \leq E_n \leq 740$ MeV

$$\frac{d\sigma}{d\Omega}(n\text{-}p) = A_1 + B_1\mu^3 \quad 0 \leq \mu \leq 1.$$

For $0 \leq E_n \leq 300$ MeV,

$$\frac{d\sigma}{d\Omega}(n\text{-}p) = A_1 + B_2\mu^4 \quad -1 \leq \mu \leq 0. \qquad (1.7)$$

For $300 \text{ MeV} \leq E_n \leq 740$ MeV,

$$\frac{d\sigma}{d\Omega}(n\text{-}p) = A_1 + B_3\mu^6 \quad 0 \leq \mu \leq 1.$$

The values of A_1, B_1, B_2, and B_3 that were used are given at representation energies in table 1.2

The binominal expressions along with these coefficients represnt the expeerimental data either within or just outside of the experimental errors at all energies.

E) Meson production model

For the particle-particle reaction that lead to the production of π-meson, the Sternheimer-Lindenbaum isobar model [SL,58,61] is employed in the intra-nuclear-cascade calculation (NMTC and HETC); this model is applicable to incident particle energies up to a few GeV. Pion production is assumed to take place through the decay of an isobar that is formed by a nucleon when it is excited in a collision. For example, $N + N \rightarrow N + N^*$,or $\rightarrow N^* + N^*$ with each $N^* \rightarrow \pi + N$. However, the final state momentum distributions of the recoil and decay products are unspecified because neither the angular distribution of the decay pion nor the angular distribution of the isobars themselves is specified.

E1) Steinheimer-Lindenbaum isobar model[SL,58,61]

The Lindenbaum-Steinheimer isobar model was selected for these codes because of its simplicity and because it reproduces the main features of the pion-production process over the energy range under consideration for both pion-nucleon and nucleon - nucleon reactions. The Olsson and Yodh model, as formulated, is limited to single pion-production reactions in nucleon-nucleon collision below about 700 MeV. The formalism could be extended to higher energies and to nucleon-nucleon collisions, but, among other things, it would necessitate the inclusion of additional resonances, such as the ρ, and no one has attempted this yet.

E2) The one-pion-exchange model

The one-pion-exchange (OEP) model will reproduce experimental data reasonably well in most cases, but for consistent reproduction of data in extensive comparisons, OEP requires the use of form factors, absorption corrections, or, more recently,phenomenological fits of a free parameter, R, to each partial wave contributing to the vertex functions.

The isobar model of Sternheimer and Lindenbaum only account for single- and double-pion production in nucleon-nucleon collisions and single-pion production in pion-nucleon collisions. Since the practical thresholds for ternary-pion production by nucleons and double-pion production by pions are about 3.5 GeV and 2.5 GeV, respectively, the pion-production model used in these codes limits the maximum nucleon and pion energies that may be treated using the intranuclear-

Table 1.1

REPRESENTATIVE VALUES OF THE SEMIEMPIRICAL PARAMETERS USED TO DESCRIBE THE NUCLEON-NUCLEON DIFFERENTIAL SCATTERING CROSS SECTIONS[a]

Incident Particle Laboratory Energy (Mev)	n-p Parameters (mb/sr)				p-p Parameters (mb/sr)	
	A_1	B_1	B_2	B_3	A	B
0	1592.0	0	0	0		
40	12.0	7.0	7.0			
80	5.2	8.1	8.3			
120	3.3	6.6	9.0			
160	2.3	3.9	7.7			
200	2.0	3.6	6.5			
240	1.9	3.6	6.2			
280	1.8	3.6	6.0			
320	1.7	3.6		7.8		
360	1.5	3.6		7.4		
400	1.4	3.6		7.0		
440	1.3	3.6		6.7		
480	1.2	3.6		6.4		
520	1.1	3.6		6.1	3.33	1.70
560	1.0	3.6		5.8	3.19	4.00
600	1.0	3.6		5.6	2.80	9.00
640	0.9	3.6		5.4	2.05	8.84
680	0.8	3.6		5.1	1.92	7.[illegible]

Table 1.1 (continued)

Incident Particle Laboratory Energy (Mev)	n-p Parameters (mb/sr)				p-p Parameters (mb/sr)	
	A_1	B_1	B_2	B_3	A	B
720	0.7	3.6		4.9	1.64	8.75
760					1.40	9.40
800					1.20	9.70
840					0.99	9.85
880					0.80	9.90
920					0.69	9.90
960					0.60	9.90
1000					0.[illegible]8	9.90

[a] Parameters defined in text on pages 19 and 22.

cascade sub-program. To treat the higher energy reactions, the extrapolation model of Garthier [Ga] is provided as discussed in HETC.

F. HETC Extrapolation model [GA,70].

HETC determines the energy, angle, and multiplicity of the products from non-elastic nucleon-nucleus and pion-nucleus collisions at higher energies (>3GeV) than the NMTC code by using the extrapolation method of Gabriel et al., This extrapolation method employs the particle-production data obtained from an intranuclear-cascade calculation for intermediate- energy, (3 GeV), nucleon-nucleus and pion-nucleus collisions, together with the energy, angle, and multiplicity scaling relations that are consistent with the sparse experimental data available for high- energy collisions, to estimate the particle production for higher energy (>3 GeV) collisions. This method is applicable only to those particles produced in the cascade phase of the collision; particle emission resulting from the de-excitation of the residual nucleus remaining left after the emission of the cascade particles is determined by performing an evaporation calculation in the same manner as that for intermediate-energy collisions.

Here we describe the extrapolation method used in HETC code. Consider a particle-nucleus collision by a particle (nucleon or charged pinon) with energy E_0 and a collision with the same nucleus by the same type of particle but at some higher energy E_0, where E_0 and E_0' are kinetic energies in the laboratory system. The extrapolation model for relating the products from the " slow" collision at E_0 to the products from the " fast collision at E_0' is based upon the following four assumptions:

(i) The total nonelastic cross section above E_0 is independent of the energy of the incident particle - i.e.: $\sigma(E_0') = \sigma(E_0)$.

(ii) The residual excitation energy after the fast and slow collisions is the same.

(iii) The transverse momentum in the center of momentum (CM) system of each particle produced is assumed to be the same in the fast and slow collisions - i.e.

$$P_{ci}' \sin\theta_{ci} = P_{ci} \sin\theta_{ci} \qquad (1.8)$$

where c denotes CM quantities, i denotes the particle type (neutron, proton, π^+, π^-, or π^0), P is the momentum, and θ is the polar angle with respect to the direction of the incident particle. To make this transformation unique, it is further assumed that the sign of $\cos\theta_{ci}$ is the same as the sign of $\cos\theta_{ci}$.

(iv) To relate the energies of the particles produced in the fast and slow collisions, the following scaling relation for kinetic energies is postulated :

$$\frac{E_{c1}'}{E_{c0}'} = \frac{E_{c1}}{E_{c0}} \qquad (1.9)$$

By using the above assumptions, we can determine the conservation of energy in the CM system for the fast and slow collision and momentum for the fast collision in the laboratory system, and the results of the intranuclear-cascade calculation at E_0, the energy and direction of each emitted particle and the excitation energy, the recoil energy, and the mass of the residual nucleus are determined for collisions at E_{co}'. Further emission of particle due to the de-excitation of the residual nucleus is obtained by performing an evaporation calculation. An intranuclear- cascade extrapolation-evaporation calculation is performed by HETC for each high energy (>E) non-elastic nuclear collisions that occur during the transport calculation.

In HETC, E_{max} is fixed at 3.5 GeV for nucleon-nucleus collisions and at 2.5 GeV for pion - nucleus collisions since these are the maximum energies allowed by the intranuclear-cascade routines. Calculated results using the evaporation method are compared with experimental data for protons in the energy

range from 12.5 to 70 GeV incident on Be, Al, Pb, and W nuclei. In most cases, there is only approximate agreement. However, these "thin-target" comparisons were made for the results of a rather different nature (mainly proton and charged-pion energy spectra in narrow angular intervals). Thus, the extrapolation method may still be satisfactory for predicting the nucleon-meson cascade in thick targets where usually only the properties of the cascade resulting from the average of the product of many nuclear collision induced by particles over a wide energy range is required. In fact, the primary purpose of the comparisons non-elastic nucleon collisions and charged-pion collisions with hydrogen nuclei at energies above 3.5 GeV and 2.5 GeV,respectively, are calculating by the method of Gabriel et al. This method utilizes experimental data for the total non-elastic n-p, p-p, π^+-p and π^--p cross sections and the analytic fits to experimental data by Ranft and Baric [RB.]to determine the particle type, the energy , and the direction of the collision products. Special provisions are made to insure the energy and nucleon are conserved for each collision.

G) Charged-particle Energy Loss

The energy loss of protons, charged pions, and muons due to the excitation and ionization of atomic electrons is treated by the well-established stopping power formula based on the continuous slowing-down approximation. Range straggling is not taken into account. The density-effect correction to the stopping-power formula is calculated using the asymptotic form of the correction.

Range-energy tables for each material in the system are computed for protons. these same tables are used for charged pions and muons by using scaling relations.

After the intra nuclear cascade (including evaporation and fission processes) is complete, calculation of the inter-nuclear cascade can proceed.

H) Multiple Coulomb Scattering

Multiple Coulomb scattering of primary charged particles is treated using Fermi's joint distribution function for angular and lateral spread, and Rutherford's single-scattering cross-section formula. The scattering is implemented in the manner described by Kinney, in which the charged particle angel is arbitrarily divided into sub-trajectories (nominally set equal to one - tenth of the range) and the lateral-spread and angle-charge corrections due to multiple Coulomb scattering are applied at the end points of the sub-trajectories. HETC is presently programmed to allow multiple Coulomb scattering only for the primary charged particles.

4.2 ISABEL (Vegas) code

The similar Monte Carlo Nuclear cascade code Vegas was developed by K. Chen, Z.Fraenkel, G.Friedlander, J.R. Grover, J.M.Miller, and Y. Shimamoto [CFF,68,CFM,68] at BNL. This code is takes into account the refractive process which is neglected in the NMTC and HETC codes, and Vegas is intended to calculate the cascade process up to about 380 MeV nucleon energy. Three alternative models for the nuclear density distribution of (a) a constant-density nucleus of radius $r = r_0 A^{1/3}$ with $r_0 = 1.3 * 10^{-13}$ cm ;(b) a trapezoidal density distribution, and (c) an step-function density distribution are used. However, the original Vegas code did not take into account meson production as does the NMTC and HETC codes, because nucleon energy is limited to the rather low energy of 380 MeV. This code was extended to the calculation of meson production, using the isobar model and the nucleus-nucleus collision by Y.Yarif and Z.Fraenkel [YF,79,81]; for the calculation of the collision between antiproton and nucleus the model by M.R.Clover, R.m. DeVries, N,J. DiGiacomo and Y. Yariv [CD,82] was used.

The code named as ISABEL, which was developed from the VEGAS code, is used in the LAHET code [Pr,89] together with the HETC code, for calculating the nuclear cascade calculation at LANL.

4.3 The cascade calculation for light mass nucleus.

As discussed in the previous section, the cascade and evaporation models give the reasonable results for the high mass number nucleus, but they are not applicable to the light mass nucleus.

The original NMTC code does not taken into account the nuclei which mass is between 2 and 7. This is due to the lack of accuracy in the model describing the nuclear reaction. In the NMTC/BNLF and NMTC/JERIE, this limitation is simply relaxed to encompass a mass range between 2-5, so that Li-6 and Li-7 can be handled in this code. (When the medium contains a large amount of light elements, the energy conservation law is not satisfied and the calculation is stopped by printing the error message. When the medium contain a small amount of the light elements, such as Li the calculation can proceed without stopping but a warning is printed in the NMTC/JAERI code.)

Deuteron is treated as two protons in the NMTC/JAERI codes,because the binding energy of the deuteron is only 2.2 Mev.

4.4 Fermi's breakup model

In the LAHET Code, Fermi's breakup model, which was developed by T.S.Suberamanian et al. [Su,83], has replaced the evaporation model for disintegration of light nuclei; It treats the de-excitation process as a sequence of simultaneous breakups of the excited nucleus into two or more products, each of which may be stable or may have an unstable nucleus or nucleon. Any unstable product nucleus is subject to subsequent breakup. In the Fermi break-up model, channel probabilities and particle momenta are determined by phase-space considerations. In the improved model,the following features have been added:

1. Particle-unstable levels are allowed as intermediate states, thus permitting sequential decay processes.
2. A two-body breaking up channel uses a Coulomb barrier penetration factor which is calculated by the approximated Coulomb wave functions, while multi-particle modes use a breakup threshold adjusted for Coulomb energy.
3. The two-body breakup of levels with known spin and parity are restricted to conserve parity and isospin, and they are inhibited by neutral-particle angular momentum barrier penetration factors.
4. Up to seven body breakup modes are allowed.
5. Experimental data are used for mass excesses, and for the excitation energies, spins, and isospins, and parities of nuclear level.

In the LAHET, the models apply only to residual nuclei with A≤17, replacing the evaporation model for these nuclei.

4.5 The Pre-equilibrium model

In the NMTC and HETC calculations the reaction process is assumed to be two-step process of spallation and evaporation: it is assumed that after spallation, the residual nucleus comes to thermal equilibrium and the particles are emitted by evaporation, However, it is more appropriate to consider that after spallation the residual nucleus is not in a state of equilibrium and emits particles from this state. This pre- equilibrium model has been studied by M.Blann [Bl,71], A.V.Ignatyuk, G,N. Smirenkin and A.S. Tishin, [IS,75] E.D.Arthur [AR,88], R.E.Prel and M.Bozoian [PB,88], and many other authors (C. Kalbach,[KA,85],Y.Nakahara, T, Nishida [NN,86].

In these theories, the pre-equilibrium states are described by the exciton state which is the many particle and hole state of the single particle state. The particle emission and transition between the each exciton state can be expressed by the master equation of the exciton states. However, the theory developed so far, assumes that the exciton states are function of the excitation energy only, and not a function of the angular moments, so that the theory does not properly describe the angular dependence of the emitting particle. Many approximation methods have been devised for taking into account the angular dependence of the emitting particles.

The Griffin's exciton model [Gr,66], which used in the JAERI code, is a simple statistical model, and it neglects nuclear angular momenta and shell

structures. When the incident particle is a proton, however, the neglect of angular momenta is not such a crude approximation. Shell structures have little effect on the particle emission process, because the excitation energy of the residual nucleus at the end of intra-nuclear cascades is sufficiently large i.e., in the order of 100 MeV, for sufficiently energetic incident protons with the energy of the order of 1GeV. Griffin's model [Gr,66] was programmed by Kalbach [Ka,81,85]for calculating pre-equilibrium.

In the LAHET code, the multi-stage pre-equilibrium model (MPM) is used for emission of neutron, proton, deuteron, He-3, and alpha particle at each stage of exciton states. The MPM terminates upon reaching the equilibrium exciton number; then, the evaporation model (or the Fermi's breakup model) is applied to the residual nucleus with the remaining excitation energy.

When the ISABEL intra-nuclear cascade model is invoked, it is possible to determine explicitly the particle-hole state of the residual nucleus, since a count of the valid excitations from the Fermi sea (and the filling of exciting holes) is provided by one count for each intra-nuclear collision for which both exciting nucleons are below the top of the nuclear potential well. This method is the only option implemented in the LAHET to link the MPM with ISABEL INC. It has not yet been implemented in the MPM model with Bertini's INC.

4.6 The fragmentation of the nucleus

When the incident proton energy is increased the nuclear can fragment. This process produces heavier nuclei with mass number A=20-40 even though this probability is much smaller than the probability of emitting the nucleon, deuteron, tritium, He-3, and alpha particles. This process occurs during /or immediately after the intra-nuclear cascade process. Various explanations, not all necessarily contradictory, have been proposed. It has been conjectured that multi-fragmentation is the manifestation of a liquid-gas phase transition occurring during a compression - expansion of nuclear matter.[Ai, 84]. Other models or theories are based on either a statistical and chemical equilibrium picture, or a fast break up process in which only minimal statistic assumptions are made[Mo,85]. But the actual process of fragmentation is so complicated that none of the theories has sucsseded in offering a convincing explanation [CDE,84].

4.7 Discussion

The neutron spectrum in the spallation reaction using the rather thin block target has a small bump in the region of 20 - 80 Mev. In the NMTC calculation, the reaction is assumed to be two step process of spallation and evaporation. To explain this bump in the neutron spectrum, several models have been proposed. One of them is a pre-equilibrium model, in which neutrons are emitted before reaching the equilibrium state. For this reaction process the several models are adopted and the results are compared with the experimental results. Some improvements are seen but this model can not comp;eetly explain the bump in the neutron spectrum. Another model is the multiple temperature model the parameter of which are obtained by analyzing the experimental data. However, there are no available data for actinide nuclei. This method cannot be applied, and there is no predictability in this model unless the multitude temperatures can be explained on a physical basis. The other model is a moving source model, which assumes that the excited nucleus created by the spallation reaction is moving, and explaing the some of neutrons are emitted in the forward direction is explained but this also has no predictability in theory.

This discrepancy is not very important for neutron yield in the accelerator incineration of actinide where its magnitude is small compared to the large yields of the neutron. Specifically, when the assembly composed of actinide nuclei is in a subcritical state of k=0.9-0.97, most of the neutrons that contribute to the incineration of actinide come from the fission process, not from the spallation process itself. But to the problem of neutron and gamma-ray shielding in the rear-end direction of assembly this high energy neutron spectrum might be important.

The spallation products including the fission products and evaporation products have been extensively studied by Nishida and Nakahara[NN,86]. They showed that the mass formula which is not covered by presently known isotopes is not enough, and the newly evaluated mass formula by Yamada et al [UY,81] is used in this study. This kind of work is important in evaluating the radiation level and radiation hazard to maintain the accelerator operation.

5 High energy fission model

5.1 General

To evaluate the yields of neutrons and reaction products in a heavy mass target irradiated by a high energy proton beam, it is very important to take into consideration the high energy fissions. The several high energy fission models have been proposed and incorporated into the high energy nucleon meson transport code HETC by Atchison [At,71], and Alsimiller et al.[Al,81] and NMTC by Takahashi [Ta,84] and Nakahara[Na,80]. Armstrong and Filges [Ar,83] have compared neutron yield calculated by these models. Balashenkov et al.[Ba,78] have developed independently a high energy fission model.

Theoretically, all of these models are based on the statistical theory of fission, but they are different in practice in their computational schemes, physical assumptions and data used in the calculations of fission probability, mass and charge distributions of fission fragments, excitation, and kinetic energies of residual nuclei. The assumptions and values of the physical parameters are so closely interdependent in each model that it is difficult, and indeed, seems of little value to make comparative evaluations of particular assumptions.

In the original NMTC and HETC codes in which fission is not taken consideration, the high energy reaction is treated as a two-step process. The first step is an intra-nuclear cascade described as a series of two-body collisions of free Fermions inside the nucleus. The second step is an evaporation process, describing the emission of particles such as n, p, d, t, He-3 and α as a de-excitation of the residual nucleus of the cascade process.

When there is a possibility of fission, it can be considered to occur in competition with evaporation. The fission process itself can be treated as a two-step process. At the moment of fission a nucleus splits into two fragments, from which particles subsequently would or would not evaporate according to the excited levels.

The π-meson emitted from the nucleus during the intra-nuclear cascade can also participate in the reaction process.

5.2 Branching ratio of fission to neutron emission.

The competition between fission and evaporation is obtained by calculating the ratio of

$$P_f = \frac{\Gamma_f}{\Gamma_f + \Gamma_n} \qquad (2.1)$$

where Γ_f and Γ_n are partial widths for fission and for neutron emission, respectively. Since we consider the possibility of emissions of p, d, t, He-3, and α particles also, the numerator of Eq (2.1) should have been $\Gamma_f + \Sigma_j \Gamma_j$. The values of Γ_j other than Γ_f and Γ_n, however, can be considered to be very small in comparison with Γ_f and Γ_n, so that Eq(2.1) may be used as a good approximation.

The statistical theory of Weisskopf [WE,37] for particle evaporation and that of Bohr-Wheeler [BW,52] for fission give a following expression of the width ratio Γ_n / Γ_f.

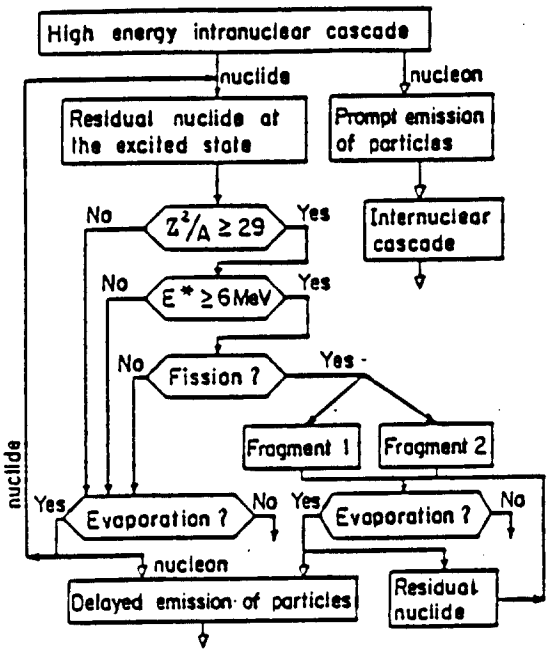

FIGURE 1 Competition of fission and evaporation processes

$$\frac{\Gamma_n}{\Gamma_f} = \frac{4A^{2/3}a_f(E-B_n)}{K_0 a_n[2\sqrt{a_f(E-E_f)}-1]} \qquad (2.2)$$

$$x\exp[2\sqrt{a_n(E-B_n)}-2\sqrt{a_f(E-E_f)}]$$

where some small terms are dropped for simplicity and physical parameters are defined as:
A= mass of a compound nucleus,
a_f and a_n = level density parameters appropriate to the saddle point of fission and the equilibrium deformation, respectively,
E = excitation energy of a compound nucleus,
B_n= binding energy of a neutron.
E_f= fission barrier,
$K_0 = h^2/2mr_0$,m and r_0 being the neutron mass and the nucleus, respectively.
Below we describe the model adopted in each laboratory.

A) RAL model[At,79]

In the RAL (Atchinsons) model, the branching ratio of fission to neutron emission is calculated using the systematic of Vandenbosh & Huizenga for Z ≥ 90 nuclei;

$$\log\frac{\Gamma_n}{\Gamma_f} = \phi(Z)A+\psi(Z) \qquad (A.1)$$

where Γ_n and Γ_f are the widths for neutron emission and fission, A is the mass number of the fissioning nucleus. Here it is assumed that $P_f = 0$ for $E^* < 6$ MeV and $P_f = (1+ \Gamma_n/\Gamma_f)^{-1}$ for $E^* > 6$ MeV. With the Γ_n/Γ_f values is calculated using the tabulated value of $\rho(z)$ and $\Psi(z)$.

For the sub-actinide region of Z < 90, the other statistical model is used, which fits the experimental data. This model uses separate level density parameters for neutron emission and fission, and a fission barrier. Both the saddle-point level density parameters and the fission barrier show systematic variation with the fissionability parameter Z^2/A.

The expressions for subactinide fission are: (for nucleus Z,A excited to E^*).

$$\Gamma_n = 0.3518099(1.68I_0+1.93A^{1/3}I_1+A^{2/3}(0.76I_1-0.051I_0)) \qquad (A.2)$$

$$I_0 = \frac{4.0}{a_n}[(s_n-1.0).e^{s_n}+1.0] \qquad (A.3)$$

$$I_1 = \frac{2.0}{a_n^2}[(6.0-6.0.S_n+2.0.S_n^2)e^{s_n}+s_n^2-6.0]$$

$$S_n = 2.0\sqrt{a_n(E^*-BE')}$$

BE' = Separation energy - pairing energy [as computed by HETC function energy]
Hence

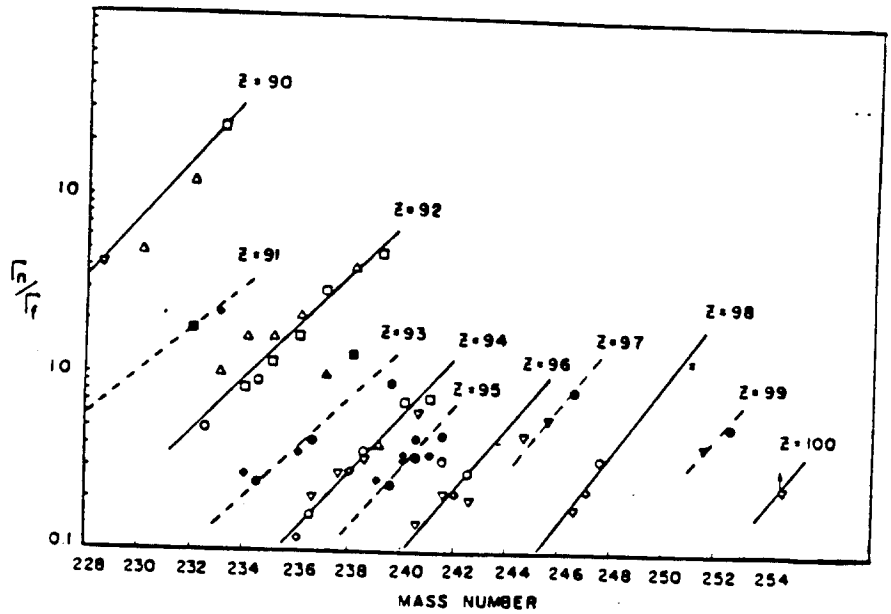

FIGURE A.1 Ratio of the width for neutron emission to the width for fission for various atomic numbers versus nuclear mass.

$$a_n=(A-1.0)/8.0$$

$$\Gamma_f=[(S_f-1.0)e^{S_f}+1.0]/a_f$$

$$S_f=2.0\sqrt{a_f(E^*-E_f')} \qquad \text{(A.4)}$$

$$E_f'=BE'+321.175-16.70314\frac{Z^2}{A}+0.2185024\left(\frac{Z^2}{A}\right)^2 \qquad \text{(A.5)}$$

$$\frac{a_f}{a_n}=1.089257+0.01097897.\left(\frac{Z_2}{A}-31.08551\right)^2 \qquad \text{(A.6)}$$

$$P_f=\frac{1.0}{1+\frac{\Gamma_n}{\Gamma_f}} \qquad \text{(A.7)}$$

These probabilities rise very rapidly to a fairly constant value in most case: This saturation value is reached by -6 MeV excitation energy.

B) ORNL model

The ORNL model adopts Hahn and Bertini's fission model[BE,72]. Their model is essentially same as the simple model developed by Sikkeland, Ghiorso, and Nurmia [SG,68], which is formulated as

$$\log_{10}(\Gamma_n/\Gamma_f)= \begin{cases} -0.276Z+5.46+0.14N & \text{for } N \le 153 \\ 19.23+0.05N & \text{for } N \ge 153 \end{cases} \qquad \text{(B.1)}$$

For odd-Z nuclei, 0.12 is added to the equation.

This simple formula reproduces the experimental Γ_n/Γ_f values for actinide nuclei with $Z \ge 91$ as well as or better than theoretical formulas that depend explicitly upon excitation energy, neutron binding energies, and fission-barrier heights. The fact that this formula, derived from heavy-ion reaction studies at many tens of MeV of excitation, can reproduce Γ_n/Γ_f values obtained with low-energy neutrons, γ rays, and α particles also supports the idea that Γ_n/Γ_f is not energy-dependent in the heavy elements. In this ORNL model, the fission of nuclei whose z number is less than 90 is simply neglected.

In the JAERI and BNL models, more elaborated models than the RAL and ORNL models are adopted.

C) JAERI model

The JAERI model takes into consideration the possibility of fission only for nuclei with masses greater than 175 (for Lu). To implement fissions of nuclei with intermediate masses around A=90, Eq.(2.2) must be extended to cover the entire range of the fission.

The fission barrier heights for almost all nuclei have been calculated and evaluated by Il'inov et al [IC,77,80]. using liquid drop model due to Meyers-Swiatecki[MS,66,67] and Nix[NI,69], which permits the extrapolation to the region of nuclei with A < 150 where no experimental results. The fission barriers calculated by Il'linov et al. are shown in fig.(1) with the experimental values; the bold solid curve corresponds to the calculation without shell corrections and the thin solid curve represents the effects of shell corrections. The dashed and

dash-dotted curves are the calculations madewith the Pauli-Ledergerber[PL,73] and the Krappe-Nix [KNS,79] parameters without shell corrections, respectively.

JAERI model uses the fission barrier corresponding to the bold solid curve in Fig.1 for the nuclei with A < 180. As seen in Fig.1, neglect of the shell effects results in a great error for nuclei with masses of 180 < A < 225.

For these sub-actinide nuclei, it is better to use the results with shell corrections. For simplicity, the following approximate expressions are devised for E_f(MeV)

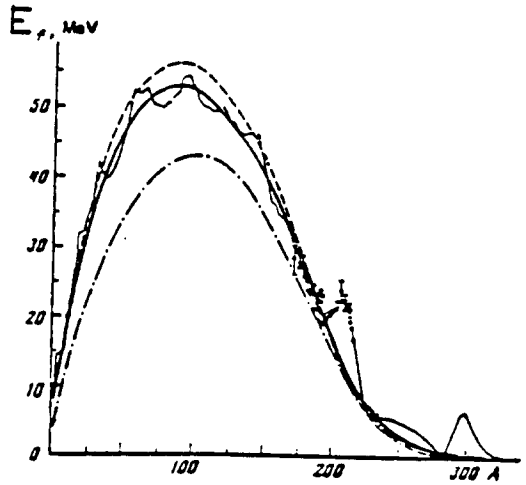

Figure 1 Fission barrier heights

The solid curves are calculations with (thin line) and without (thick line) shell corrections based on the parameters of Swiatecki et al.

The dashed and dash-dotted curves are calculations with the Pauli-Ledergerber and Krappe-Nix parameters, respectively, without shell corrections.

$$E_f = \begin{cases} 52\exp[-(\frac{A-90}{70.7b})^2] & \text{for } A < 90, \\ 52\exp[-(\frac{A-90}{91.7b})^2] & \text{for } 90 < A < 180, \\ 23\exp[-(\frac{A-210}{11.0b})^2] & \text{for } 210 < A \le 225, \\ 52\exp[-(\frac{A-90}{91.7b})^2] + 23\exp[-(\frac{A-210}{11.0b})^2] & \text{for } 180 < A < 210, \end{cases} \quad (C.1)$$

where b= 1/ln2.

The level density parameter, a_n, is calculated from the LeCouteur's expression [LC,50]:

$$a_n = \frac{A}{B_0}[1+1.5(\frac{A-2Z}{A})^2] \quad (C.2)$$

where B_0 is a universal constant and B_0 = 8 is used in NMTC and NMTC/JAERI. (Atchison [At,79], and Alsmiller et al.[Al,81] use different values for B_0). B_0 seems to range from about 8 to 20 MeV, but the best value has not been evaluated.

The level density parameter for fissioning nucleus, a_f, was fitted to the experimental data compiles by Vandenbosh and Huizenga [VH,58]. The fitting is represented by the following simple equation linear in Z^2/A,

$$a_f/a_n = 1.0+0.1(Z^2/A-29.0) \quad (C.3)$$

The neutron binding energy, B_n, can be obtained in the same way as in the subroutine DRESS of NMTC.

For the fission of the actinide nuclei, it has been shown by Strutinski [St,67] that the shell effects substantially influence the fission of heavy nuclei not only in the initial final states but also in all intermediate stages during its evolution. He also showed that the shell correction to the nuclear energy is an oscillating function of the deformation and, as a consequence, E_f in the actnide region has a double-humped shape. The direct application of the traditional systematic of Vandenbosh-Huizenga [VH,58] fitting to this region is difficult, so that JAERI model follows the procedure proposed by Kupriyanov et al [Ku,80].

The potential energy of the nucleus can be expressed as the sum of two components: the liquid drop energy $V(\alpha)$ and the shell correction $\delta W(\alpha)$,where α is a deformation parameter. Accordingly, the heights of the two humps, E_f nd E_{fb}, can be written as

$$E_f^i = V(\alpha_i) - \delta W_g - \delta W_f^i, \quad i=A,B \quad (C.4)$$

where δW_g =the shell correction of the ground state of a nucleus of equilibrium deformation relative to the ground state if the liquid drop model ~V(0),

δW_f^i= the shell correction to the i-th maximum of the potential energy at a corresponding deformation.

The potential and shell corrections are shown in Fig.2. The relative

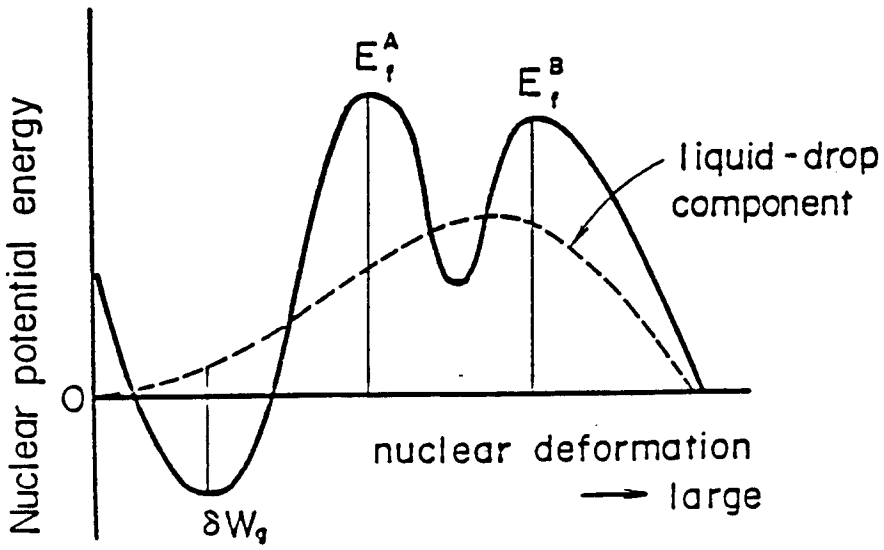

Figure 2 Schematic illustration of double-humped fission barrier

magnitudes of E_f^A and E_f^B changes at uranium;

$$E_f^A \leq E_f^B \quad \text{for } Z \leq 92,$$

$$E_f^A > E_f^B \quad \text{for } Z > 92. \tag{C.5}$$

Numerical values of E_f^A and E_f^B have been estimated by Kupriyanov et al. [Ku,80] and are summarized in table 1.

The fission barrier derived from the liquid drop model can be written as :

$$\overline{E_f} = E_s^0 \, \xi(x) \tag{C.6}$$

where x and E_s^0 have been defined already for Eq(3) and can be calculated using the following expressions obtained by Meyers and Strtinski [MS,66,67]

$$X = \frac{C_3}{2a_2} \frac{Z^2}{A} \frac{1}{(1-kI^2)} \tag{C.7}$$

where a_2 , c_3 and k are the parameters in their mass formula and I=(N-Z)/A,and

$$E_s^0 = a_2 A^{2/3}(1-kI^2). \tag{C.8}$$

On the other hand, Cohen and Swiatecki [CS,63] derived an approximate expression of $\xi(x)$ that is satisfactorily applicable in the region of interest to us up to x = 0.6:

$$\xi(x) = (1-x)^3[0.7259-0.3302(1-x)+0.6387(1-x)^2 \\ -0.78272(1-x)^3-12.006(1-x)^4] \tag{C.9}$$

Meyers and Swiatechki [MS,66,67] performed a fit of a parameters of the liquid drop model a_2, c_3, and k to the experimental data on nuclear masses which give consistent values of the nuclear potential and δW_g:

$$a_2 = 17.9439 \; MeV, \quad c_3 = 0.7053 \; MeV, \quad k = 1.7826 \tag{C.10}$$

Using the value of δW_g also obtained by Meyers and Switecki [MS,66,67] and the experimental data on E_f^A and E_f^B ,Kuriyanov et al. calculated the values of W_f^A and W_f^B, which turned out to be taken as independent of N and Z. These values

$$\delta W_f^A = 2.8 \; MeV \quad \delta W_f^B = 0.5 \; MeV \tag{C.11}$$

provide the best agreement with the experimental data for nuclei with Z > 92.

For nuclei with the double-humped fission barrier,the width ratio Γ_n/Γ_f can be expressed as follows,

$$\frac{\Gamma_n}{\Gamma_f} = G \exp\left[\frac{E_f^M - \langle B_n \rangle}{T}\right] \tag{C.12}$$

where

Table 1 Double-humped fission barrier heights (MeV)

Element	A	E_f^A	E_f^B	Element	A	E_f^A	E_f^B
Ra	225	5.69	7.89	Np	233	5.69	5.21
	226	5.50	7.68		234	6.10	5.69
	227	5.08	7.30		235	6.02	5.68
	228	5.07	7.34		236	6.171	5.926
					237	5.96	5.79
Ac	326	5.69	7.35		238	6.17	6.08
	227	5.42	7.14		239	5.815	5.79
	228	5.26	7.04				
				Pu	237	6.25	5.34
Th	227	5.45	6.58		238	6.22	5.39
	228	5.59	6.79		239	6.40	5.65
	229	5.42	6.68		240	6.16	5.48
	230	5.48	6.80		241	6.17	5.46
	231	5.45	6.84		242	5.94	5.41
	232	5.41	6.86		243	5.92	5.52
	233	5.29	6.79		244	5.71	5.32
	234	5.24	6.80		245	5.67	5.34
Pa	230	5.57	6.26	Am	239	6.40	4.87
	231	5.45	6.21		240	6.59	5.15
	232	5.65	6.48		241	6.34	4.98
	233	5.48	6.38		242	6.44	5.16
					243	6.09	4.89
U	231	5.67	5.75		244	6.26	5.13
	232	5.79	5.95		245	5.82	4.77
	233	5.97	6.20		246	5.92	4.94
	234	5.92	6.23		247	5.37	4.45
	235	5.91	6.29				
	236	5.83	6.28	Cm	241	6.56	4.50
	237	5.89	6.40		242	6.45	4.38
	238	5.65	6.23		243	6.53	4.54
	239	5.63	6.26		244	6.41	4.50
	240	5.42	6.12		245	6.54	4.72
					246	6.32	4.57
					247	6.32	4.65
					248	6.10	4.50
					249	5.89	4.36
					250	5.48	4.02

$$G = G_A \exp\left[\frac{E_f^A - E_f^M}{T}\right] + G_B \exp\left[\frac{E_f^B - E_f^M}{T}\right] \qquad (C.13)$$

$$E_f^M = \max(E_f^A, E_f^B) \qquad (C.14)$$

$$\langle B_n \rangle = \frac{1}{2}\left[B_n(Z,M) + B_n(Z,N-1)\right]. \qquad (C.15)$$

The value of a parameter T can be fixed as $T = 0.5$ MeV, which has been justified by Linn . The relative weights G^A and G^B consistent with this T value have been determined by Kupriyanov et al. as follows ,

$$G_A = 0.41, \quad G_B = 0.90 \qquad (C.16)$$

The systematic described above may become less accurate for the pre-uranium nuclei (Th, Ac, Ra), because of the experimental data on $\ln(\Gamma_f/\Gamma_n)$ study outside the region corresponding to the limit $G_{min} < G < G_{max}$.

D) BNL model

The BNL model uses the brnching ratio developed by Il'inov et al [IC,77,80]. This formula is expressed in the following equation,

$$\Gamma_j = \frac{(2s_j+1)A_j M_n A_{fj}^{-1/2} \alpha_j I_0^2}{\pi h^2 a \exp\left[2(aA_c E^*)1/2\right]} \times \left\langle (E_j^* - B_j')\left[\exp(\kappa_j)(\kappa_j - 1) + 1\right] - \frac{1}{4aA_{fj}}\left[6 + (\kappa_j^3 - 3\kappa_j^2 + 6\kappa_j - 6)\exp(\kappa_j)\right]\right\rangle \qquad (D.1)$$

and

$$\Gamma_f = \frac{\exp(\kappa_f(\kappa_f - 1) + 1)}{4\pi A_c a_f \exp\left[2(aA_c E^*)^{1/2}\right]} \qquad (D.2)$$

where

$$\left.\begin{aligned} B_n' &= B_n - \beta \\ A_{fj} &= A_c - A_j \\ \kappa_j &= 2\left[aA_{fj}(E^* - B_j')\right]^{1/2} \\ \kappa_f &= 2\left[a_f A_c (E_f^* - B_f')\right]^{1/2} \\ E_j^* &= E^* - h^2 M^2 / 2I_j \end{aligned}\right\} \qquad (D.3)$$

$$E_f^* = E^* - h^2M^2/2I_f .$$

In the derivation of Eqs.(1) and (2), the Fermi gas approximation for the level density of Eq.(D.4) is used.

$$\rho(E^*) = const.\exp[2(aAE^*)^{1/2}] \qquad (D.4)$$

In Eq.(D.1) and (D.2), M_n is the nucleon mass, A_j and S_j are the mass number and spin of nucleus, a and a_f are, respectively, the level density parameters of the undeformed nucleus and of the nucleus, having a configuration corresponding to the saddle points of fission. The parameters r_0, a_j ,and β, which describe the cross section for the inverse process of abssorption of the particles by the nucleus , were taken from I .Dostrovsky et al.[Do,58]. The binding energies of the particles were calculated from the formula used in the NMTC code.

In Eq,(D.3), B_f is the fisson barrier height which is determined by the liquid drop model, shown as follows:

$$B_f^{LDM} = E_s b(x) \quad , \quad x = E_c/2E_s \quad , \qquad (D.5)$$

where: E_s and E_c are the surface and Coulomb energies of a spherical nucleus, respectively, and b(x) is formulated as Eq.(D.6) As discussed the above, Il'inov et al. [IC,77,80] recommend using the value calculated by Nix[Ni,69]. However, the semi empirical formula obtained by Cohen and Swiatecki [CS,63] is used in the BNL model. In table , the b(x) calculated in this formula is compared with the tabulated value by Nix. This shows reasonable agreement between the two values except in the range of x > 0.8.

$$\begin{aligned} b(x) &= 0.38(0.75-x) \quad , 0 < x < 2/3 \\ &= 0.83(1-x)^3 \quad , \quad 2/3 < x < 1 \end{aligned} \qquad (D.6)$$

In Eq. (D.5), E_s and E_c are obtained from the same formula as Eq.(C.8):

$$E_s = a_s(1-\kappa[(N-Z)/A]^2)A^{2/3} \qquad (D.7)$$

and

$$E_c = a_c Z^2/A^{1/3} \quad , \qquad (D.8)$$

The calculations used in this study are based on the set of liquid drop parameters of Meyer and Swiatecki[MS,67]:a_s=17.944, a_c=0.7053, k=1.7826,which are same as Eq.(C.10).

To take into account the effect caused by the change of properties of highly excited nucleon the nuclear feasibility, Illinov et al. used the thermal dependence of the Coulomb and surface energy coefficients as :

$$\begin{aligned} a_c(E^*) &= a_c(1-cT^2) \\ a_s(E^*) &= a_s(1-sT^2) \end{aligned} \qquad (D.9)$$

where: T is the nuclear temperature which is expressed by:

$$T = (E^*/aA)^{1/2} \text{ and } c = 10^{-3}MeV^{-2},\ s = 6.316*10^{-3}MeV^{-2} \qquad (D.10)$$

For calculating the fission barrier height, this formula is used.

The level-density parameters of a and a_f in the Eq(D.3) are sensitive to determine the branching ratio. Il'inov et al. used the ratio of a_f/a which is a function of the incident proton as follows. In the case of ; a=0.1 MeV^{-1} (B_0 =10 MeV),the ratio of a_f/ a are 1.05,1.03 and 1.02 for proton energies of 150, 660, and 1000 MeV.

As shown in the previous section, the B_0 value used in our calculations is 8 MeV or 10 MeV, and we took the ratio of a_f/a as 1.05 for excitation energy E^* < 150 MeV and 1.01 for E^* > 150 MeV.

In the calculation of the branching ratio, the excitation energy (E^*) dependent value of a is calculated by formula :

$$a(E^*,A,Z)=a[1+[1-\exp(-0.061E^*)]*\Delta M/E^*] \qquad (D.11)$$

where: ΔM = shell correction to the nucleus mass A= (0.1343-1.21 $x10^{-4}$ A) (MeV^{-1}) asymptotic value of the level density parameter (for large E). This is very close to the level density parameter B_0 =10 MeV for the U-238 nucleus.

5.3 The mass and charge distribution after scission.

If it has been decided that fission will occur, the masses, charges, and other parameters such as kinetic and excitation energies have to be selected for the fission fragments. These parameters are also determined using the statistical model ,in which it is assumed that the fission process is so slow that an instantaneous equilibrium state will be established at every moment of the process. Thus, the relative probability of occurrence of a fission mode is determined from the instantaneous equilibrium at the moment just before the two fragments separate from each other. The probability is calculated from the density of quantum states of the different nuclei configuration at the moment just before scission. These values are calculated by the liquid drop model used in the calculation of the branching ratio discussed above.

We next describe the models adopted by various laboratories.

A) RAL [At,79] and JAERI [Na,80] models

In the RAL and JAERI models, these distributions are determined by the statistical theory based on the fluctuation probability and on the experimental data.

If the most probable value, x, of a certain parameter x is known, the statistical theory provides the fluctuation probability:

$$P_y(x) \propto \exp\left[- \frac{(x-\bar{x})^2}{\langle \Delta x \rangle^2} \right] , \qquad (A.1)$$

where

$$\langle \Delta x \rangle^2 = \left[\frac{T}{2} \frac{\partial^2 W}{\partial x^2}_{x=\bar{x}} \right]^{-1} , \qquad (A.2)$$

T = the temperature at the moment of rupture,
W = the total energy.

The index y in Eq.(A.1) denotes the distribution of x for a fixed value of y.

In the RAL model, the mass distribution after scission is determined for actinide region by taking into account the two competing modes, asymmetric division (dominant at low excitations) and symmetric division (which takes over at high excitation).

For nuclei in the sub-actinide region, the mass split is always assumed to be a symmetric, i.e., about A/2 (E.F. Neuzel & A.W. Farhall [Nf,63]) and for the distribution the following expression is obtained from analysis and adopted in as the calculation model.

$$1/2 \text{ width at } 1/2 \text{ height} = E_{cn^*} - E_f + 7 \qquad (A.3)$$

where E_f is the fission barrier for the fissioning nuclei.

For the charge distribution function, the equal charge density postulate is adopted,

$$Z_1/A_1 = Z_2/A_2 = Z/A. \qquad (A.4)$$

The charge distribution function for the one fragment (the heavy one in the case of asymmetry) is assumed to have a gaussian distribution with a two charge unit for the width. The charge of the other fragment is determined from conservation of the number of protons.

The total recoil kinetic energy correlates well with the Coulomb repulsion parameter $Z^2/A^{1/3}$, and this RAL model takes the correlation of E from E.K. Hyde[Hy,64]

$$T_{tot} = 0.1065\ Z^2/\ A^{1/3} + 20.1 \qquad (A.5)$$

where $Z^2/A^{1/3}$ is computed for the fissioning nucleus.

This model computes the excitation of the fragment assuming a uniform distribution of both excitation and binding energy in the fissioning nucleus plus conservation of energy.

In the JAERI model, Pik-Pichak and Strutinskii's model [PS,76] is used to determine the mass and charge distributions of the fission fragments[20]. When the mass A of a fission fragment has been determined for fissioning nucleus of the mass A_0 and charge Z_0, the most probable charge of the fragment is given as follows,

$$\bar{Z}=-\frac{1}{10}\frac{e^2}{r_0\beta}\left(\frac{A_0}{2}\right)^{2/3}\left(1-\frac{5}{8Q}\right)\frac{Z_0}{2} + \frac{AZ_0}{A_0}\left[1+\frac{1}{10}\frac{E^2}{r_0\beta}\left(\frac{A_0}{2}\right)^{2/3}\left(1-\frac{5}{8Q}\right)\right] \qquad (A.6)$$

which is consistent with the Cameron's mass formula [Ca,57]. In Eq. (A.6) β is a parameter in the Cameron's mass formula, the value of which is given by him as β= -31.4506MeV ; 2ρ is the distance between the center of mass of each fragment.

The fluctuation relative to Z bar is given by the expression:

$$\frac{1}{\langle\Delta Z\rangle^2}=-\frac{16\beta}{A_0T}\left[1+\frac{\phi}{\beta}\left(\frac{2}{A_0}\right)^{1/3}-0.055\frac{e^2}{r_0\beta}A_0^{2/3}\right] \qquad (A.7)$$

where ϕ =44.2355 MeV and is also a parameter in the Cameron's mass formula. In deriving Eqs.(A.6) and (A.7), the pairing energy and symmetry energy correction terms in the mass formula have been neglected, because their contributions are $\pm$2 MeV at most.

Pik-Pichak and Strutinskii also derived the expressions of A bar and $1/\langle\delta A\rangle^2$ for subactinides. The overall shape of the distribution may be expressed very well by the triple-folded normal distribution:

$$P(A)=\frac{2}{\sqrt{\pi}b\langle W_{1/2}\rangle[2\alpha+\beta]} \times\left(\alpha\exp\left[-\frac{(A-A_1)^2}{b^2\langle W_{1/2}\rangle^2}\right]+\beta\exp\left[-\frac{(A-A_2)^2}{b^2\langle W_{1/2}\rangle^2}\right] +\alpha\exp\left[-\frac{(A-A_3)^2}{b^2\langle W_{1/2}\rangle^2}\right]\right) \qquad (A.8)$$

The same half-width at half maximum is assumed for the three normal distribution in Eq. (A.8). The constant b is the normalization factor. We fitted the heights of the two side peaks alpha and the central peak beta (or valley) to the data obtained by Grass et al.[Gr,56] on Pu-239 fission induced by a helium ion;

$$\alpha(E)=\begin{cases}\exp(0.5991E-13.1869), & 6\text{MeV} < E < 25\text{ MeV}\\ \exp(0.08026E-0.2149), & 25\text{MeV} < E < 40\text{ MeV}\\ \alpha(40\text{ MeV}) & 40\text{MeV} < E\end{cases} \qquad (A.9)$$

$$\beta(E)=\begin{cases}\exp(0.7013E-17.5325), & 6\text{ MeV} < E < 25\text{ MeV},\\ \exp(2.2672E^{1/2}-11.34321), & 25\text{ MeV} < E < 48\text{ MeV},\\ \beta(48\text{ MeV}), & 48\text{ MeV} < E,\end{cases} \qquad (A.10)$$

Since the binding energy of alpha particle is approximately 6 MeV, the relation between E and the excitation energy E^* of the fissioning compound nucleus is given as $E = E^* + 6$. Because there are insufficient experimental data and theoretical models to get general expressions of alpha and beta for a wide range of nuclides, we assume that Eqs.(A.9) and (A.10) would be applied to all

actinides.

Fitting parameters A_1, A_2 and A_3 in Eq.(A.8) are chosen as

$$A_1 = 2/5\ A_0, \quad A_2 = 1/2\ A_0\ , \quad A_3 = 3/5\ A_0. \qquad (A.11)$$

The width $\langle W_{1/2} \rangle$ is assumed to have the same expression [NF,63]:

$$\langle W_{1/2} \rangle = E^* - E_f + 7 \qquad (A.12)$$

as for the subactinides, which is used in the RAL (Athcison's) computational scheme in the sub-actinide region.

It is not obvious how to make a random sampling of A from the distribution given by Eq.(A.8). To avoid substantial and complicated computationa, a simplified, expedient procedure is employed in the JAERI model.

If $\alpha > \beta$, β is taken to be equal to 0. In this approximation, the asymmetric fission is overestimated and the symmetric one is underestimated. Hence, we generate a random number x from the folded normal distribution:

$$f(x) = \frac{1}{\sigma\sqrt{2\pi}} \left[\exp\left[-\frac{(x-\mu)^2}{2\sigma^2}\right] + \exp\left[-\frac{(x+\mu)^2}{2\sigma^2}\right]\right] \qquad (A.13)$$

where $x > 0$,

$\mu = (A_1 - A_3) / 2$, $\sigma = b \langle W_{1/2} \rangle / 2^{1/2}$.

Then masses of two fission fragments are obtained as

$$A_1 = x + 1/2\ (A_1 + A_3), \quad A_2 = A_0 - A_1\ . \qquad (A.14)$$

If $\alpha < \beta$, α is taken to be equal to zero and the normal distribution:

$$f(x) = \frac{1}{\sigma\sqrt{2\pi}} \exp\left[-\frac{(x-\mu)^2}{2\sigma^2}\right], x>0 \qquad (A.15)$$

with $\mu = A_2$, $\sigma = b \langle W_{1/2} \rangle / 2^{1/2}$ is used to generate a random number and get

$$A_1 = x, \quad A_2 = A_0 - A_1 \qquad (A.16)$$

In this case, the asymmetric fission is an underestimate and the symmetric one is overestimated. It is expected optimistically that the cancellation of errors due the to over- and under-estimate will result in the reasonable value of number of neutrons produced. Once the masses of fragments have been determined, their charges can be obtained immediately by generating random number x from Eq. (A.15) with

$\mu = \bar{Z}$, $\sigma = \langle \Delta Z \rangle / \sqrt{2}$

where $\bar{Z}$ and $\langle \Delta Z \rangle$ can be calculated by the use of Eqs. (A.6) and (A.7).

$$z_1 = x, \quad Z_2 = Z_0 - Z_1 \qquad (A.17)$$

The total kinetic energy E_k of the fission fragments is determined by the Coulomb repulsion at the moment of splitting i.e.,

$$E_k = \frac{Z_1 Z_2 e^2}{r_1 + r_2} \qquad (A.18)$$

where r_1 and r_2 are nuclear radius fragments. Exactly speaking, E_k depends on the excitation energy and angular momentum of the fissioning nucleus.

In actual calculations it is convenient to use the experimental formula [VH,73]:

$$E_k=0.1071Z^2/A^{1/3}+22.2 \quad (MeV) \tag{A.19}$$

The recoil energies of fragments are determined by the relations:

$$E_{k_1}=\frac{A_2}{A_1+A_2}E_k, \qquad E_{k_2}=\frac{A_1}{A_1+A_2}E_k. \tag{A.20}$$

The total energy released at the moment of fission of a nucleus of the excitation energy E* is given by the relation:

$$E_T=M(A_0,Z_0)+E^*-M(A_1,Z_1)-M(A_2,Z_2) \tag{A.21}$$

where M(A, Z) is the Cameron's mass formula[Ca,57]. The total excitation energy of two fragments is obtained from the conservation of energy as follows,

$$E^{*\prime}= E_T- E_k \tag{A.22}$$

According to the statistical theory, the excitation energy of a nucleus is proportional to its mass.

Finally, the total excitation energy $E^{*\prime}$ can be distributed among fragments as

$$E_1^{*\prime}=\frac{A_1}{A_1+A_2}E^{*\prime}, \quad E_2^{*\prime}=\frac{A_2}{A_1+A_2}E^{*\prime} \tag{A.23}$$

B) BNL [Ta,84] and ORNL [Al,81] models

In the BNL and ORNL models, the Fong's statistical model [Fo,69] is adopted instead of the empirical formula used in the RAL and JAERI models. As discussed earlier, the fission process is considered to be so slow that an instantaneous equilibrium state will be established at every moment of the process. Thus, the relative probability of occurrence of a fission mode is determined from the instantaneous equilibrium at the moment just before the two fragments separate from each other. The probability is calculated from the density of quantum states of the different configuration of the nuclei at the moment just before scission.

According to the Fong's statistical theory, the probability of producing fission product fragments (A_1, Z_1) and (A_2 Z_2) are expressed by the function of the following quantities; C (the mutual Coulomb energy of a fission pair at the moment just before scission), k (the total translational energy of the same) , D (the total deformation of two fission fragments), and E (the total energy available to the compound system C minus k), with a given partition of excitation energy E_1,E_2 and with given angular momenta, j_1 and j_2 , for the two fragments, where it is assumed that j=0 and there is no orbital angular momentum. The probability is expressed as:

$$N(A_1,A_2,z_1,Z_2,C,D,k,E,e_1,j_1,j_2)=c_1c_2(2j_1+1)(2j_2+1)$$

$$\exp\left[-\frac{(j_1+\frac{1}{2})^2}{2g_1T_1}-\frac{(j_2+\frac{1}{2})^2}{2g_2T_2}\right]\cdot\frac{4\pi V}{k^3}\sqrt{2\mu^3k}\exp\left[2\sqrt{a_1E_1}+2\sqrt{a_2(E-E_1)}\right]dE_1\cdot dk \tag{B.1}$$

where c is the parameter which depends on A as:

$$c=0.38e^{-0.005A} \tag{B.2}$$

and $a_i = aA_i$, g, T, and μ are given as

$$g=\frac{2}{5}\frac{MR^2}{h^2}A^{5/3} \tag{B.3}$$

(M and R are the mass and radius of nucleus, respectively).

$$t=\sqrt{E/a} \tag{B.4}$$

$$\mu=\frac{m_1m_2}{m_1+m_2}=\frac{A_1A_2}{A_1+A_2} \tag{B.5}$$

and V is volume of space in which the translational energy of the pair (k) is normalized.

Incorporation of this most general distribution function of fission product into the calculation to the intra-nuclear cascade code is very time consuming. Therefore in the BNL model, a simplified distribution function of few variables is derived by carrying out the summation of j, and the integration of k in Eq.(B.1). The distribution function of partition masses A_1 nd A_2 with the most probable value for the other variables can be written as:

$$N(A_1,A_2)\sim c_1c_2\frac{(a_1a_2)^{1/2}}{(a_1+a_2)^{13/4}}\left(\frac{A_1^{5/3}A_2^{5/3}}{A_1^{5/3}+A_2^{5/3}}\right)^{3/2}\left(\frac{A_1A_2}{A_1+A_2}\right)^{3/2}$$

$$\frac{(Z_{p_1}Z_{p_2})^{1/2}}{(B_{A_1}+B_{A_2})^{1/2}}E^{11/4}\left(1-\frac{5}{2}\frac{1}{\sqrt{(a_1+a_2)E}}\right)e^{2\sqrt{(a_1+a_2)E}} \tag{B.6}$$

where E is to be calculated for the model of most probable charge division $Z_{p1}:Z_{p2}$ and most probable kinetic energy release and deformation energy for the given mass division A_1 , A_2.

In EQ. (B.6)

$$Z_{P_1}=\frac{B_{A_1}Z_{A_1}-B_{A_2}Z_{A_2}+Z(B_{A_2}-\frac{1}{2}C_{12})}{B_{A_1}+B_{A_2}-C_{12}} \tag{B.7}$$

$$Z_{P_2}=Z-Z_{P_1} \tag{B.8}$$

$$B_A=0.041505/Z_A \tag{B.9}$$

and

$$Z_A=A/(1.980670+0.0149624A^{2/3}) \qquad \text{(B.10)}$$

c_{12} in Eq. (B.6)and (B.7) is constant with respect to charge division as:

$$k=c_{12}z_1z_2 \qquad \text{(B.11)}$$

The excitation energy E is expressed by

$$E=M^*(A,Z)-M^c(A_1,Z_1)-M^c(A_2,Z_2)-K-D \qquad \text{(B.12)}$$

where $M(A_i, Z_i)$ is mass of nucleus (A_i and Z_i).
The total fission fragment kinetic energy K in Eq. (B.12) is expressed by:

$$K=c+k \qquad \text{(B.13)}$$

where c is Coulomb repulsion energy of fission fragment at the moment of scission point. The value of k turns out to be very small (about 0.5 MeV) compared with c, so that it can be neglected in the calculation. The Coulomb repulsion energy for fission fragments which have deformation parameters, of α_{31} and α_{32} is respectively expressed by;

$$c(\alpha_{31},\alpha_{32})=Z_1Z_2e^2[r_{01}(1+\alpha_{31}(1-\frac{3}{7}\eta_1^2))+r_{02}(1+\alpha_{32}(1-\frac{3}{7}\eta_2^2))]^{-1} \qquad \text{(b.14)}$$

where

$$r_0=1.5X10^{-13}A^{1/3} \qquad \text{(B.15)}$$

$$629\eta_1=\eta_2=0.4 \qquad \text{(B.16)}$$

The total deformation energy of the fission fragments is :

$$D=D_1(\alpha_{31})+D_2(\alpha_{32}) \qquad \text{(B.17)}$$

where

$$D_i(\alpha_{3i})=0.7143\alpha_{3i}^2E_{si}^0-0.2041\alpha_{3i}^2E_{ci}^0 \qquad \text{(B.18)}$$

$$E_s^0=0.014A^{2/3}(AMU) \qquad \text{(B.19)}$$

and

$$E_c^0=0.000627Z^2/A^{1/3} \qquad (AMU) \qquad \text{(B.20)}$$

In this calculation, the most probable combination of deformation parameters α_{31} and α_{32}, is determined by minimizing the value of $D_1(\alpha_{11})+D_2(\alpha_{32})$ and the their values are calculated by minimizing the value of $C(\alpha_{31},\alpha_{32})+D_1(\alpha_{31})+D_2(\alpha_{32})$. After determining the partition of mass number A_1 and A_2 , according to

Eq.(B.6), the partition of charge number of Z_1 and Z_2 is calculated by using the distribution function of:

$$N(Z_1, Z_2) \sim (Z_1, Z_2)^{1/2}\left(1-\frac{5}{4}\frac{1}{\sqrt{(a_1+a_2)E}}\right)E^{5/2}e^{2\sqrt{(a_1+a_2)E}} \qquad \text{(B.21)}$$

The distribution functions for the total fission fragment kinetic energy K and deformation energy D are not taken into account; these are represented by their most probable ones. The total excitation energy is partitioned into the two fission fragments with the assumption of equal nuclear temperature:

$$E_1 : E_2 = (a_1 T^2) : (a_2 T^2) = a_1 : a_2 = A_1 : A_2 \qquad \text{(B.22)}$$

Thus, the excitation energy of fragments (A_1, Z_1) in the state far from scission point is expressed by:

$$E_1 = \frac{A_1}{A_1+A_2}E + D_1 \qquad \text{(B.23)}$$

The nucleus with excitation energy loses its energy by evaporating particles.

In the ORNL model [Al,81], the statistical functions at the scission and evaporation times are derived according to Fong's theory, but more reliance is placed on the empirically derived function than on the above models. Since the details of their formalism [Al,81] has been published, we do not repeat here[Al,81].

5.4 Photo-fission

In recent years, growing interest in investigations of electromagnetic interactions of heavy nuclei at intermediate energies is evident. Such a information provides information on the nature of nuclear force, mechanism of intranuclear cascade, etc. Wide program for nuclear photo-fission and photo-fragmentation studies using back-scattered laser photons is carrying out.

At present, photo-fission both of U-238 and Np-237 has been carried out by D.I.Ivanova et al.[II,89]. They desired to analyses their experimental results by detailed calculation including the double-humped structure of the fission barrier, in the cascade-evaporation model[Iv,89].

6. Codes for analyzing the accelerator incinerator

6.1 Accelerator Reactor code system

To analyze the accelerator breeder and high intensity neutron source facility code systems were developed combining the nuclear cascade code and the conventional neutron and photon transport code used for the nuclear reactor at BNL, JAERI and LANL.

A. BNL code system[Ta,80][NT,,82,89]

Fig.A.1 shows the code system developed at BNL for analyzing the accelerator breeder and accelerator tritium production. The BNL computer code system used in this analysis consists of six main programs: NMTC/BNLF, HIST3D ,EPR, (DLC-2) ,TAPEISN,TWOTRAN-II, and three auxiliary programs:FIND, SURF,MULTISUM. Figuure 8 shows overall interrelations of these programs.

The nuclear cascade part is calculated using the nucleon meson transport code (NMTC) with the BNL fission model; the neutron transport is treated either by two dimensional Sn code TWOTRAN II or three-dimensional Monte Carlo code MORSE-CG. The neutron source distribution to be used in the TWOTRAN calculations is prepared by HIST3D, which was designed to analyse the collision events file created by NMTC/BNLF. HIST3D also prepared a one-dimensional source distribution for use in the one-dimensional neutron transport Sn code ANISN [AN,67].

The basic neutron cross-section are ENDF/B -III data stored on the magnetic tape in DLC-2 format. They are 100 energy group data processed by SUPERTOG-III [WG,69]. The program DLC2 is used to process the data in the magnetic tape to compile a new file on the magnetic disk for specified nuclei. The data on the new file are processed again by TAPEMAKER to get the microscopic or macroscopic cross sections obtained by the mixing procedure in the FIDO format. The FIDO formatted cross sections of the 100 groups are collapsed by ANISN to prepare cross section sets of few groups, micro, or macroscopic, for use in TWOTRAN or MORSE-CG.

MORSE-CG is a version of Monte Carlo code MORSE with a combinatorial geometry package. Dicade ago it was very expensive to obtain sufficient numbers of samples for the Monte Carlo calculation. MORSE-CG code was used only when detailed three-dimensional geometry had to be taken into consideration to get the correct information.

For the output from TWOTRAN-II processing programs FIND and SURF were prepaired to provide graphic representations.

B. RAL code system[At,69]

The code system which was developed at RAL is shown in Fig.B.1, this is based around HETC code. This contains two major codes: HET which transport for RAL's particular case the incident protons and the produced neutrons, pions and muons. The second part is O5R which takes neutrons from 77 MeV to 0.14 m eV. The answer boxes are shown at the bottom of figure. The low energy neutron escapes are the ones which are passed onto the TIMOC code, a time based neutron transport code, which is used in the moderator calculation by A.Taylor. The energy deposition is very important because the target has to be cooled and in particular with uranium.

For O5R it needs a library of cross-sections. The cross-sections are put into a suitable form by the pre-processor code XSCEND; this is a new group averaging code written at RAL to allows to use the ENDF/B IV neutron cross-sections. A fair part of ENDF/B is held in resonant parameter form, which requires inclusion of an extra program RESEND. to unfold the resonances.

Operating O5R takes three tapes and three disc channels. Again the output is on history tape (or the analysis could alternatively be done in core). In the analysis it can pick up capture γ's to go the γ-transport code. Most important quantities in the RAL project is the first source of low energy neutrons useable for moderator calculations. Also it get a contribution to energy deposition and some more contributions to the nuclide distribution.

The γ-transport code will be MORSE which be implemented such as to fit in their overall program system.

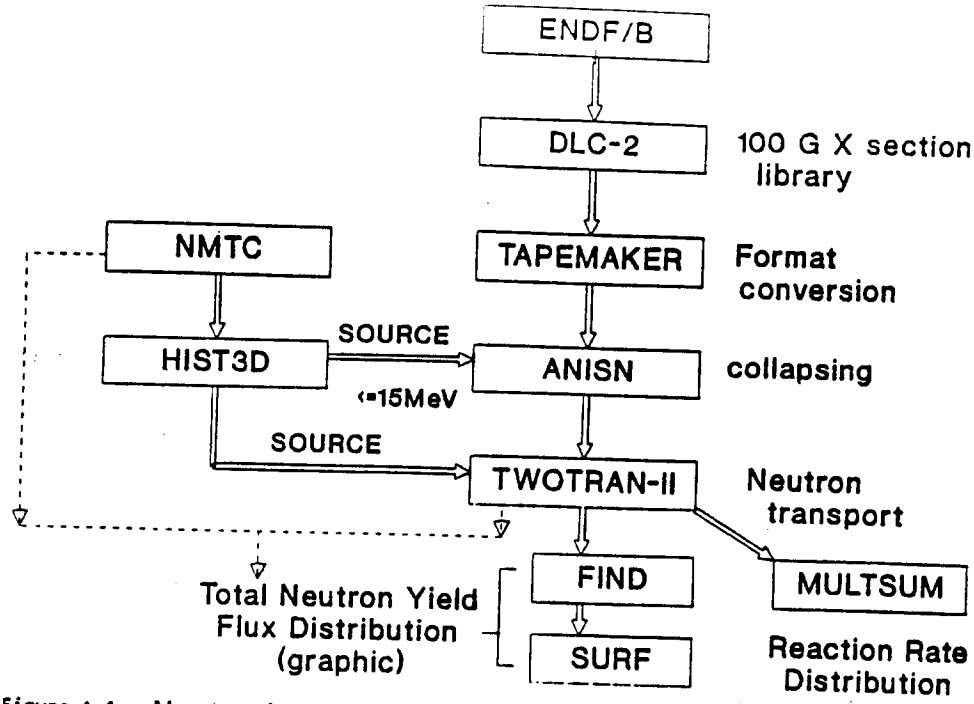

Figure A.1 Neutronics Part of BNL Code System for LAR's

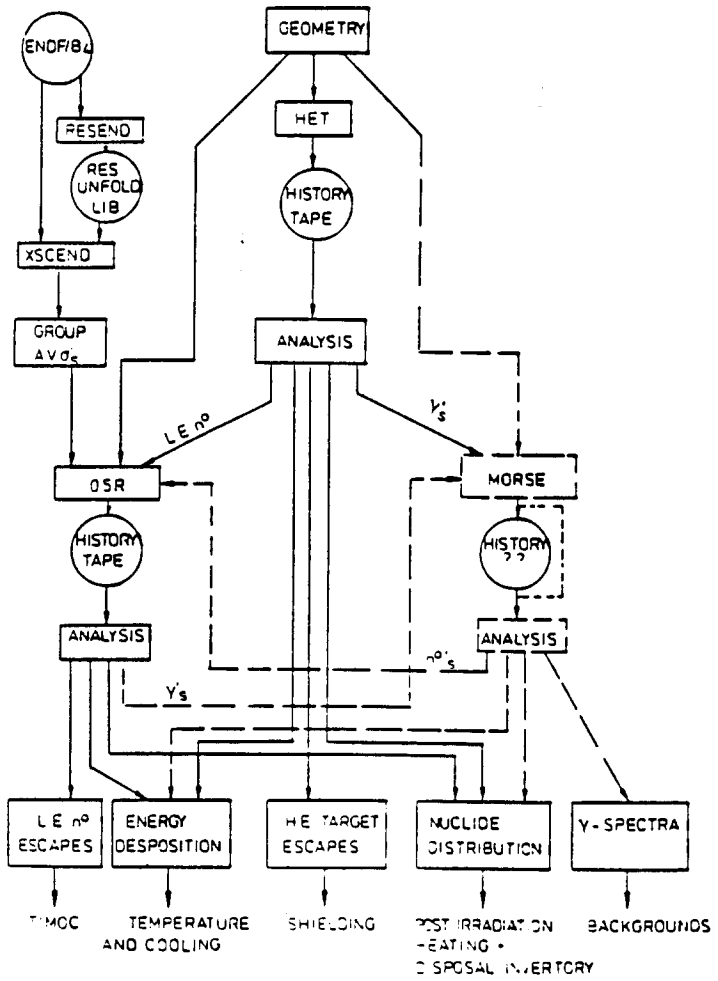

Figure B.1 Flow chart diagram of the neutronic calculations used for target calculations

C. JAERI code system [NT,89,82]

Figs. C.1 and C.2 show the Accelerator code system (ACCEL)[NTT,81] code system and its new version developed at JAERI. This system originally was developed from the BNL code system, so that there is lot of similarity between ACCEL and BNL systems. The nuclear cascade is calculated by NMTC/JAERI, which uses Nakahara's fission model [Na,80].

In the NMTC/JAERI,(see Table C.1) the calculation of the neutron transport uses the ENDF/B-4 nuclear data file library. The library is processed by SUPERTOG-JR and TAPEMAKER to create the GAM-type cross section of the 100 energy group. The ANISN code [EN,67] collapes the cross-section energy group from 100 to small number of groups to reduce the size of store memory required in the calculation.

The neutron sources used for 1D-transport ANISN and 2D-transport TWOTRAN calculation are, respectively, prepared by using HIST3D/A and HIST3D/B processing codes of the neutron files created by NMTC/JAERI. These processing procedures are similar to the original BNL code system. This system also uses the Sn transport code TWOTRAN and the Monte carlo code, MORSE-DD (JAERI version of MORSE-GC) to calculate a neutron transport below the cut-off energy 15 MeV. When the MORSE code is used, the processing codes HISTO3D is not necessary. The neutrons created in the NMTC/JAERI are supplied directly as the neutron source for the Monte carlo calculation.

The fragmentation process, which produces nuclei, such as Na, of a the somewhat large mass are observed in the experiment. But the code does not handle this kind of fragmentation process because the physics behind it is not well established.

As discussed in a later section, when the BNL and JAERI code systems are applied [NT,79],[Ta,84]to analyzing the Vasilkov's experiment for neutron yield (rigorously for the production rate of Pu) [Va,78]. The agreement between experiments and calculations is very much improved by taking into account the high-energy fission reaction.

The original NMTC code does not take into account nuclei with mass between 2 and 7. This omission is due to a lack of accuracy in the model describing the nuclear reaction. However, both, the NMTC/BNLF and NMTC/JAERI have relaxed this restriction to a mass range between 2-5 so that Li-6 and Li-7 can be handled in these codes. NMTC/JAERI code, calculates a medium which contains a large number of light elements, the energy conservation law might not be satisfied; then, the calculation is stopped by printing the error message. In the case of a calculation involving a medium containing a small amount of light elements such as Li, the calculation proceeds without stopping but warning is printed. Also, in the NMTC/JAERI code, deuteron is treated as two protons system ,because the binding energy of the deuteron is only 2.2 Mev .

The pre-equilibrium state is included the ACCEL code systems. It is known that neutrons emitted from the pre-equilibrium state have spectra harder than these evaporated from the compound state. The exciton model has the advantage in its generality of formulation, which is very useful in incorporating it into the systematic simulation flow. As discussed in the previous section, the problem in incorporating the pre-equilibrium decay process into the spallation reaction lies in the difficulty in defining the definite stages of transitions from the intra-nuclear cascade to the pre-equilibrium decay, and from the pre-equilibrium to compound decay. The JAERI system adopted the cascade-exciton model of Gudima et al.[Go,75],[GM,83], where the initial exciton state is chosen parametrically. Also, this system uses the exciton model proposed by Griffin [Gr,66].

This is a simple statistical model which neglects nuclear angular momenta and shell structures. Neglect of angular momenta is not a crude approximation when the incident particle is a proton and neglect of the shell structure has little effect on the particle emission process because the excitation energy of the residual nucleus at the end of the intra-nuclear cascades is sufficiently large i.e.,of the order of 100 MeV, for there to be sufficiently energetic incident protons with energy of the order of 1GeV. The Griffin's model was programmed by Kalbach [Ka,81,85] to calculate pre-equilibrium and direct reaction double-differential cross-sections.

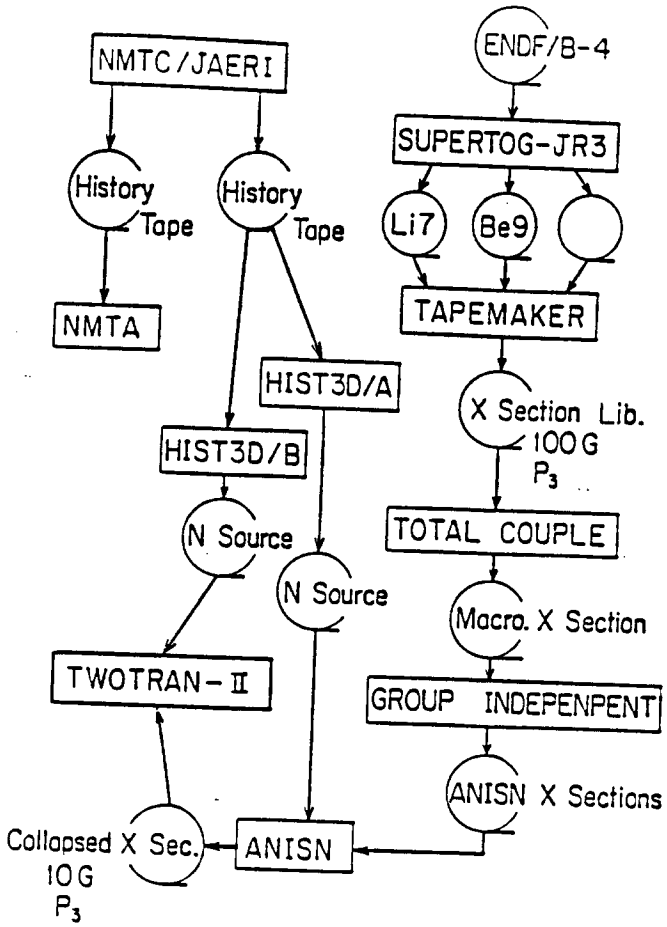

Figure C.1 Flow of neutronics calculations

The base of NMTC/JAERI is the NMTC version revised at LASL and BNL.

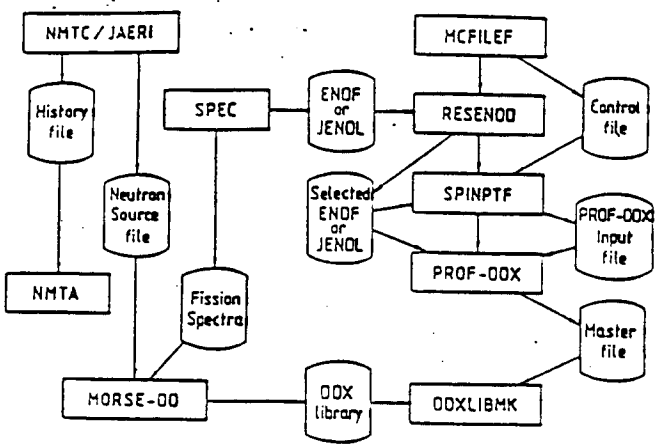

Figure C.2 Code system developed for spallation & transport calculation

Table C.1 Computer codes for the nucleon transport calculations in the nucleon energy range above the cascade cut-off and process codes of history tapes

NMTC/JAERI	performs the intra- and inter-nuclear cascades, evaporation and fission calculations by Monte Carlo method and produces history tapes.
HIST3D/A [A1]	edits a history tape prepared by NMTC to make a source neutron distribution for the ANISN calculation.
HIST3D/B [A1]	edits a history tape prepared by NMTC to make a source neutron distribution for the TWOTRAN-II calculation.
NMTA [A2]	analyzes a history tape prepared by NMTC to compute (a) flux and current from boundary crossing, (b) flux and spectrum from collision density, (c) residual nuclei distribution, etc.

A1) H. Takahashi, J. Beerman, D. Hillman and Y. Nakahara; unpublished.

A2) T.W. Armstrong and K.C. Chandler; "Analysis Subroutines for the Nucleon-Meson Transport Code NMTC", ORNL-4736 (1971).

Table C.1 b Computer codes for the neutron transport calculations in the nucleon energy range below the cascade cut-off

SUPERTOG-JR3[A3]	generates the cross sections for the neutron transport calculation, the energy deposition factor and the atomic displacement factor.
TAPEMAKER[A3]	collect group cross sections for each element or material generated by SUPERTOG-JR3.
TOTAL COUPLE[A3]	makes a coupled neutron and gamma-ray multigroup cross sections and regions-wise macroscopic cross sections.
GROUP INDEPENDENT[A3]	selects the cross section tables for required materials and produce a group independent cross section tape in order to obtain forward or adjoint solutions by ANISN effectively.
ANISN[A4]	solves the one-dimensional neutron and gamma-ray transport problem by the S_n method and produces the collapsed effective cross sections for heterogeneous zones.
TWOTRAN-II[A5]	solves the two-dimensional neutron transport problem by the S_n method.

A3) K. Koyama et al.; "RADHEAT-V3, a Code System for Generating Coupled Neutron and Gamma-ray Group Constants and Analyzing Radiation Transport", JAERI-M 7155 (1977)

A4) W.W. Engle, Jr.; "ANISN, a One Dimensional Discrete Ordinate Transport Code", RSIC ORNL, CCC-82.

A5) K.D. Lathrop and F.W. Brinkley; "TWOTRAN-II: An Interfaced, Exportable Version of the TWOTRAN Code for Two-Dimensional Transport", LA-4848-MS (1973).

The program system developed at JAERI for accelerator incinerator are listed in TABLE C.1. Complementary descriptions are given below.

(1) NMTC/JAERI

The origin of NMTC/JAERI is a 1978 version of NMTC, which was developed at ORNL and later revised at LANL and BNL. The fission process is treated by using Nakahara's fission model, and the range of mass number of target nuclides has been extended from [A=1-8,A < 239] to [A=1 ~ 6,A < 250].

(2) NMTA/JAERI

This is a JAERI version of NMTA; new subroutines have been added for calculating the total heat deposition and the spatial distribution of the heat deposition density in a target. This version also calculate the mean excitation energy in all recoiling residual nuclei. Gamma heating is not calculated.

(3) NUCLEUS

This program was developed by modifying and combining the Monte Carlo program NMTC/JAERI and NMTA/ JAERI. Several plotting routines have been provided to rapidly process a huge amount of output data.

(4) ACCEL

This code system is composed of the codes NMTC/JAERI and NMTA/JAERI described above. With it are associated the following three subroutines:

(i) The subroutine which edits the stored neutron files as the input source data for the Sn transport calculation by ANISN and TWOTRAN-II.

(ii) The subroutine that calculates the neutron transport in the energy range below 15 MeV using the ANISN and TWOTRAN and also by 3-dimensional Monte Carlo MORSE-DD.

(iii) The subroutine that prepares the neutron and gamma-ray group cross-section set by a code system RADHEAT-V3 developed by K.Koyama et al at JAERI.

(5) DCHAIN-SF

This system is an extended version of a one- point depletion code DCHAIN2, which can treat only reactions induced by neutrons with low energy. This DCHAIN-SF code can treat build-up and decay process of nucleides with proton and cascade nucleons.

(6) SPD

SPD calculates the following quantities related to beta decay:

i) Q value,
ii) half-life,
iii) all the energy convertible to thermal energy,
iv) kinetic energy of electrons,
v) energy of the gamma-ray, following beta-decay,
vi) gamma-ray energy released by the annihilation of electron positron pair.
vii) kinetic energy of neutrons.

Beside these codes developed at JAERI, K.Ishibashi et al. have improved the program HETC. To extend the two-step model to a three-step model, they [NT,89] introduced the pre-equilibrium process into HETC.[RS,77]

D. The LANL code System (LAHET) [Pr,89]

Los Alamos National Laboratory has developed a code system based on the LANL version of the HETC Monte Carlo code[RS,77]. Many new features were added at LANL, therefore the code was renamed LAHET, the system of codes based on LAHET designed as the LAHET code System (LCS). Fig.D.1 shows the LAHET code system [Pr.89].

The geometric transport capability in LAHET is that of LANL's continuous energy neutron-photon Monte Carlo code MCNP. LAHET includes two models for fission induced by high-energy interactions: the ORNL model by Alsmiller and others, and the Rutherford Appleton Laboratory model by Atchinson; the fission-models are employed with the evaporation model of Dresner.

HETC uses the intranuclear cascade model of Bertini to describe the physics

Table(2a) Computer Programs developed and being developed at JAERI for simulating nuclear spallation and transmutation processes

Name	Prolem solved	Processes included	Data used

NUCLEUS (Ref.(2))	•spallation of a single nucleus, induced by a proton, neutron or pion.
	•mass of a target nucleus should be A=1, 6≤A≤250.
	•upper limit of the energy range = 3.5 GeV, but for pions = 2.5 GeV.
		•Intra-nuclear cascade,
		•evaporation,
		•high energy fission.
			•nuclear radius,
			•nucleon density distribution,
			Fermi energy,
			•nucleon-nucleon cross sections:
			for (π^-,p), (π^o,p), (π^+,p), (π^o,n),
			•elastic scattering cross sections,
			•charge exchange cross sections,
			•differential scattering cross sections,
			•absorption cross sections,
			•inelastic scattering cross sections for 1π production,
			for (n,p), (p,p)
			•elastic scattering cross sections,
			•differential scattering cross sections,
			•inelastic scattering cross sections for 1π and 2π productions.

NMTC/JAERI (published) (Ref.(3))	•high energy (≥ 20 MeV) nucleon transport in a heterageneous bulk medium.	•inter-nulear nucleon transport, •spallations of nuclei.	•same as those used in NUCLEUS, except for geometry related data.

TABLE C.2 b (continued)

Name	Prolem solved	Processes included	Data used
NMTA/JAERI (published)	•edit of the output data from NMTC/ JAERI: spallation product distribution, heat deposition density distribution.	•ionization loss of charged particles, •kinetic energy of recoil nuclei, •excitation energies of residual nuclei.	•output from NMTC/JAERI.
ACCEL (unpublished)	•nuclear design calculations of accelerator target-blanket systems for actinide transmutation and fissile breeding.	•nucleon transport ($\geq$15 MeV) and neutron transport ($\leq$15 MeV) processes	•same as those in NUCLEUS for high energy nucleons, •ENDF/B data in the energy range below 15 MeV
DCHAIN-SF (unpublished)	•time evolution analysis of spallation and fission products	•build-up and decay of spallation and fission products	•data of fission products, •data of spallation products, prepared with the use of NUCLEUS.
SPD (unpublished)	•calculation of half-lives of spallation product niclei, •β and γ decay energies.	•β^--decay, •β^+-decay, •γ -decay.	•mass formulas: Myers and Swiatechi, Wapstra and Cameron, Uno and Yamada.

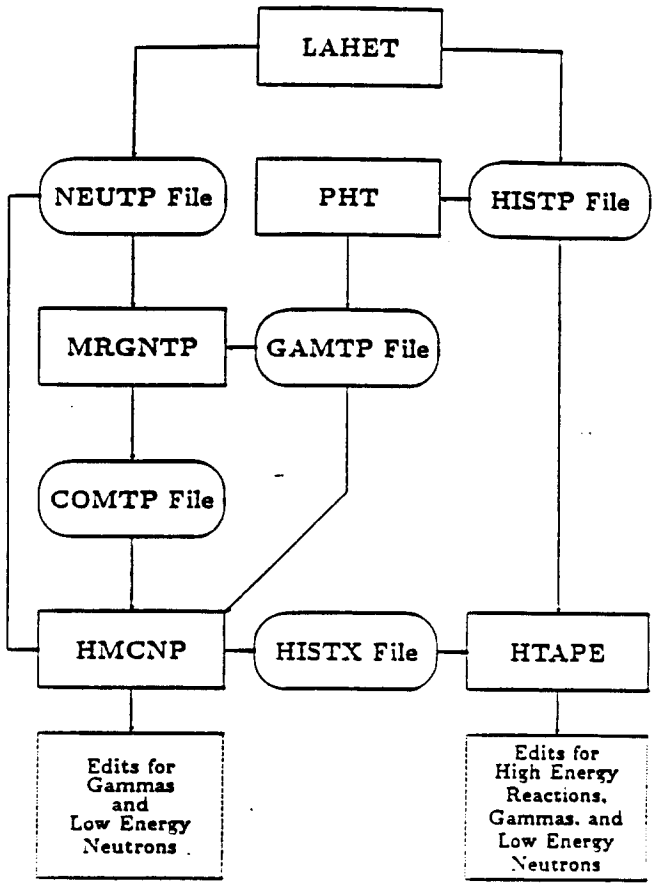

Figure D.1 Code Linkage and Data Flow for the LAHET Code System

of nuclear interaction. In LAHET, an alternative intranuclear cascade model was adopted from the ISABEL code which allows hydrogen and helium ions and antiprotons as projectiles. The ISABEL intranuclear cascade model itself is derived from the VEGAS intranuclear cascade code. For the breakup of light nuclei, the Fermi breakup model has replaced the evaporation model . As an intermediate stage between the intranuclear cascade and the evaporation phase of a nuclear interaction, a multistage pre-equilibrium excitation model was implemented. Alternative level density parameterizations have been added. A library of calculated neutron elastic scattering data has been provided.

The HETC code treats all interactions by protons, pions,and muon within HETC, but treats neutron interactions only above a cutoff energy, typically 20 MeV at LANL. Any neutron arising from a reaction with energy below the cutoff energy is recorded on a neutron file (NEUTP) for subsequent transport by a Monte Carlo code utilizing ENDF/B-based neutron cross-section libraries. For LAHET, a version MCNP (HMCNP) which was modified to accept NEUTP as an input source is used to complete the particle transport: recent developments allow the proton and deuteron records to be passed to HMCNP[BR,86] for transport with multi-group option of MCNP version 3B.

The results from the HMCNP phase of the computation may be obtained by using the standard MCNP tallies. The tallies of the initial LAHET run are obtained by subsequent processing of data record on the history file (HISTP) using the HTAPE code. The history file may contain a nearly complete description of the events occurring during the LAHET computation. The HMCNP allows a history file called HISTX to be written in a format similar to that of HISTP. The HISTX file may then proceed through the HTAPE code to obtain edits available only in HTAPE or in the same format as was obtained for the high-energy edits.

The HMCNP computation may be executed as a coupled neutron-photon problem; however, to obtain a photon source from a high energy interactions computed by HETC, it is necessary to execute the PHT code. PHT accepts HISTP as an input file and produces a gamma file(GAMTP) containing a photon source for HMCNP in the same format as NEUTP. At presnt, the gamma source arises from two processes.

* The decay of neutral pions produced in the intranuclear cascade, and
* The de-excitation of residual nuclei after all evaporation has ceased.

The two files of NEUTP and GAMTP can be merged with the code MRGNTP to make a source for HMCNP in a coupled neutron-photon problem which describes the transport of the entire neutron and gamma-ray source in the system. Alternatively, the two source files may be processed separately to analyze the effects of gamma arising from the high-energy interactions and from neutron-induced reactions (below 20 MeV). The relationships of the various codes in the LCS and the files that carry information from one to another are shown in Figure D.1.

LAHET may also be used to compute cross sections directly. With this option, transport is turned off and the primary particle is assumed to interact directly with the specific material at the incident energy. The history file produced then is processed with the XSEX code to generate double differential cross-sections of particle production.

HMCNP code

HMCNP is a modification to the MCNP code which accepts the NEUTP file from LAHET (for neutrons and perhaps protons and deuterons), the GAMTP file from PHT (for Photons), or a merged COMPT files as an input source. In addition, a TALLYX subroutine has been included which provides some tallying options which have proved to be of interest to LAHET users and which will, in addition, cause the writing of a surface crossing files which subsequently be edited by HTAPE. Versions of HMCNP are identified by the version of MCNP from which they are obtained (currently 3A and 3B).

PHT code

The PHT code is used to construct a gamma-ray file from the collision information recorded on LAHET history file for use as a source for HMCNP in a mode 1 or 2 problem. PHT may also be use to calculate gamma production cross sections from LAHET run.

The gamma ray output of PHT arises from two sources: from the decay of neutral pions and from the de-excitation of residual nuclei. For the decay of neutral pions, only two gamma decay mode is allowed. For the de-excitation of the residual nuclei, the assumption is made that all particle decay modes have been exhausted; thus gamma emission does not compete with particle emission.

XSEX code

XSEX is the code which analyzes a history files produced by LAHET and generates double-differential particles production cross-sections for primary beam interactions cross-section plots may also be generated.

6.2 Burn-up codes

The code system described above do not include the burn-up calculation of the target lattice. The burn-up of actinide can be calculated with the conventional burn up code used in the nuclear reactor if it takes into account the change in the neutron spectrum due to spallation neutrons [LH,69]. When the multiplication factor k of the target is small, then the fission reaction in the energy range above the cut off energy (15 Mev or 20 MeV) contributes to burn-up; thus, it is necessary to take the reaction of this high energy range into account. Our incinerator operates close to 1, so that the contribution of this high energy fission is small compared to fission under the cut-off energy. Thus, we can use the conventional burn up code used in the reactor calculation.

For the conceptual design study, a 0 dimension burn-up code origin2 is mostly used. A one dimensional burn-up code sizzle has been used to calculate the depreciation of fissile material in the accelerator LWR fuel regenerator together with the EPRI-CELL burn- up code. A two-dimensional burn-up code 2DB is also used for the calculation of accelerator breeder. The short description of these codes are given in the following.

A.ORIGIN-2[Be,73]

ORIGIN2 is a versatile point-depletion and radioactive-decay code for use in simulating nuclear fuel cycles and calculating the nuclide compositions and characteristics of material contained therein. It represents a revision and update of the original ORIGIN computer code, which was developed at the ORNL.

The decay, cross-section, fission products yields,and photon emission data bases had been extensively updated, and the list of reactor can simulated includes PWR, BWR, FFTF, CANDU, HTGR reactors. The code uses the matrix exponential method to solve a large system of coupled, linear, first-order ordinary differential equations with constant coefficients.

B.SIZZLE [SP,61]

The SIZZLE code is a reactor burn up code based upon the AIM-6 one dimensional neutron diffusion equation code. Its primary purpose is to make possible rapid and reasonably accurate reactor burn-up calculation for intermediate to fast reactor systems.

There is no provision in the SIZZLE code for a computation of the adjoint fluxes. The only criticality search permitted in a concentration search.

C.2DB [LH,69]

2DB is a two-dimensional (X-Y, R-Z, R-θ,triangular), multi-group diffusion code for use in fast reactor criticality and burn-up analysis.

* Compute K_{eff} and perform criticality search on buckling, time absorption (α), reactor composition, and reactor dimensions by means of either a flux or an adjoint model,
* compute material burn-up using a flexible material shuffling scheme,
* compute flux distributions for an arbitrary extraneous source.

6.3 Monte carlo codes used often in the accelerator reactor calculation bellow cut-off energy (15 or 20 MeV).

A) MORSE code [SS,77]

The MORSE code is a muti-purpose neutron and gamma-ray Monte Carlo transport code. Through use of the multi-group cross-section, the neutron and gamma-ray,or neutron-gamma ray problems may be resolved in the forward or adjoint mode. Time dependences for shielding and criticality problem are provided. General three-dimensional geometry may be used as an albedo option available at any material surfaces.

Standard multi-group cross-sections such as those used in discrete ordinate code may be used as input; either ANISN or DTF-IV cross-section formats are acceptable. Anisotropic scattering is treated for each group-to-group transfer using a generalized Gaussian quadrature technique. The modular form of the code with a built-in analysis capability for all types of estimates make it possible to solve a complete neutron-gamma ray problem as one job, without the use of tapes.

The use of multi-group cross-sections in a Monte Carlo code reduces the effort required to produce cross-section libraries. Coupled neutron gamma-ray sets are available from the Radiation Shielding Information Center at Oak Ridge National Laboratory.

Cross-sections may be read in either the DTG-IV format or ANISN and DOT format. The ANISN-DOT type may be in either fixed or free form. The auxiliary information gives the number of groups, elements, and coefficients from the random walks models. The possible transport cases that can be treated include the neutron only, gamma ray only, coupled neutron-gamma-ray, gamma-ray from a coupled set, and fission, with all of the above options or either a forward or adjoint case and for isotropic or anisotropic scattering up to a P16 expansion of the angular distribution. The option of storing the Legendre coefficients for use in a next-event estimator is also provided.

B) MCNP Code[Br,86]

The MCNP code was developed at LANL and it is a general-purpose Monte Carlo code that can be used for neutron, photon, or coupled neutron/photon transport, including the capability to calculate eigenvalue for critical systems. The code treats an arbitrary three-dimensional configuration of materials in geometric cells bounded by first- and second-degree surfaces and some special fourth-degree surfaces (elliptical tori).

Pointwise cross-section data are used. For neutron,all reaction given in a particular cross-section evaluation (such as ENDFB-V) are accounted for.

The neutron energy regime ranges from 10^{-1} mev to 20 Mev, and the photon energy regime from 1 kev to 100 Mev. The capability to calculate k-eff eigenvalues for fissile system is a standard feature.

MCNP uses continuous-energy nuclear data libraries. The primary sources of nuclear data are evaluation from the Evaluated Nuclear Data File (FNDF) system, the Evaluated Nuclear Data Library (ENDL), and the Activation Library (ACTL) compilations from Livermore and evaluations from Applied Nuclear Science (T-2) Group at Los Alamos. Evaluated data are processed into a format appropriated for MCNP by codes such as NJOY [PSR,118]. The processed nuclear data libraries retain as much detail from the original evaluations as feasible.

6.4 Sn transport codes

A.ANISN-W [CCC,25]

This code was written by Westinghouse, and can be obtained from RSIC. This code is very familiar to the nuclear engineer, and is an old but very useful multi-group one-dimensional time-independent discrete-ordinates transport code for neutrons and photons less than 20 MeV. The outputs of this code are neutron and photon fluences, fission rate, dose rate, and activation through " activities" . This code is well proven, widely implemented, and runs fast.

B.Dot4 [RC,82]

This code is also well known to the nuclear engineer, and was written by ORNL: it can be obtained from RSIC. The code calculates multi-group two-dimensional time-independent discrete- ordinates transport for neutrons and photons less than 20 MeV. The output is neutron and fluences.

C. OneDant [CCC-428]

This code was written at LANL and can be obtained from RSIC. It calculates multi-group one dimensional time-independent discrete-ordinate transport problems for neutrons and photons less than 20 MeV. Output is the neutron and photon fluences.

D. TWOTRAN [LB,73]

TWOTRAN-II solves the two-dimensional multi-group transport equation in (x,y), (r,θ) and (r,z) geometries. Both regular and adjoint, inhomogeneous and homogeneous (k_{eff} and eigen-value searches) problem subject to vacuum, reflective, periodic, white or input specified boundary flux conditions are solved. General anisotropic scattering is allowed and anisotropic inhomogeneous sources are permitted.

As method of solution the discrete ordinates approximation for the angular variable is used in finite difference form which is solved with central (diamond) difference approximation. Negative flux are eliminated by a local set-to-zero and correct alogarithm. Standard inner (within-group) and outer iterative cycles are accelerated by coarse-mesh rebalancing on a coarse mesh which may be independent of the material mesh.

E. TWODANT [CCC,456]

This code also was written at LANL and can be obtained from RSIC. It calculates multi-group two-dimensional time-independent discrete transport problem for neutrons and photons less than 20 MeV. The output is neutron and photon fluences.

F. TORT

Three-Dimensional Oak Ridge Transport Code (TORT) calculates the flux or fluence of particles throughout a two- or three-dimensional geometric system due to incident flux upon the system from an extraneous source or generated internally by interaction within the system. The principal application is to the deep-penetration transport of neutron and photons. Certain reactor eigenvalue problems can also be solved.

The Boltzmann transport equation is solved using the method of discrete ordinates to treat the directional variable, and finite-difference methods to treat partial variables. Energy dependence is treated using a multi-group formulation. Time dependence is not treated.

Anisotropic scattering is represented by a Legendre expansion of arbitrary order. TORT can run in either R0Z or XYZ geometry, as well as in several 2-D geometries. Cross-section input files are supplied in formats familiar to ANISN and DOT.

All discrete codes are geometries limited, but the calculation time is much faster than the Monte Carlo codes.

Many other codes have been developed for neutron and photon transport problems in the analytical and Monte Carlo method which are familiar to Nuclear Engineers, so they are not cited here.

6.5 Diffusion codes

A. 2DB [CCC,134]

(See Burn up code section)

B. 3DB [CCC,328]

3DB is designed explicitly for use in fast reactor analysis; available geometries include X-Y-Z, R=θ-Z,and triangular-Z. Eigenvalues are computed by standard source-iteration techniques. Group rebalancing and successive over-relaxation with line inversion are used to accelerate convergence. Adjoint solutions are obtained by inverting the input data and redefining the source terms.

6.6 Computer codes for electron cascade shower

We did not discuss the electron accelerator in this report. The following codes are useful for shielding calculatiion of electron accelerator.

A. EGS4

This code is written by W.R.Nelson, H. Hirayama ,and D.W.Rogers at SLAC and will calculate various parameters of the electron photon in the range of 10 TeV down to few ten keV by using the Monte Carlo methods. Output of this code include particle flux distributions, and energy deposition. The advantage of this program is the QED process that is very well understand and there are lot of numerical examples.

B. ITS (Integrated Tiger Series)

This code was written by J. a, Halbleib and T.A. Melhorn; it is kept at RSIC or Sandia National Laboratories. This code calculates time-independent coupled electron/photon radiation transport from 1 GeV down to 1 KeV with or without theinclusion of macroscopic electric or magnetic fields that is calculated by the Monte Carlo method. Slab, spherical, cylindrical, or combinatorial geometries can be handled.

The output of this code is the fluence of electrons and photons, their energy and charge deposition. The main advantage of this code is that it is user friendly but rigorous, and can run on Cray, IBM, Vax, and CDC.

7. Analysis of the experimental data (code verification and its limitation)

To verify the validity of the theoretical model and code system developed for the accelerator breeder and the high intensity neutron source, the comparison between the experimental results and calculated results is described in this section. There are few integral experiments using non-fissile and fissile materials. To evaluate the accelerator breeder concept, Fraser's group made measurements in collaboration with ORNL. Similar experiments were repeated at LANL's and Fraser's group [Fa,75],[Fa,80], Vasilkov's group [Va,78] mesured the production rate of Pu using large, block-size uranium.

7.1 Microscopic Analysis

A. Alsmiller's Analysis of the fission reaction [Al,81].

Before discussing these experiments, we first discuss the comparison between the experimental results for neutron yield from the proton U-238 nucleus collision and the theoretical results performed by Alsmiller et al using the ORNL fission model.

In Fig.A.1 the calculated non-elastic cross-section and the calculated fission cross section of the proton on U-238 are shown as function of incident proton energy. Also shown in Fig.A.1 is the large varietion the experimental measurments of the fission cross- sections for proton of various energies on U-238. The values of fission cross section values shown in the figure were calculated with B_0 = 10 MeV, but these results are not as sensitive to the values used. However, the fission cross section are sensitive at the higher energies (> 500 MeV). Because of the spread of the experimental data, it is difficult to judge whether the calculated results agree with the experimental data; however, in the 100-MeV to 1 Gev energy range, the calculated and experimental results are in approximate agreement.

Below 100 MeV the calculated fission cross section increases slightly although a few experimental points do not show this increase. In Fig.A.2, the calculated number of emitted neutrons per non-elastic collision with kinetic energy < 12.5 MeV is shown as function of incident proton energy on U-238 with the experimental results. The calculated results are given for B_0 values of 8, 10, and 15MeV; these results include both cascade and evaporation neutrons with kinetic energies < 12.5 Mev. The points on the curves in FiG.A.2 indicate the actual calculated values. At the lower proton energies, the calculations are not sensitive to the value of B_0 used. but this is not the case at higher energies. Because of the spread of in the data , it is not possible to determine the best value of B_0, but B_0 = 10 MeV gives a reasonable representation of the data.

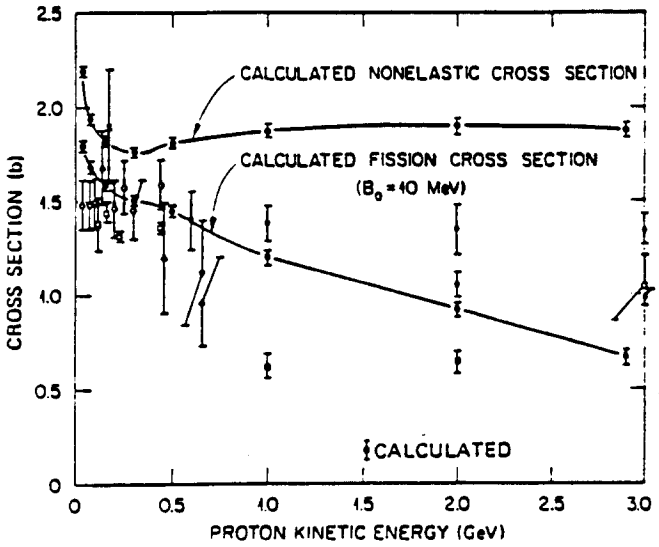

Figure A.1 Nonelastic and fission cross sections versus incident proton kinetic energy for protons on ^{238}U.

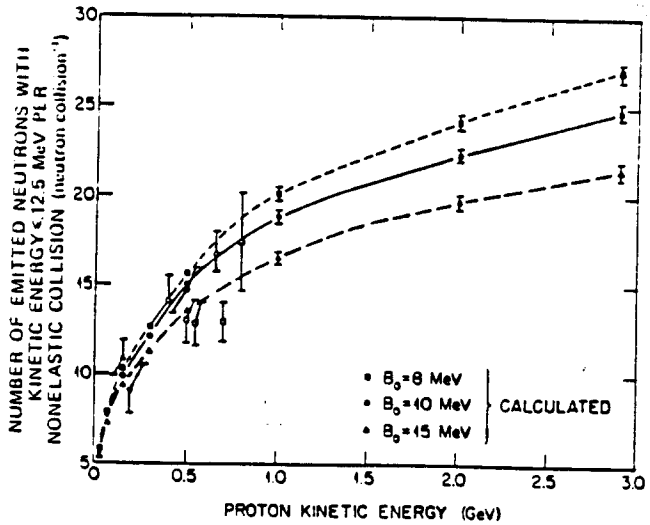

Figure A.2 . Number of emitted neutrons with kinetic energy ≤12.5 MeV per nonelastic collision versus incident proton kinetic energy for protons on ^{238}U.

In Fig.A.3, the total number of emitted neutron per non-elastic collision is shown as a function of incident proton kinetic energy on U-238. Also shown are the results calculated by Batashhenkov and Shnakov and those calculated by Hahn and Bertini. Barashenkov and Shmakov used B_0 = 10 MeV and therefore their calculations should be directly comparable with the results calculated here for B_0 = 10 MeV. The fact that the two sets are significantly different, particularly at higher energies, indicates the kind of differences that can arise because of differences in theory and in the physical data used.

B Armstrong and Flige's analysis [AF,81].

Similar calculations were carried out by T.W. Armstrong and D. Flige to examine the difference between the ORNL and RAL fission models using the modified HETC code which accommodated these fission models. They calculated the proton energies of 0.3, 1.0 & 2.9 GeV on the thin U-238 target; i. e. for a target thickness sufficiently small that the secondary particle created could escape from without undergoing further collision.

Fig.B.1 shows the fission cross-sections calculated by the RAL and ORNL models compared with experimental data. The fission cross section predicted by the RAL mode is about 15-20 % lower than for the ORNL model for beam energies below 1.0 GeV, and the energy dependence of the cross-section predicted above 1 GeV also differs. The spread of the experimental data is too large to judge the correctness of either model. Also shown in Fig.B.1 are the non-elastic cross sections from the two calculations, which are in agreement, as expected, since both use the same intranuclear cascade model.

Figs. B.2 and B.3 are comparisons of neutron multiplicity from evaporation only (taken to be < 12.5 MeV) and over all energies (evaporation plus intranuclear cascade), respectively. For the standard B_0 values used in the two models (B_0 = 14 for RAL, B_0 = 10 for ORNL), the RAL model predicts a lower neutron emission by about 20-25 %. These comparisons also show the sensitivity of neutron production to the values assumed for B_0. The variation in neutron production over the range of B_0 parameters suggested as reasonable from present experimental data are about the same as the model differences.

To further consider the influence of B_0, Armstrong and Flige have calculated the spectrum of low energy neutron production of for 1-GeV protons using the RAL model (Fig.B.4). The integral neutron production below 12.5 MeV is 20 % higher for B_0=8 than for B_0= 14. Also shown in Fig.B.4 is the neutron spectrum obtained when high-energy fissioning is neglected. With fission included. the neutron productions about 8% higher, and there is evidence of some" spectral hardening" for neutron energy which is important because it corresponds approximately to the energy threshold for neutron induced fission for U-238. Thus, the magnitude of spectral hardening on total neutron production in thick U-238 targets can be amplified by providing a larger source of neutrons that can cause multiplication via low-energy fissioning.

C. The neutron spectrum in the spallation reaction

The neutron spectrum in the spallation reaction using the rather thin block target produces small bump in the region of 20-80 Mev. In the NMTC calculation the reaction process is assumed to be a two-step process of spallation and evaporation. Several models have been proposed to explain this bumps. One is a pre-equilibrium model in which neutrons are emitted before reaching the equilibrium state. For this reaction several models are adopted and the results are compared with the experimental results. Some improvements are seen but this model cannot completely explain the bump in the neutron spectrum. Another model is the multiple temperature model whose parameters are obtained by analyzing the experimental data. However no data are available for actinide nuclei, so that this method cannot be applied, and further, there is no predictability in this model unless multi-temperatures can be explained from physical basis. The other model is a moving source model, which assumes that the excited nucleus created by the spallation reaction is moving and the some of the neutrons are emitted in a forward direction; however this explanation also has no predictability in theory.

First study of this problem was made by Nakahara and Tsukada [NT.] who took

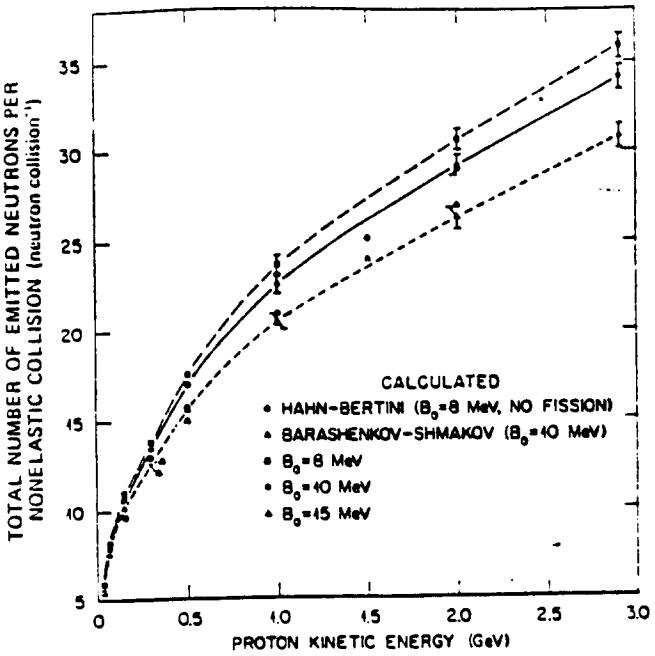

Figure A.3 Total number of emitted neutrons per nonelastic collision versus incident proton energy for protons on ^{238}U.

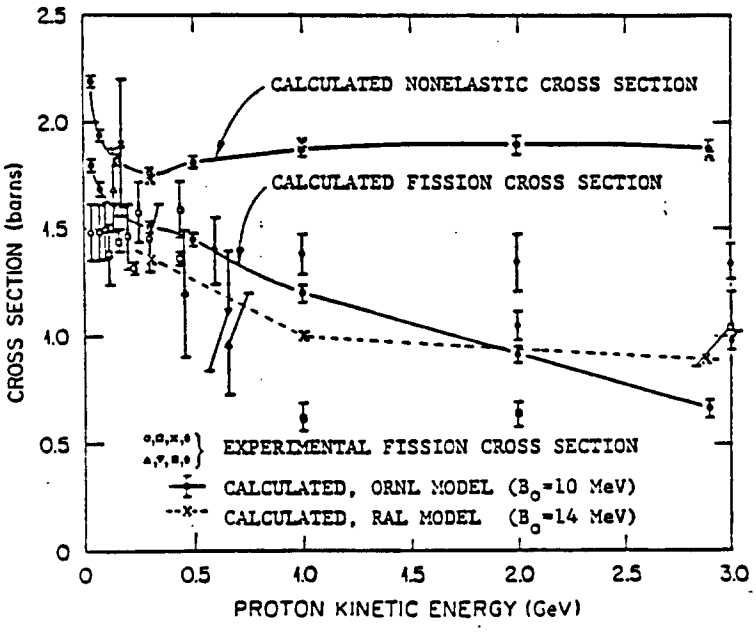

Figure 8.1 Comparison of calculated cross sections using the RAL and ORNL fission models for the case of protons incident on thin U-238 target.

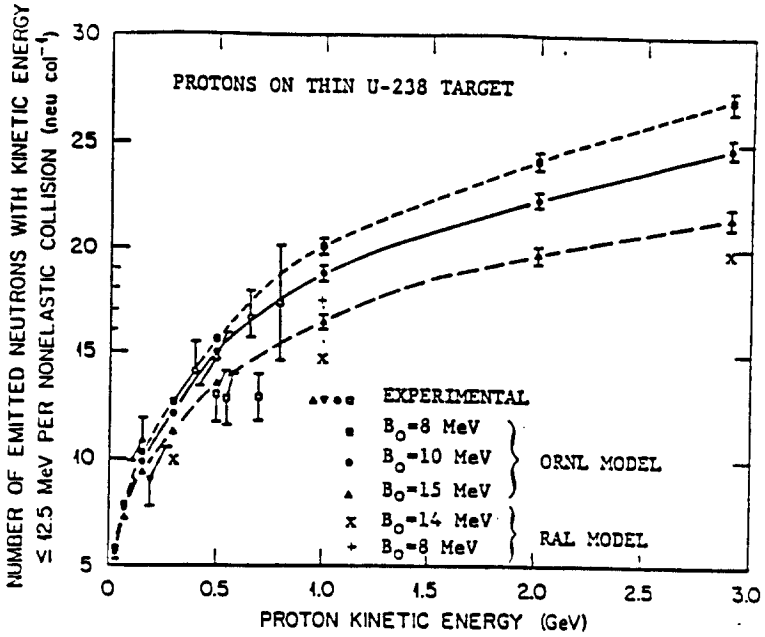

Figure 8.2 Comparison of RAL and ORNL fission model predictions for neutron production below 12.5 MeV.

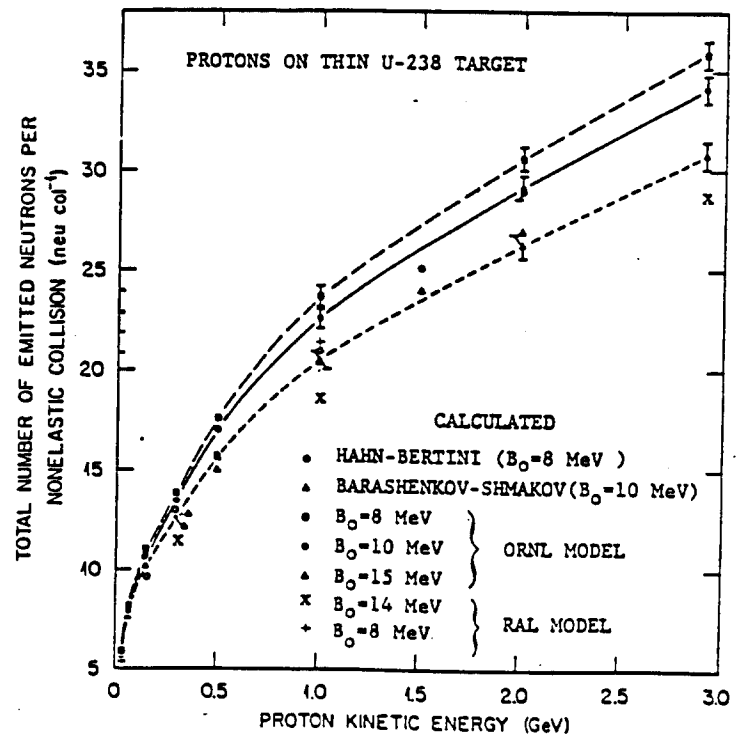

Figure 8.3 Comparison of total (evaporation plus cascade) neutron production predicted using RAL and ORNL high-energy fission models. Also shown are the results of Barashenkov and Shmakov using the Dubna fission model . The calcualtions of Hahn and Bertini were made neglecting fission .

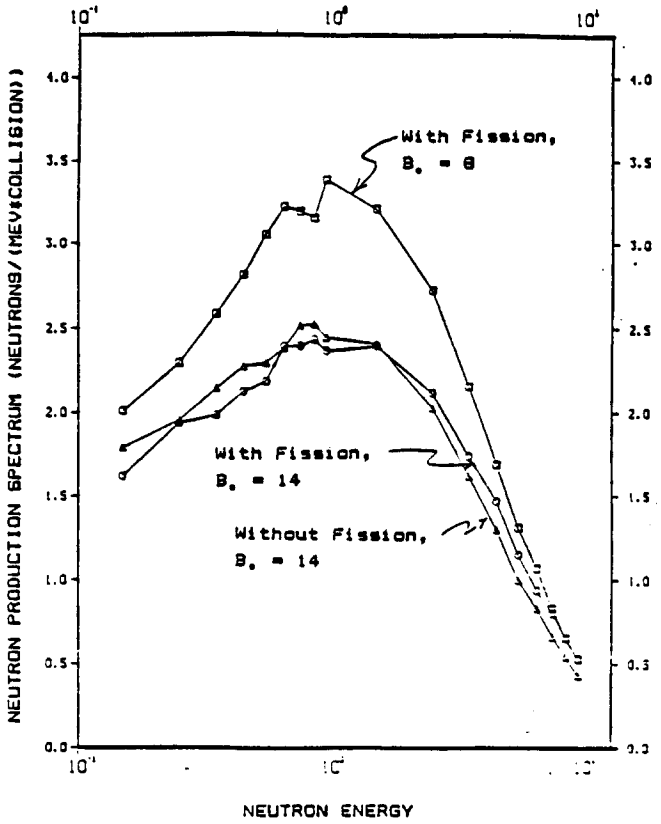

Figure 8.4 Low-energy neutron production spectrum calculated using RAL fission model, 1-GeV proton beam on thin U-238 target.

into account the large mean free path of the nucleon inside nucleus in the high energy spallation process.

Prael [PB,88] analyzed the LANL experimental data for 113 Mev and 256 MeV proton on stopping-length targets and thick target using the MCM model described the above. The neutron yield was measured for beryllium, carbon,aluminum, iron, and depleted uranium at angles of 7.5, 30, 60, and 150. He examined the several options of combining the Bertini's [Be,69] and ISABEL INC (Vegas) [CFF,68] and with MPM and without MPM, the Fermi-break up model. He concluded that the motivation for introducing the MPM has been to improve agreement with experiment at back angle, where the calculation without MPM have serious under-predicted the emission in the some combination of INC and with MPM or without MPM is conclusion spectrum. The study indicated shows that the MPM generally removes this defect.

With use of the Bertini INC and the normal MPM, the 150 MeV comparisons at 113 MeV for Fe and U are excellent; The comparisons for AL and C show a slight under prediction. But the generally there is no clear advantage of one intranuclear cascade model over the other than cost the ISABEL INC requires considerably greater computing time. Figs. C.1 - C.2 show examples of their comparison.

D. Spallation products

The spallation products including the fission products and evaporation products have been extensively studied by Nishida and Nakahara [NN,86] ,who showed that the mass formula which is not covered by presently known isotope is not enough; they used a newly evaluated mass formula by Yamada et al [UY,81] for their study. This kind of work is important in evaluating the radiation level and radiation hazard to maintain the accelerator operational. Fig.D.1 shows the mass yield distribution of products with even Z from 92 to 82 for 1 GeV incident proton energy.

7.2 Integral Experiment

A. Chalk River TRIUMF Experiment (FERION Experiment)[Fr,80]

To obtain data for the high intensity neutron source, several experiments were performed using a small block of uranium surrounded by a water bath.

Fraser et al. at Chalk River made a series of measurements with several sizes of uranium blocks using the 480-MeV proton beam of the TRIUMF facility. The experimental geometry in this series of measurements is shown in Fig.A.1. The target was composed of closely packed cylindrical uranium rods. Each rod was 1.616 cm radius 30.48 cm long, 18.94 g/cm^3 density, with a U235 content of 0.22 wt% . The target rod assembly is surrounded by a water moderator, shown in Fig.A.2. The incident proton energy is approximately uniform over a 1-cm radius circular area. The number of thermal neutron captures in the surrounding water was measured.

The results analysed using the NMTC/BNLF for this assembly are shown in the Table A.1. To examine the effects of the level density parameter B_0, two parameters were studied, of B_0= 8 and 10 MeV. The results indicate that the calculation with B_0 = 8MeV gives reasonable agreement with the experimental finding, except for the case of a single rod. Since this calculation is performed with a rather small number samples for the Monte Carlo calculation, the statistical error is somewhat large. The results using the B_0 = 10 Mev are about 15% smaller that the experimental value, and are close to Alsmiller's calculation [Al,81a] in which the level density parameter B_0 also has the same value of 10 MeV. Garvy's calculation , in which the high energy fission process is neglected, shows a smaller number of the captured neutron than either BNL's or Alsmiller's calculations.

In the case of the single rod target the experimental value is smaller than the calculated value. The reason for this small experimental value might be because the small-angle multiple scattering for the incident proton was neglected in the calculation. The small-angle scattering makes the angular diffusion of the incident proton leak out from a side surface, and does not contribute to the neutron yield. When several rods are closely packed, the protons leaking out from

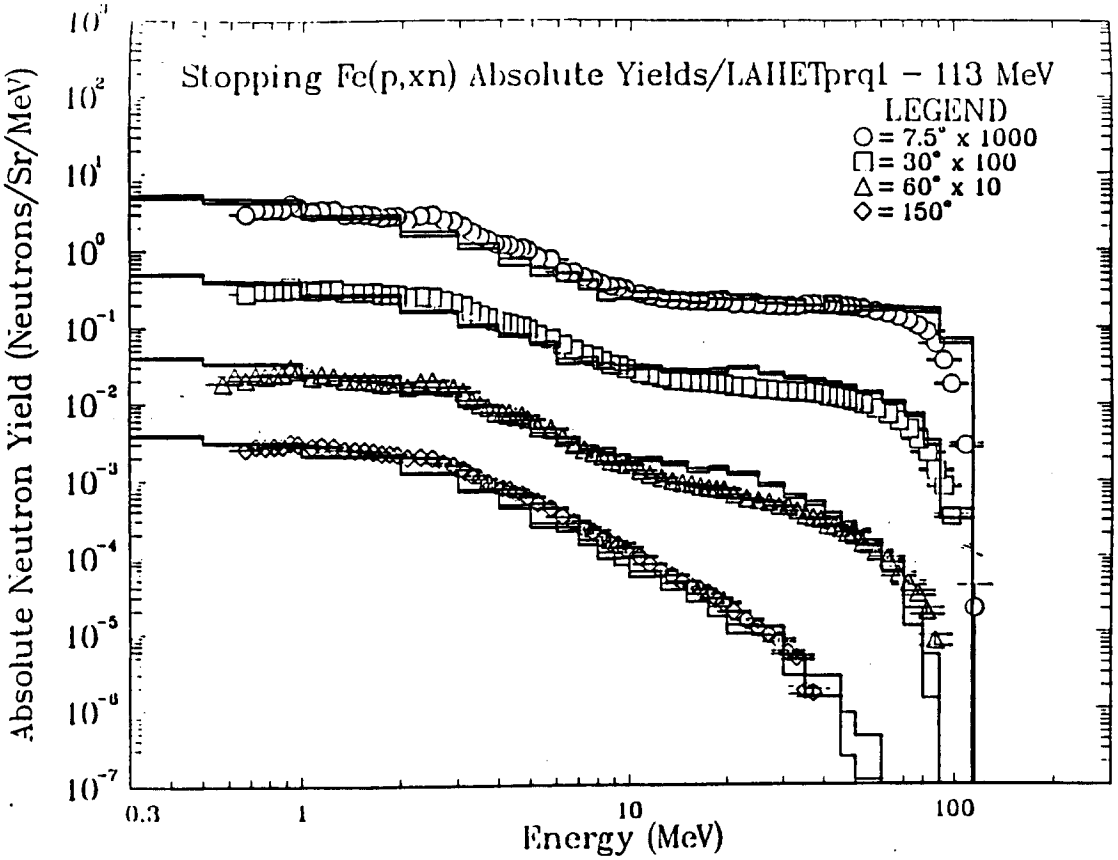

Figure C.1

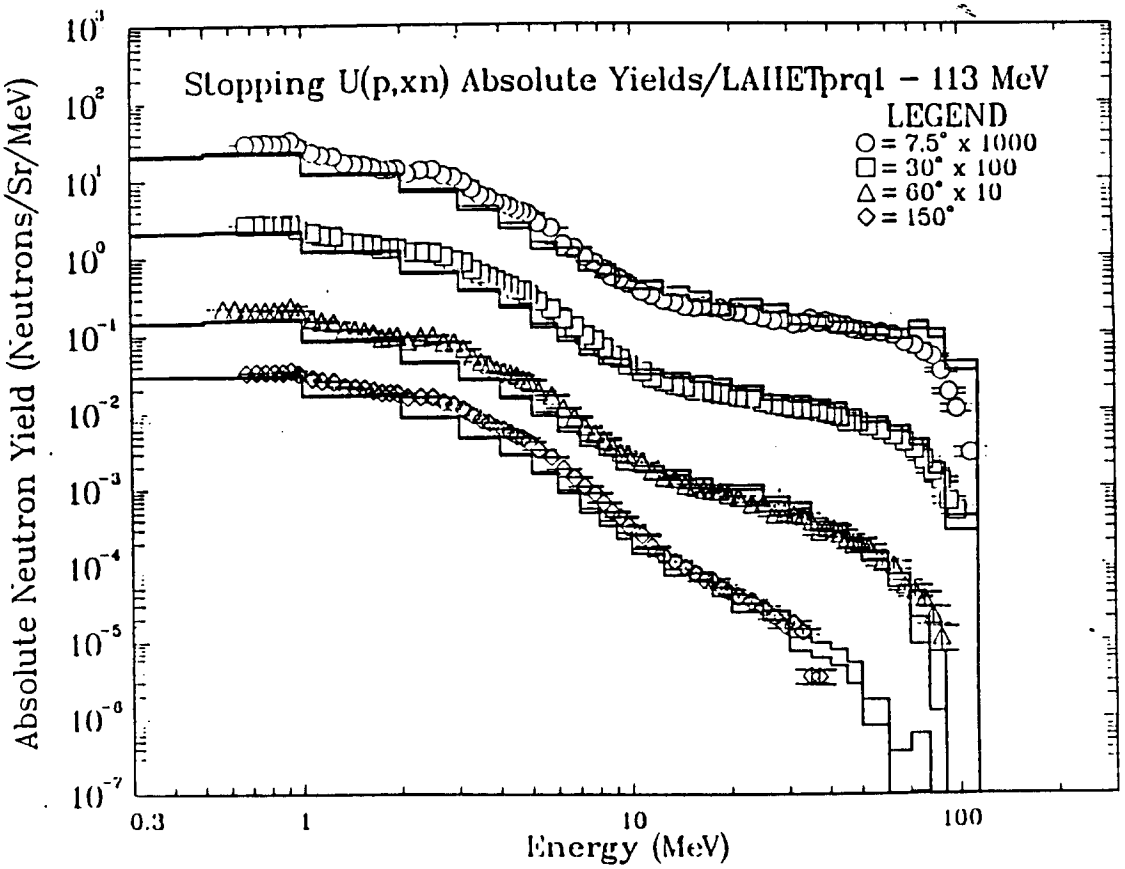

Figure C.2

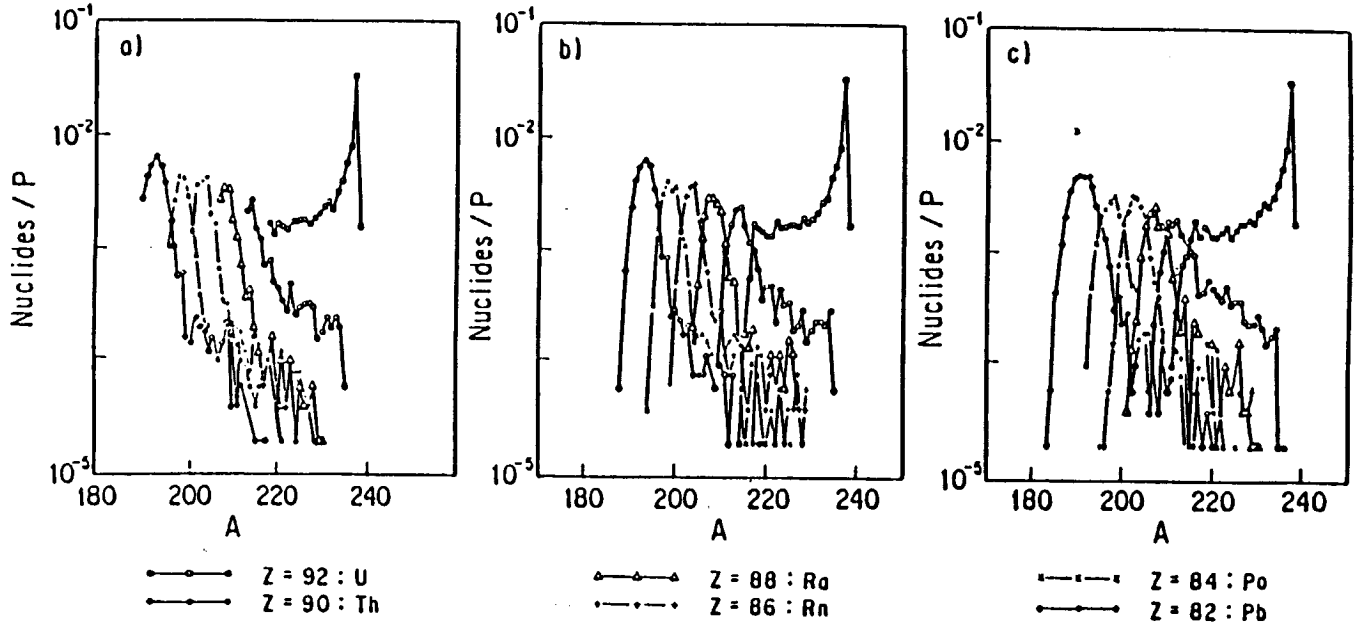

Figure D.1 *Mass yield distribution of products with even Z from 92 to 82 for 1 GeV incident proton energy. a) old mass formula and region; b) old mass formula and extended region; c) new mass formula and extended region*

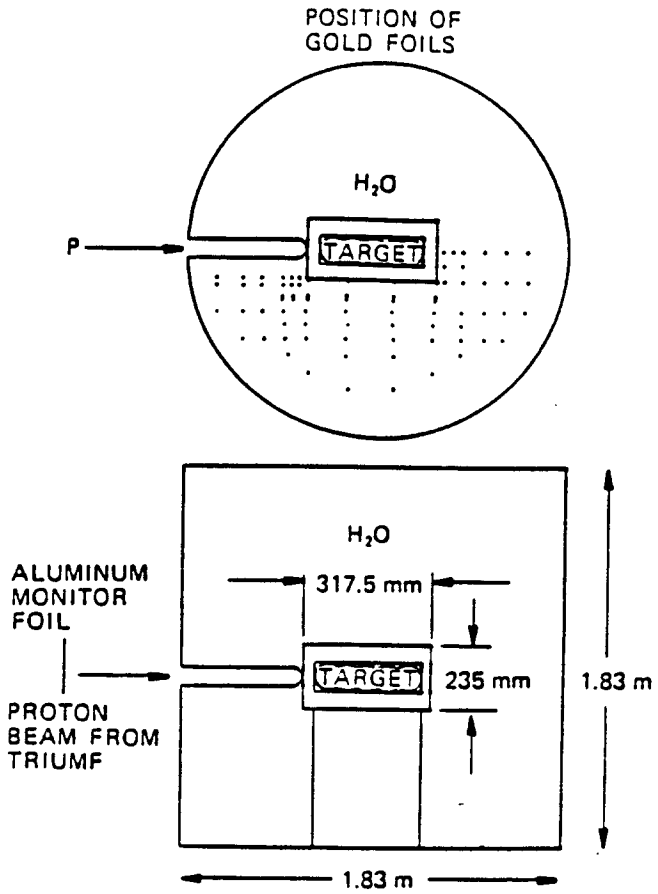

Figure A.2 Water tank and target assembly for FERICON experiments.

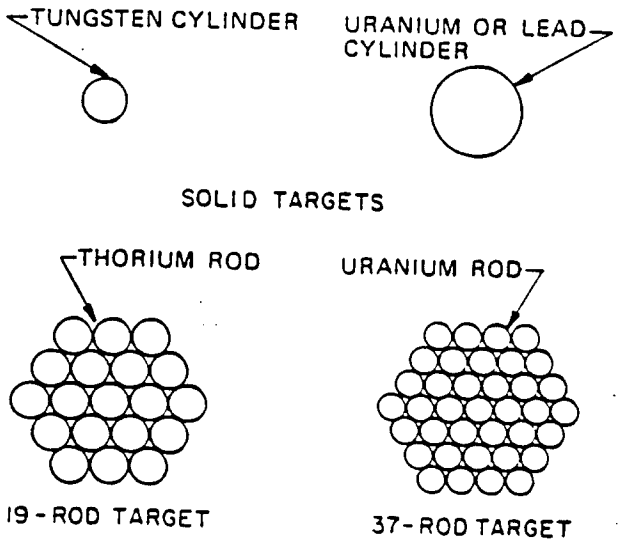

Figure A.1 Target used in the LANL FERICON experiments.

Table A.1

Thermal Neutron Capture in H_2O for 480-MeV Proton Incident on Uranium Targets

(Experiment of Fraser et al. using TRIUMF facility)

Uranium Target	Thermal Neutron Capture in H_2O per Incident Proton				
Number of Rods	Experiment	BNL Calculation		Alsmiller et al. Calculation	Garvey Calculation
		$B_0 = 8$ MeV	$B_0 = 10$ MeV		
U-1	9.6 ± 0.7	11.97 ± 1.0	11.08 ± 1.25	11.8 ± 0.4	10.1 ± 0.4
U-7	14.1 ± 0.9	13.95 ± 0.9	11.96 ± 1.06	---	10.9 ± 0.4
U-19	15.2 ± 1.0	14.10 ± 1.4	---	---	12.4 ± 0.4
U-37	17.1 ± 1.0	16.93 ± 1.0	14.75 ± 1.57	14.1 ± 0.6	12.3 ± 0.4

Note: Uranium = 0.22 wt% ^{235}U
Rod density = 18.94 g/cm^3
Rod length. = 30.48 cm
Radius = 1.616 cm.

Table A.2

Fission and Capture Reactions in Rod Regions for 480-MeV Protons Incident on Uranium Target

Number of Rods	Fissions >15 MeV		Fissions <15 MeV		Neutron Captures by ^{238}U	
	BNL[a]	Alsmiller et al.	BNL	Alsmiller et al.	BNL	Alsmiller et al.
U-1	0.74 (0.684)	0.72	0.55 (0.50)	0.54	0.36 (0.34)	0.35 ± 0.01
U-7	0.92 (0.798)	---	1.51 (1.30)	---	1.8 (1.53)	---
U-19	1.08	---	3.12	---	4.83	---
U-37	1.21 (1.01)	1.09	5.18 (5.12)	3.21	5.87 (5.10)	5.76 ± 0.19

[a]The values of the BNL calculation without and with parentheses are calculated with $B_0 = 8$ and 10 MeV, respectively.

Table A.3

Thermal Neutron Capture in H_2O for 800-MeV Protons Incident on Uranium Target

(Russel et al. experiment using LAMPF facility)

Experiment	BNL Calculation		Alsmiller et al. Calculation
	$B_0 = 8$ MeV	$B_0 = 10$ MeV	
25.3	29.75 ± 2.8	28.34 ± 2.7	27.2 ± 1.2

Table A.4

Fission and Capture Reactions in Rod Regions for 800-MeV Protons Incident on Uranium Target

Fissions Above 15 MeV		Fissions <15 MeV		Neutron Capture by ^{238}U	
BNL[a]	Alsmiller et al.	BNL	Alsmiller et al.	BNL	Alsmiller et al.
1.68 (1.66)	1.47	4.39 (4.5)	3.72	7.37 (7.24)	4.77 ± 0.22

[a]The values of the BNL calculation without and with parentheses are the ones calculated with $B_0 = 8$ and 10 MeV, respectively.

single rod enter the surrounding rods, thus making neutron production possible. Thus, the effects of the small-angle scattering of the injected proton is small in the case of the clustered rods.

In Table A.2, the calculated fission and captured reaction are shown together with the Alsmiller calculation. The values in parenthesis are calculated using B_0=10 MeV. They have a larger statistical error than the value for neutron capture by H_2O, because of the small number of samples.

In the Table A.3, the calculated thermal neutron capture in the surrounding water is shown with the experimental value and with the calculation of Alsmiller et al..

Both the calculated values with B_0= 8 and 10 MeV are larger than the experimental value. Although both are within the statistical error, the Value with B_0 =10 Mev is a little smaller than the one calculated with B_0 = 8 MeV and it is closer to Alsmiller's calculation.

Table A.4 shows the fission reaction and neutron capture in the uranium rod. Our calculated values are large compared with Alsmiller's calculation.

B. Chalk River ,ORNL Experiment[Fr,75]

In collaboration with Oak Ridge National Laboratory, Fraser's group performed similar experiments long before the second experiment described above. They used the 3 GeV cosmotron at BNL and made a series of experiments using different sizes and material of Be, Pb, and U. The data obtained in this small size target experiment are often refered to as the basic data for the accelerator conceptual design. The target geometry is qualitatively similar to that in Russel's experiment [Ru,81]discussed in the later section. The uranium target analyzed was a solid cylinder of 5.08 cm radius, 60.96cm in length with density of 18.94 g/cm^3; the enrichment of the U235 was o.22 wt%. The incidents proton beam energies were 540, 720, 970, and 1470 MeV, The calculation assumed that the proton beam is uniform over a circular area with 1-cm radius.

In Table B.1, the calculated value of thermal neutron capture in the surrounding water are compared with Fraser's experimental values and Alsmiller's calculations. The values not in parenthesis are Fraser's original data; the values in parenthesis were obtained Alsmiller's paper, who got them by private communication with Garvey. For the 540 and 720 Mev incident proton energies, our calculations using B_0 = 8 MeV are closer to the original experimental values than that calculated with B_0 =10 MeV. For 960 MeV, the calculation with B_0 = 10 Mev gives reasonable agreement with the experiment, although the statistical errors of the calculation and the experimental are substantial. For the higher energy of 1470 MeV, both our calculation with B_0 = 8 and 10 Mev give higher values than the experimental values. By using the larger B_0 value as the incident proton increase, the number of the captured neutrons becomes closer to the experimental value. However, B_0 is related to a single particle energy level, and we could not find any physical reason for the increase in B_0 as incident proton energy increases.

All Alsmiller's calculated values are smaller than our calculated values and close to the experimental values supplied by Garvey, except in the case of 1470 MeV. Neglecting the high-energy fission of the nuclei ($Z \leq 90$) in the Alsmiller's calculation results in smaller neutron yield. Without the high energy fission nuclei ($Z \leq 90$) our calculation shows a reduction of 12% for neutron capture.

Table B.2 shows the reaction rate of fission and capture in the target rod, together with the values calculated by Alsmiller's group.

C. LANL experiment[Ru,81]

Other experiments similar to the Fraser's original experiment were performed by LANL's group for cluster type fuel rod, are analyzed using the LAHET code system. The physical characteristics of the clustered 37 rod uranium and 19 rod thorium targets are given in Table C.1. In the case of Fig. C.1 is an illustration of the cluster target used in the conversion measurements, showing the location of the foils in an array and the foil positions within a rod.

Table B.1

Thermal Neutron Capture in H_2O for Protons Incident on Uranium Targets

Incident Proton Energy (MeV)	Neutron Capture			
	Experiment[a]	BNL Calculation		Alsmiller et al. Calculation
		$B_0 = 8$ MeV	$B_0 = 10$ MeV	
540	18.1 ± 0.9 (15.1 ± 0.8)	18.1 ± 2.2	16.71 ± 1.4	15.2 ± 0.8
720	29.1 ± 1.5 (23.2 ± 1.0)	---	26.40 ± 1.8	23.3 ± 0.8
960	40.5 ± 2.0 (32.3 ± 1.6)	---	39.72 ± 3.8	33.7 ± 1.0
1470	56.8 ± 2.8 (44.8 ± 2.2)	71.4 ± 4.8	67.71 ± 4.3 59.5 ± 1.3[b]	53.6 ± 1.5

[a]The Fraser et al. first experiment using the BNL cosmotron.
[b]This value is calculated by neglecting the high-energy fission for nuclei with atomic numbers ≤90.

Table B.2

Fission and Neutron Capture Reactions in Rod Region Protons Incident on Uranium Target

Incident Proton Energy (MeV)	Fissions Above 15 MeV		Fissions Less Than 15 MeV		Capture in ^{238}U	
	BNL[a]	Alsmiller et al.	BNL	Alsmiller et al.	BNL	Alsmiller et al.
540	1.36 (1.38)	1.06	2.67 (2.8)	2.13	4.00 (4.3)	3.64 ± 0.19
720	1.63	1.42	4.05	3.65	6.86	5.89 ± 0.25
960	2.32	1.96	6.36	5.61	10.72	8.82 ± 0.28
1470	3.91 (4.62)	2.89	11.04 (11.6)	8.61	18.28 (19.0)	14.1 ± 0.3

[a]The values in the BNL calculation without and with parentheses are calculated with $B_0 = 8$ and 10 MeV, respectively.

Table C.1

Physical Characteristics of the Targets

Material	Number of Rods	Density (g/cm^3)	Diameter (cm)	Length (cm)
Depleted uranium[a]	37	19.04	19.70[b]	30.46
Thorium	19	11.38	18.28[c]	36.31

[a]0.251 wt% ^{235}U.

[b]Effective diameter of the clustered target ($D = d\sqrt{n}$) with an individual rod diameter of 3.239 cm.

[c]Effective diameter of the clustered target with an individual rod diameter of 4.194 cm.

Table C.2 Calculated Depleted Uranium Target Characteristics

	ORNL		RAL	
	B_0 = 10 MeV	B_0 = 14 MeV	B_0 = 8 MeV	B_0 = 14 MeV
Protons				
Leakage >20 MeV (proton/proton)	0.0293 ± 0.0016	0.0287 ± 0.0016	0.0312 ± 0.0018	0.0311 ± 0.0017
$\bar{E}$ (MeV)	284 ± 25	287 ± 25	284 ± 25	287 ± 25
Neutrons				
Leakage >20 MeV (n/proton)	0.810 ± 0.008	0.844 ± 0.008	0.769 ± 0.007	0.796 ± 0.007
$\bar{E}$ (MeV)	84 ± 1	82 ± 1	85 ± 1	83 ± 1
Leakage <20 MeV (n/proton)	34.5 ± 0.2	33.5 ± 0.2	31.5 ± 0.2	29.7 ± 0.2
$\bar{E}$ (MeV)	1.42 ± 0.02	1.48 ± 0.02	1.33 ± 0.02	1.43 ± 0.02
$\bar{\nu}$ <20 MeV (n/fission)	3.03 ± 0.03	3.07 ± 0.03	2.99 ± 0.03	3.04 ± 0.03
$\bar{\Phi}$ <20 MeV ($n/cm^2 \cdot s$)[a]	(4.98 ± 0.04) × 10^{13}	(4.79 ± 0.04) × 10^{13}	(4.59 ± 0.03) × 10^{13}	(4.25 ± 0.03) × 10^{13}
Fissions				
High-energy >20 MeV (fission/proton)	1.84 ± 0.01	1.83 ± 0.01	1.68 ± 0.01	1.61 ± 0.01
Low-energy neutrons <20 MeV (fission/proton)	5.15 ± 0.04	5.15 ± 0.04	4.46 ± 0.04	4.43 ± 0.04
Energy deposition				
E >20 MeV (MeV/proton)	768 ± 2	773 ± 2	753 ± 2	752 ± 2
E <20 MeV (MeV/proton)	997 ± 7	996 ± 7	865 ± 6	856 ± 6

[a]Average neutron flux inside target for 100 μA of 800-MeV protons.

Calculation using the ORNL and RAL Models (without high energy fission) showed that either version could predict radiative capture in uranium or thorium to within 7% of the measured values. However, the models gave lower number of fissions by factor of ~ 1.5 in uranium and ~3 in thorium. Table VI shows the computation with high energy fission for the uranium target using both the ORNL and RAL models: each fission model is shown with different values of the level density parameter B_0. Although ~73% of the fissions were from neutrons < 20 Mev in each calculation, the total fissions predicted by ORNL were higher by ~15%. Because MCNP does not tabulate the yields of individual fission products from neutrons < 20 MeV, 14 MeV and fission-spectrum neutron fission yields were combined in proportions of 12 and 88 %, respectively ,to reach calculated value of ?? and generate an average mass-yield curve for low-energy fissions. Including high-energy fission in the RAL model added ~35% to energy deposition in the uranium target, and 29% in the thorium target.

Table C.2 shows that for the uranium target, the experimental fission product data agree more closely with the RAL model (B_0 = either 8 MeV or 14 MeV) than with the ORNL model (B_0 = 10MeV) . As shown in Fig.C.2, measured yields of the 10 high fission products average ~3 % lower than the RAL- calculated yields. Consequently , 3 %) fewer fissions per proton are reported; the higher number of fissions predicted by ORNL is outside the experimental values and the valley yields are underestimated by both models. However, because all three calculations gave a similar fractions in the two energy groups, the shapes of the fission yield curves (peak-to-valley ratio, etc.) are similar. Predictions of Np-238 (Pu-238 production) and U-237, but not Pa-233, are better with RAL and B_0 = 8 MeV.

Table C.3 list some of the characteristic of the thorium target computed by the RAL program with high energy fission for two values of B_0. A significant number of proton leak from the target: presumably, there are secondary protons from the cascade process.

Calculations for the thorium target including high- energy fission effects were not performed with the ORNL model because of the Z limitation (Z > 91) of the models applicability. Table C.4 compares the total integrated experimental yields with two calculated predictions for the thorium target. In Fig.C.3, the solid curve represents the total yield for each mass which is to be compared with the measured yields of isotopes (solid circles). Values for Sr-89, Sr-90, Sb-127, Ba-140, -141, Ce-143, and Nd-147 agree well with the experimental data; however, the actual yields between mass 95 and mass 112 are even higher than the calculated total mass yields. Furthermore, the RAL models yields for three neutron deficient isotopes (Sr-85, Y-87 ,and Tc-96) from the light peak (around mass 90) are higher than measured, while the predicted independent yields of the two antimony isotopes are lower than measured.

The dashed curve in Fig.C.3, fitted by the two-mode-of fission hypothesis (TMFH), agree s better than the solid curve with data in the 95 to 112 mass region. They generated the dashed curve by combing 59% of 232 14-MeV neutron fission yield curve, and 41% of A "symmetric mode" (Gaussian distribution centered about mass 107.6, with a standard derivation of 14.1 mass units). The number of fissions per proton, 1.56 (determined by summing this mass-yield curve and dividing by 2), is almost the same as RAL with B_0=8 MeV; however, the integration of the cumulative yields of the neutron-rich isotopes only (from Table C.4) resulted in 10% fewer fissions .

Part of the uncertainty in the experimental number of fissions(Table C.5) is because there is insufficient information about the charge distribution and about the yield of nuclides near stability . The experimental production of U-238 (the amount of Pa-233 formed) agrees very well with the RAL calculation (B_0=8MeV).

Of the two targets studied here, thorium provided the more stringent test of the theoretical models because over 60% of the fissions were at energies >20 MeV. For the same reason, the experimental values for many more isotopes are required the mass-yield curve can be established that will be used to determine the number of fissions.

Concerning to the level density parameter B_0, the LANL group could not

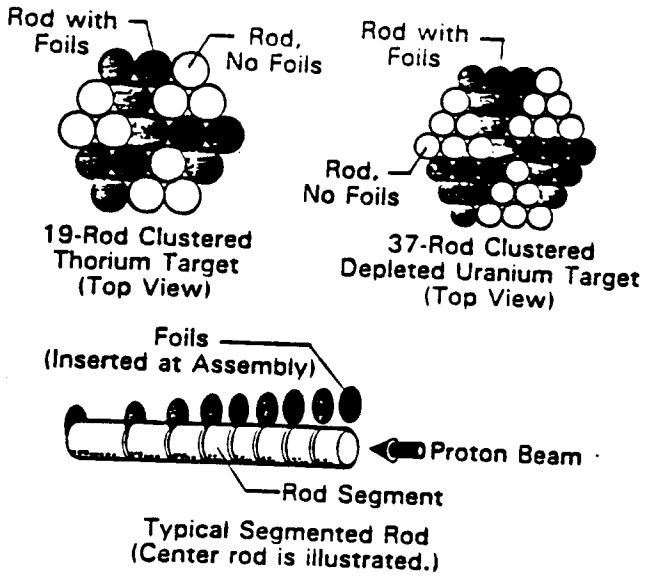

Figure C.3 Illustration of clustered targets used in the conversion measurements, the location of the foils in an array, and the foil position within a rod.

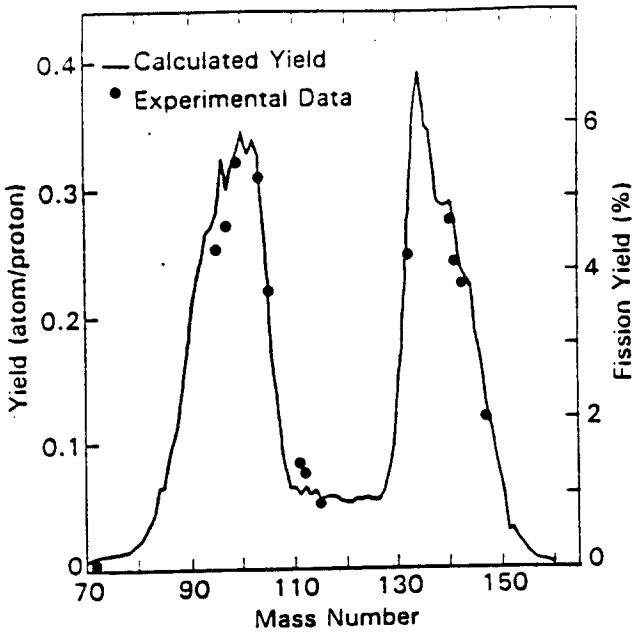

FIGURE C.2 Comparison of measured fission product yields for the uranium target to values calculated using the RAL model with $B_0 = 8$ MeV.

Table C.3

Comparison of Experimental Data from the Depleted Uranium Conversion Experiment with Calculations Using High-Energy Fission

	Total Yield[a] (atom/proton)			
		ORNL	RAL	
Nuclide	Experiment	$B_0 = 10$ MeV	$B_0 = 8$ MeV	$B_0 = 14$ MeV
^{72}Zn	0.0046 18	0.0032 4	0.0046 6	0.0041 5
^{95}Zr	0.254 1	0.314 3	0.269	0.268 2
^{97}Zr	0.272 2	0.324 3	0.281 3	0.277 3
^{99}Mo	0.322 1	0.369 6	0.320 5	0.316 5
^{103}Ru	0.310 1	0.364 20	0.319 15	0.317 17
^{105}Rh	0.221 3	0.255 10	0.228 8	0.226 9
^{111}Ag	0.0839 3	0.055 12	0.060 9	0.053 10
^{112}Pd	0.0762 16	0.048 11	0.046 8	0.044 10
^{115g}Cd	0.0524 9			
^{132}Te	0.248 1	0.293 5	0.250 3	0.251 4
^{136}Cs	0.0107 4	0.0075 7	0.0080 7	0.0070 7
^{140}Ba	0.276 1	0.320 14	0.276 11	0.272 12
^{141}Ce	0.243 1	0.306 13	0.265 10	0.263 11
^{143}Ce	0.225 1	0.258 8	0.222 6	0.220 7
^{147}Nd	0.120 4	0.146 5	0.126 4	0.127 5
^{233}Pa	0.0207 6	0.0108 9	0.0112 9	0.0124 9
^{237}U	0.954 2	1.379 16	1.079 14	1.223 16
^{239}Np	3.810 8	4.133 32	3.875 31	3.534 29
Fissions	5.90 25	6.989 41	6.144 37	6.034 37

[a]The number following each value represents the uncertainty in the last place or places.

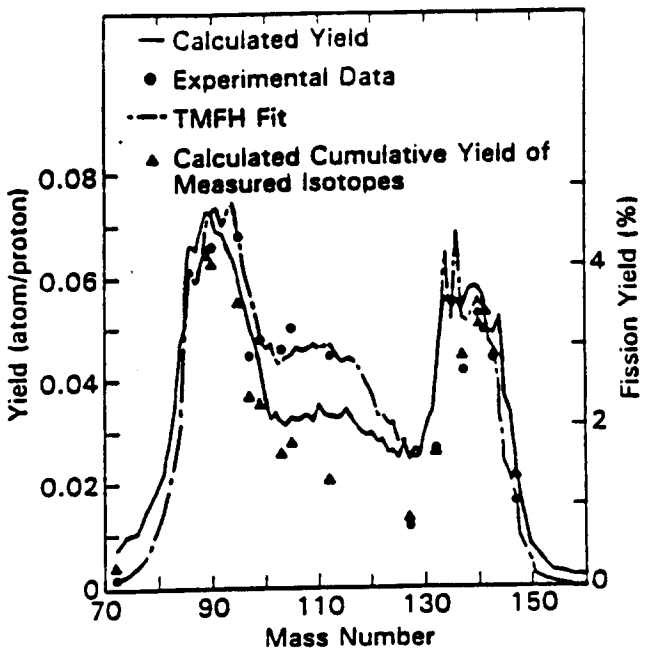

FIGURE C.3 . Comparison of measured fission product yields for the thorium target to values calculated using the RAL model with $B_0 = 8$ MeV. A TMFH fit to the experimental data is also shown.

Table C.4

Calculated Thorium Target Characteristics

	RAL	
	B_0 = 8 MeV	B_0 = 14 MeV
Protons		
Leakage >20 MeV (proton/proton)	0.228 ± 0.002	0.229 ± 0.002
$\bar{E}$ (MeV)	239 ± 3	238 ± 3
Neutrons		
Leakage >20 MeV (n/proton)	1.01 ± 0.01	1.04 ± 0.01
$\bar{E}$ (MeV)	93 ± 1	91 ± 1
Leakage <20 MeV (n/proton)	20.8 ± 0.1	18.8 ± 0.1
$\bar{E}$ (MeV)	---	2.09 ± 0.02
$\bar{\nu}$ <20 MeV (n/fission)	2.76 ± 0.03	2.84 ± 0.03
$\bar{\Phi}$ <20 MeV (n/cm^2·s)[a]	---	(2.00 ± 0.01) × 10^{13}
Fissions		
High-energy >20 MeV (fission/proton)	0.986 ± 0.005	0.884 ± 0.004
Low-energy neutrons <20 MeV (fission/proton)	0.557 ± 0.004	0.560 ± 0.004
Energy deposition		
E >20 MeV (MeV/proton)	588 ± 1	593 ± 1
E <20 MeV (MeV/proton)	124 ± 1	123 ± 1

[a]Average neutron flux inside target for 100 μA of 800-MeV protons.

Table C.5

Comparison of Experimental Data from the Thorium Conversion Experiment with Calculations Using High-Energy Fission

Total Yield[a] (atom/proton)						
			RAL			
Nuclide	Experiment		B_0 = 8 MeV		B_0 = 14 MeV	
^{72}Zn	0.00173	5	0.0037	3	0.0035	3
^{85}Sr	0.0010	5	0.0031	2	0.0020	2
^{87}Y	0.00116	3	0.0034	2	0.0023	2
^{89}Sr	0.0653	5	0.0645	17	0.0621	16
^{90}Sr	0.0661	5	0.0627	19	0.0607	18
^{95}Nb	0.0682	3	0.0553	10	0.0524	10
^{96}Tc	0.0006	1	0.0020	2	0.0012	2
^{97}Zr	0.0449	3	0.0368	12	0.0371	12
^{99}Mo	0.0479	1	0.0353	11	0.0336	11
^{103}Ru	0.0460	7	0.0257	11	0.0242	10
^{105}Rh	0.0501	5	0.0279	12	0.0257	11
^{112}Pd	0.0449	3	0.0205	14	0.0211	14
^{122}Sb	0.0058	1	0.0040	3	0.0034	3
^{124}Sb	0.0069	14	0.0039	4	0.0038	3
^{127}Sb	0.0116	1	0.0132	11	0.0131	11
^{132}Te	0.0268	2	0.0259	6	0.0257	5
^{134}Cs	0.00288	3	0.0033	3	0.0034	3
^{136}Cs	0.00393	3	0.0041	3	0.0041	3
^{137}Cs	0.0420	3	0.0445	8	0.0449	5
^{140}Ba	0.0530	3	0.0508	21	0.0486	16
^{141}Ce	0.0497	2	0.0530	19	0.0531	18
^{143}Ce	0.0441	2	0.0450	18	0.0448	18
^{147}Nd	0.0163	2	0.0215	12	0.0218	12
^{203}Pb	0.00488	6	0.0085	5	0.0112	5
^{205}Bi	0.00565	6	0.0077	4	0.0080	4
^{206}Po	0.0108	1	0.0086	4	0.0091	4
^{227}Th	0.0457	3	0.0221	7	0.0236	7
^{233}Pa	1.251	3	1.267	7	1.120	7
Fissions	1.56	25	1.543	6	1.444	6

[a]The number following each value represents the uncertainty in the last place or places.

determine the values of B_0 from the experimental data on fission product yields, number of fissions, or the measured spallation products for either target. However, they concluded that Armstrong's suggested value of B_0 = 8 MeV for proton energies < 1 GeV, in the RAL model substantiates our general finding and, furthermore, they concluded that ..." their experiments are "clean" integral experiments, but complex in the reactions taking place. The agreement between the experimental data and the calculated results is satisfactory"...

D. Vasilkov et al. 's experiment(the Large uranium block experiment)[Va,78]

So far only one experiment has been performed with large uranium block target. This experiments was carried out by Vasilkov et al. using a target assembled from rectangular block of natural (2x4x8 cm^3) and depleted (8x8x16 cm^3) uranium. The total linear dimension of the target was 56x56x64 cm^3 and it was covered with a lead layer of thickness 0 or 20 cm as (shown in Fig.D.1).

The proton beam was injected into the central part of the target through a beam hole of cross-section 8x8 cm^2 and a depth of 16 cm from the front surface of uranium block. The diameter of proton beam at the entrance into the target was 4-5 cm.

The experiment was carried out with an extracted beam of 660 MeV protons. For experiments at proton energies 30,400, and 500 MeV, the initial 660 MeV-protons were slowed down in a polyethlene attenuator.

In the diagonal plane of the target, passing through the axis of the proton beam, a system of channels was made where the detectors could be placed. The channels were arranged in parallel with the proton beam and located 6 to 45 cm from the axis at approximately 3 cm interval. The channels were 60 cm in length and 2x0.3 cm^2 in cross section.

The density distribution of (n,γ) capture was measured by Np - 239,distinguished radio-chemically from uranium samples irradiated at variouspoints in the target. Measuring the density distribution $A(z,r,\theta)$ of the (n,γ) captured in the volume of the target and integrating this distribution, Vasilkov et al obtained the total number of captures (Pu-239 yields) per one energetic proton: Vasl'kov et al's definition of neutron yield is

$$Y=\rho\int_v A(z,r,\phi)\,dV, \qquad (D.1)$$

where z is the direction of proton beam r,θ are cylindrical coordinates and ρ is the density of metallic uranium.

This experiment was analyzed by Takahashi [Ta,84],Nakahara et al.[NT,79], Garvey [Ga,79] and Barashenkov et al.[Ba,78]: Table D.1 compare the calculated and experimental values of neutrons captured by U-238 and the fission reaction of U-238 and U-235. The results are plotted in Fig.D.2.

The values of the U-238 capture reaction calculated by Nakahara, Takahashi, and Barashenkov which take into account the high energy fission are close to each other. However, Takahashi's previous calculation and Garvey's calculated value which do not take the high energy fission reaction into account are substantially smaller than those that include it.

There is fairly good agreement between the computation with the high energy fission and the experiment for neutron capture by U-238 in the case of E_p = 660 MeV; the discrepancy is a little larger for E_p = 400MeV.

One reason for this discrepancy might be the energy spread of the 400 MeV proton beam which, is produced by the slowing down of the 660 MeV proton in polyethylene. The calculation was performed by assuming the δ function type energy spectrum for incident proton of 400 MeV energy.

The table D.1 shows that the number of both U-238 and U-235 fissions calculated by Takahashi is 22-50 % lower than the experimental results for both 660 and 400 MeV proton energies. And values calculated previously by Takahashi and Garvey without high energy fission are substantially lower than the experimental values.

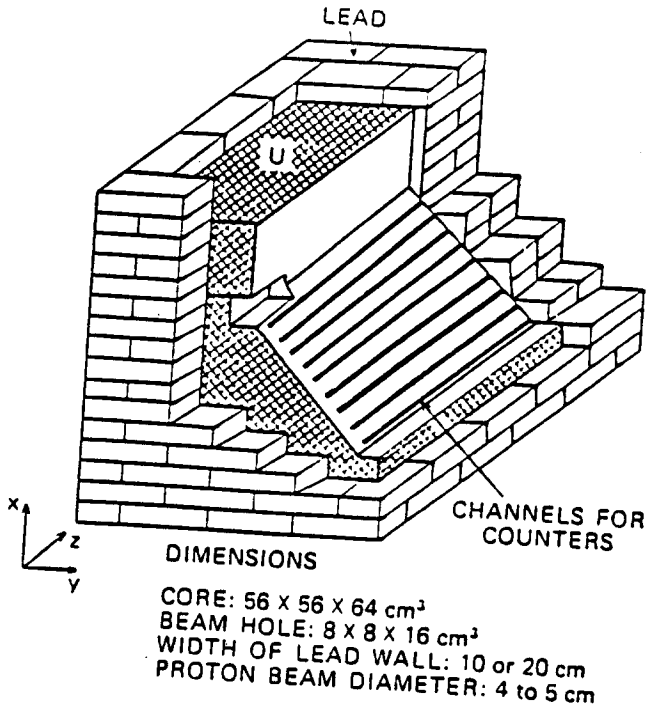

FIGURE D.1 Target in the experiment of Vasil'kov et al.

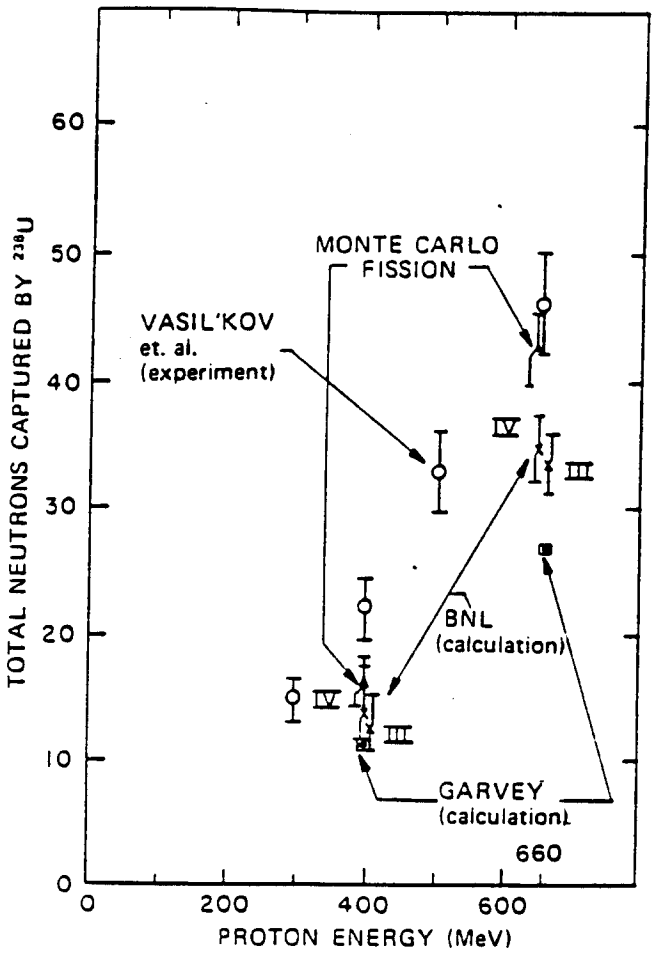

FIGURE D.2 Comparison of total neutrons captured by ^{238}U per one proton by Vasil'kov et al. Experiment and BNL calculation (III and IV for ENDF/B-III and -IV data).

Table D.1

Neutrons Captured by ^{238}U Analysis of the Vasil'kov et al. Experiment for High-Energy Proton Incident on Large Uranium Block

	Proton Energy (MeV)	Number of Captured Neutrons					
		Experiment	BNL-Present Calculation	Nakahara Calculation	Barashenkov and Shmakov Calculation	BNL-Previous[a] Calculation	Garvey[a] Calculation
Capture ^{238}U	660	46.0 ± 4.0	42.6 ± 4.8	44.9 ± 5.10	42.0	33.23 ± 3.79	26.9 ± 1.6
Fission ^{238}U	660	14.6 ± 1.3	11.3 ± 1.2	---	---	8.26 ± 0.88	5.2 ± 0.3
^{235}U	660	3.9 ± 0.4	2.44 ± 0.2	---	---	2.11 ± 0.23	1.6 ± 0.1
Total	660	18.5 ± 1.7	13.74 ± 1.4	---	---	10.37 ± 1.11	6.8 ± 0.4
Capture ^{238}U	400	22.1 ± 2.4	16.2 ± 2.0	15.96 ± 4.65	19.8	13.44 ± 0.81	10.9 ± 0.6
Fission ^{238}U	400	7.0 ± 0.8	4.5 ± 0.6	---	---	---	2.1 ± 0.1
^{235}U	400	1.9 ± 0.2	0.96 ± 0.1	---	---	---	0.7 ± 0.1
Total	400	8.9 ± 1.1	5.46 ± 0.7	---	---	---	2.8 ± 0.2

[a]High-energy fission is not included in the calculation.

E. Calculation for an Infinite U-238 block

Barashenkov[Ba,78], Alsmiller[Al,81] and Takahashi[Ta,84] also calculated neutron capture and the fission reaction in an infinite natural uranium medium. Since the medium is infinite , the spatial inter-nuclear transport of the nucleon (neutron and proton) and meson becomes irrelevant so only the cross section of energy transfer and reaction rate are involved in the calculation. In Table E.1, these results are compared for 1 GeV incident energy proton. Takahashi's values are close to those of Barashenkov; Allismiller et al's value is 15% smaller than those of Takahashi and Barashenkov.

Recently, Vassil'kov [Va,90] compared the values reported by several authors for neutrons captured including the data discussed above. He found a the large disagreement among them.

Some of the results were obtained by extrapolating the calculated value for a finite block uranium block. Figs. E.1 and E.2 show, respectively, the yields of Pu-239 atom / proton and the number of fission/proton at 1GeV as a function of the year in which the value were published. The calculated values for Pu-239 yield are scattered around two experimental values of Dubna and ORNL-CRNL at BNL, and still the uncertainty is about ± 15 %. The calculated values for the fission number/proton are about 30% smaller than those from Dubna experiment.

To overcome the lack of the experimental data, Vasil'kov is constructing an experimental facility with a cylindrical target of depleted metal uranium having a total mass of 21 metric ton, and a beamline for transporting protons or deuteron with momenta 1.4 - 3.4 GeV/c. This setup is shown in Figs.E.3 and E.4.

Table E.1

Comparison of Calculated Results for 1-GeV Protons Incident of an Infinite Natural Uranium Target

	Neutron Captures in ^{235}U	Neutron Captures in ^{238}U	Total Capture	Total Fission
BNL calculation	1.2 ± 0.1	98.8 ± 7.0	100.0 ± 7.1	27.4 ± 1.5
Barashenkov et al. calculations	1.2	100.9	102.1	28.3
Alsmiller et al. calculations	1.1 ± 0.0	84.9 ± 2.7	86.0 ± 2.7	23.1 ± 0.7

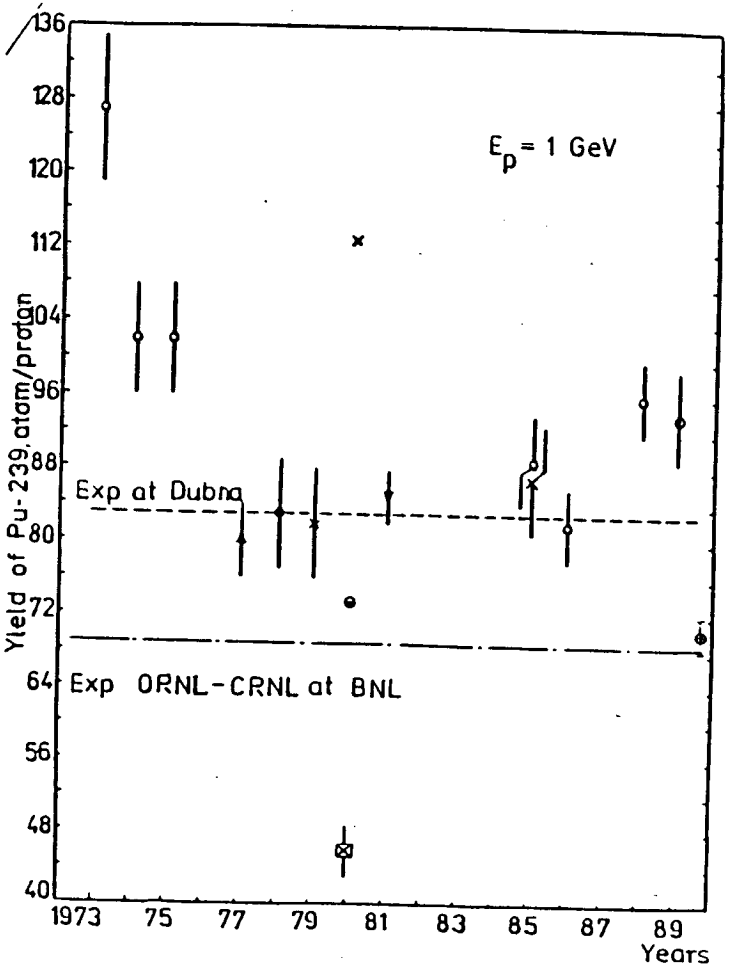

Figure E.1

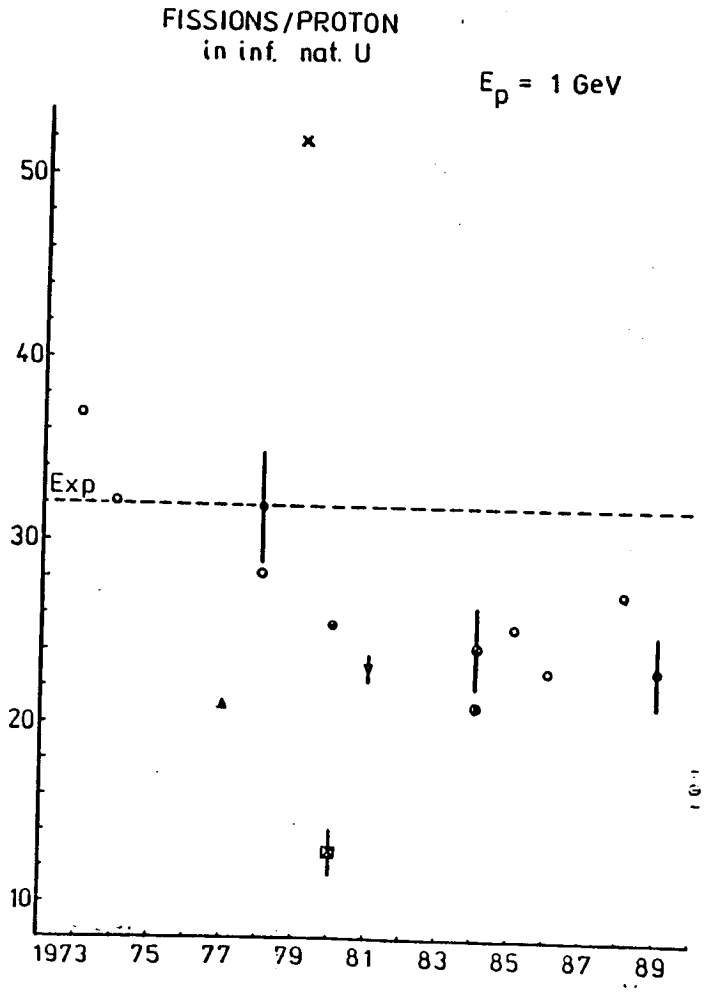

Figure E.2

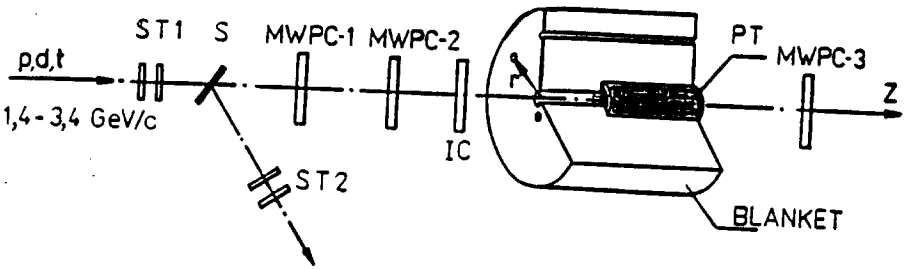

Figure E.3

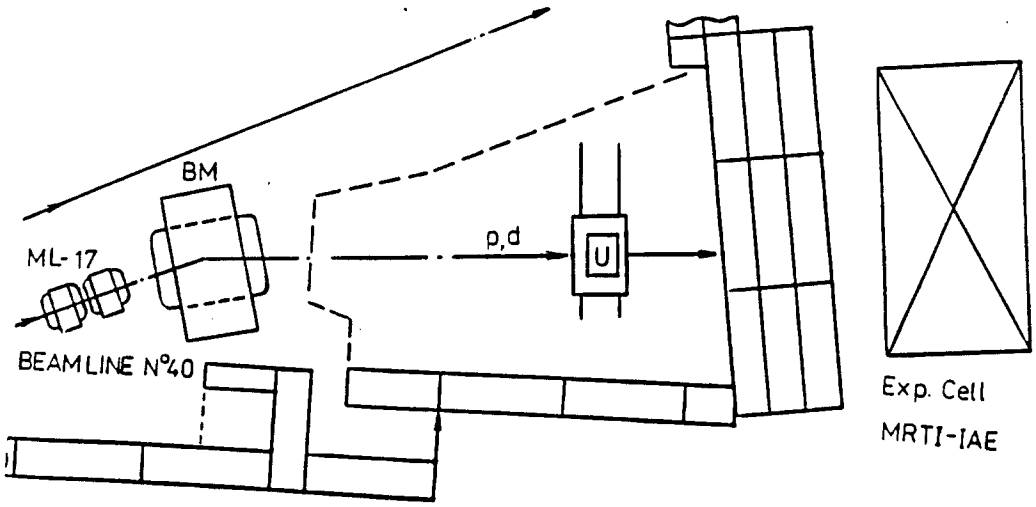

High Energy Lab., JINR
Bldg. 1B

Figure E.4

8. Cost analysis of accelerator for incinerator

It is difficult to evaluate the cost of accelerator incineration, because of large uncertainty in the data for fuel processing cost and many other items. The target reactor used in the accelerator incinerator is rather similar to the conventional fast reactor, thus, data on the cost of fast reactor can be used for estimating the target cost. Therefore we will not try to estimate the cost of incineration using this accelerator incinerator: we will limit ourselves to estimating the cost of the accelerator used for the incineration of minor actinides.

8.1 Meson factory Accelerator and other acclerators planed. [Ku,89]

Before estimating the cost of the accelerator, we describe the existing accelerator which is used as meson factory. Although these accelerators are smaller than the accelerator discussed here , the discussion will be useful as a basic point of reference.

Table 1.1 shows the specifications of the accelerator and the total costs of the facilities of TRIUMP, PSI, LAMPF, and INR Moscow Meson Factory.

The cyclotron of SPI in switzerland has been reconstructed to increase the beam intensity to 1.5 mA, and future plans are to increase the intensity to 10 mA. This is rather close to the segmented cyclotron discussed in the incinerator section. The 800 MeV proton synchrotron is a rapid-cycling, strong-focusing machine designed to provide an average 200 microamps at a repetition frequency 50 Hz.

As the other planned accelerator, KFA (Kernforshungsanlage) had the project called SNQ to construct the accelerator for high intensity neutron source. Unfortunately this project was cancelled, but they made a detailed study for the accelerator. Even though the cost analysis was not published, reference to this accelerator might be very useful. This accelerator has the following structure.

The ion source is injected into the preaccelerator of 400 kV and injected into the DT. After a 105 MeV acceleration, the beam is injected into the DAW (Disk and Washer) which is one kind of CCL, and accelerated to 1GeV. This accelerator differ from the one of a accelerator breeder; the beam current is not the continuous wave and pulsed wave with 500 ms width and repetition of 100Hz. The average current is 5mA ,and peak current is 100mA.

8.2 High power linear accelerator for accelerator breeder and incinerator[Ko,77]

There are several estimate of cost for the accelerator breeder, which uses the high power linac of 300 -400 MW proton beam power. Before discussing the costs of the linear accelerator, we first describe the linear accelerator, which is being for the accelerator breeder.

Over the past 50 years, Linac has been developed into a highly reliable and efficient research tool. There is great confidence that a high current (300 mA at 2-GeV proton), continuous wave (CW) production accelerator can be constructed at a reasonable cost. One direction of this development is toward the high current accelerator.

As part of long-range plans of the energy problem, Chalk River nuclear Laboratory in Canada, accelerator breeder concept has been systematically developed. Fig.2.1 shows this concept. In contrast to the old linac beam currents which was the pulsed type one, this accelerator is continuous wave current. Figs.2.1 and 2.2 show the components of the accelerator breeder and one specification of the breeder is that it is energy self-sufficient. The ions source is placed at the high voltage terminal of 75 KV, and, after injection , proton is accelerated by radio frequency quadrupole (RFQ). The assembled protons are accelerated by Drift Tube Linac (DTL), that is called the Alvarez Linac up to 200MeV . Since the shunt impedance $z=E_0^2/(P/L)$ (E_0 is the peak value of accelerating fields at the center axis of DTL, and P/L is the high frequency (RF) loss per one unit length of DTL) is decreased as increase of the beta value of proton, the proton is accelerated by coupled cavity linac (CCL) above 200 MeV

Laboratory	Triump	PSI	LAMPF Meson Factory	INR Moscow
accelerator type	cyclotron	cyclotron	Linac	linac
Average Current (mA)	0.15 mA	0.25 0.37**	1mA	0.5mA
Energy (MeV)	70-110 183-520	595	800	602
No. of D	2	4	-	-
Width (cm)	16,25	45.	-	-
Internal beam (part/pulse)			$5x10^{13}$	$6x10^{13}$
(part/s)			H+ $6x10^{15}$	$7.2x10^{15}$ $3x10^{15}$
Physical Dimension			800m	450m
RF.Range (MHz)	23.055	50.63	201.25(D) 805.(SC)	198.2(D) 991.(DAW)
Energy Gain in Turn	340Kev/turn	1700Kev/turn		
Total facility Cost	60M$	134MSFR	75M$	130MRouble
Construction Start	Jan.1970	1969/1974	1968	1977
First Beam obtained	Dec.1974	01/18/1974	1972	1990

** Upgrade program for max current 1.5mA underway.
***(D) :Drift tube (SC) : side coupler,

Table 1.1 Accelerators of the meson factories of TRIUMP, PSI, LAMPF, and INR Moscow

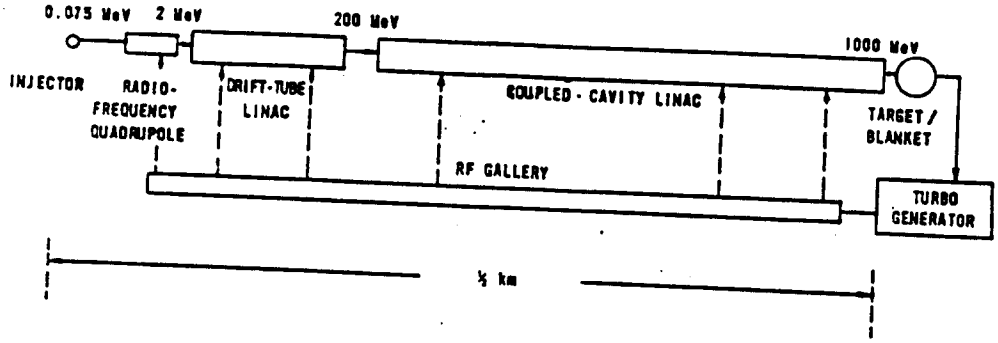

Figure 2.1 Main components of an Accelerator Breeder.

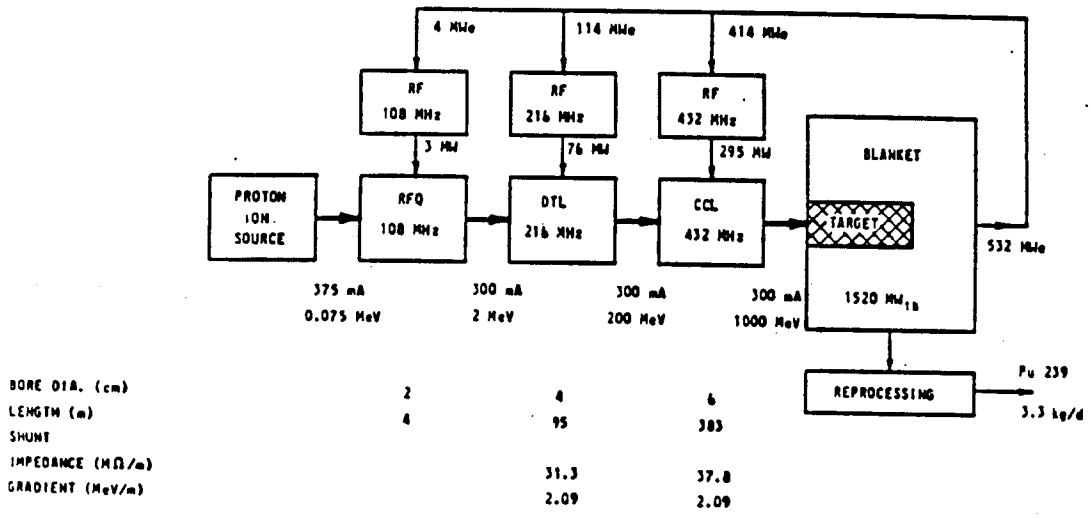

Figure 2.2 Schematic of an Accelerator Breeder that is energy self-sufficient.

Figure 3.1 *Overhead view of the Clinton P. Anderson Meson Physics Facility.*

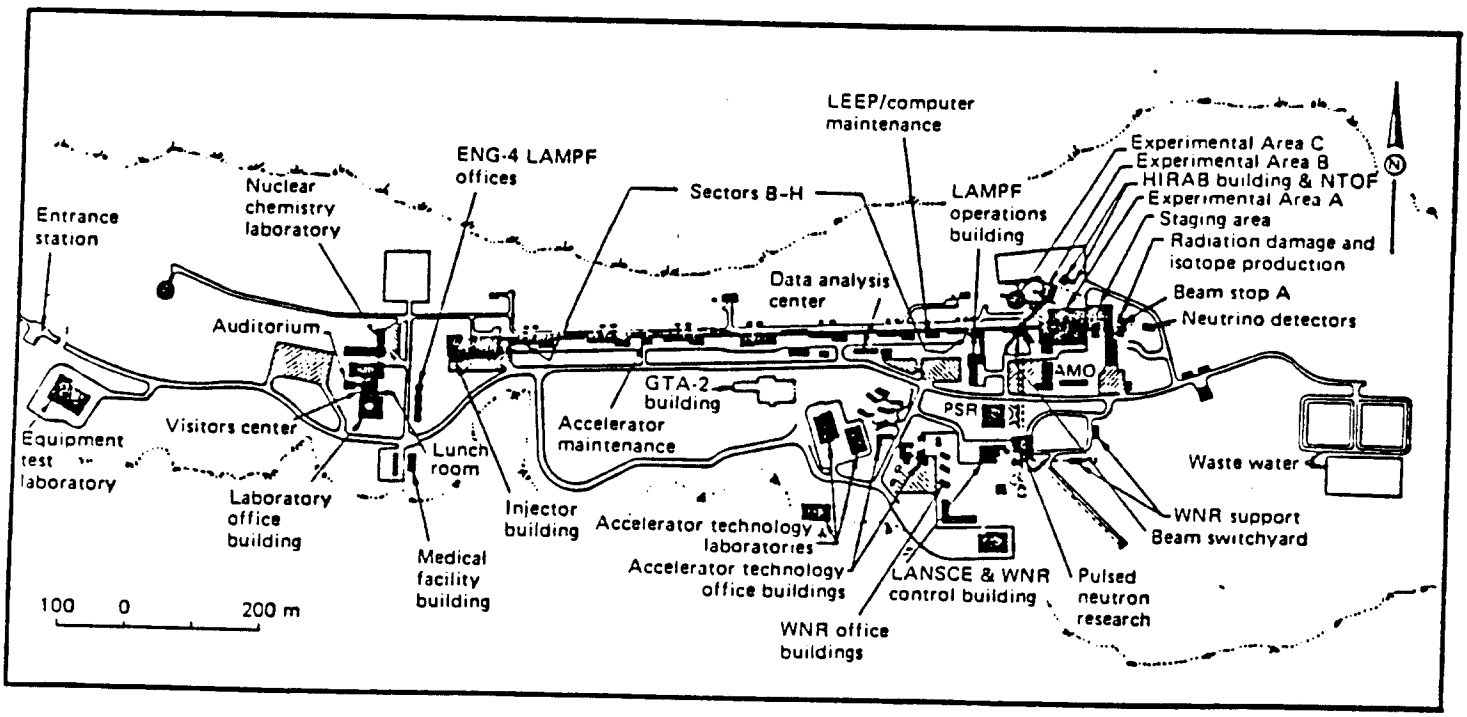

Figure 3.2 *Plan of the experimental areas of the Clinton P. Anderson Meson Physics Facility.*

energy.and reach a final energy of 1 GeV.

The accelerator for the breeder studied by BNL is very similar to the CRNL accelerator[Ko,77]. The main difference between the CRNL and BNL accelerators are (1) Injector: By improving the RFQ which has been successfully operated in many laboratory, the proton is accelerated till 2MeV. The RFQ frequency of 100 MHz is increased to the 200 MHz frequency of DTL by the funneling technique,
(2) Acceleration of high beta section:Instead of using the DAW of CCL.

The accelerator specifications of BNL are [Gr,81]

75 MHz RFQ, 0.1 - 1.5 MeV
150 Mez DTL, 1.5-150 MeV
450 MHz CCL, 150- 1,500MeV
Proton Beam Currents 300mA
Total length of accelerator 1,200 m

Although the energy of proton is 1.5 times that of the CRNL accelerator, the structure is basically same as the one at CRNL.

Recently, Russian group [BM,90b] designed the linear accelerator for incinerator-reactor. Fig.2.1 shows the diagram of the incinerator reactor linear accelerator. the accelerator involves two injectors of H^- and H^+ beams, initial part (IP), first and second parts.

The IP proposed in Moscow Radiotechnical Institute (MRTI) is based on the 5 - 8 T superconducting solenoid focusing. The solenoid contains a resonator with opposed vibrators providing for high accelerating wave amplitude E_m.

At present design stage two pairs of operating frequencies for accelerator parts are considered: 330 and 990 MHz (990 MHz is operating frequency of the second part of meson physics facility linear accelerator at the INR of the USSR Academy of Science); 200 and 600 MHz. The first frequency pair is preferable. It enables the RF generator size and cost be decreased. At the same time the beam dynamics still remain favorable with regard to the particle beam losses. Specific acceleration in both accelerator parts is chosen to be 1 MeV /m.

The implementation of RF power supply systems for continuous mode accelerators with total RF power of several hundred MW requires RF generators with at least 5 -10 MW output power, 70 -80 percent efficiency and 20 dB gain. Proposed in MRTI regotron , i.e. a relativistic electron beam generator with distributed RF power extraction system meets the aforementioned requirements.

8.3 Cost analysis of the linac

A) Formulation of cost analysis.

The cost of the high power linac accelerator for the accelerator breeder is formulated as follows; the total capital cost (C_t) can be expressed as (by neglecting the small correction.)

$$C_t = C_s P_s + C_b P_b + C_l L \qquad (3.1)$$

The first term of the right-hand side of Eq.(3.1) is the capital cost which is related to the power consumption in the accelerator structure P_s (or wall loss $P_{\text{wall loss}}$)

The second term is the one thatdepends on the beam power, Pb, which is expressed as

$$P_b = E*I(MW) \qquad (3.2)$$

and $C_b = C_{\text{RF system}} + C_{\text{cooling system}} + C_{\text{Rf building}}$

where C_{RF} system : coefficient related to the RF-power. (The major part of this is proportional to the beam power, and we neglect the part of relating to P_s.)

$C_{\text{Cooling system}}$: coefficient related to the cooling power
$C_{\text{Rf building}}$: Coefficient related to the RF power)

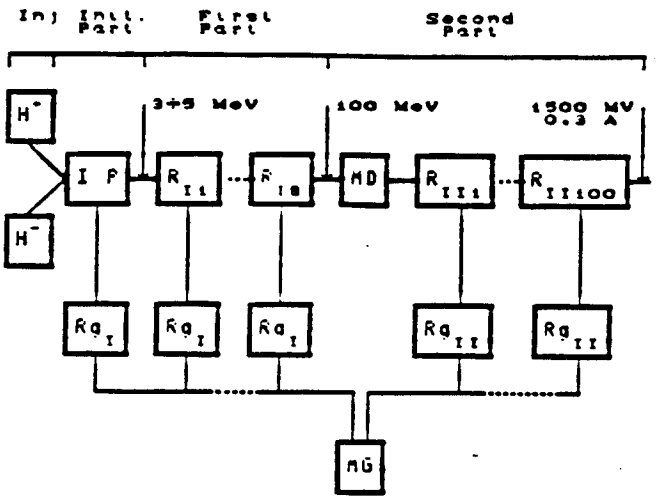

Figure 2.3 The diagram of the burner-reactor linear accelerator

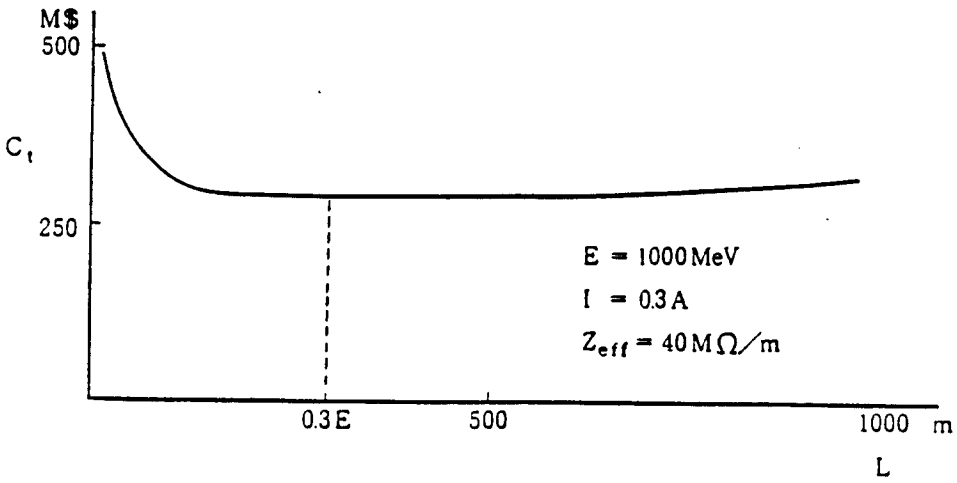

Figure 3.1 Relation between accelerator cost and length of linac

The third term of Eq(3.1) is the one related to the length of the linear accelerator, such as the tunneling type accelerator building: the building size is almost proportional to the linear accelerator length.

$$C_l = C_{Tunnel} \qquad (3.3)$$

When the beam energy and beam current are given, the minimum length of L is can be expressed as:

$$L_{min} = C_s E \qquad (3.4)$$

These values were estimated by Grand as

$$\begin{aligned} C_{Structure} &= M\$\ 0.075\ /\ MW^* \\ C_{Tunnel} &= M\$\ 0.02\ /m^* \\ C_b &= M\$\ 0.93\ /MW^* \end{aligned} \qquad (3.5)$$

(* These M $s are 1979$)

Accordingly, if we take the value of Z_{eff} = 40 MΩ /m, then we get:

$$L_{min}(m) = 0.3\ m\ (MeV)$$

From this expression, the minimum values of the total cost is obtained when the electric field is 3 MeV/m.

Fig.3.1 shows the relationship between the total cost and the length of linac for 1 Gev energy proton and its current of 300 mA, and Z_{eff} =40 M.Ω/m. The capital cost increase rapidly below L = 200 m and above this length the total capital cost becomes rather flat up to 1 Km.

Table 3.1 shows the breakdown of the capital cost estimated by LANL[KN,77], BNL[Gr,81], and Chalk River[Sr,79].

In addition of capital costs, we have to take into account the running cost for the accelerator hardware. The lifetime of the PEP klystron of 500 KW CW with frequency of 353 MHZ and the 65% efficiency is 20000 hr (experimental value). Thus the cost of this klystron is roughly $ 100 K, (in the 1980 $), and the consumption cost of Klystron is 1 ¢/RF KWH. When the beam loading factor is 5.5 and the (ratio of RF generator to beam loading)x (control range ratio)=.85, then the total power of RF generator is 420 MW ,and the consumption cost for Klystron for 420 MW is $ 4.2K /hr =M $ 2.8 / year. If we take the same life time of 20000 hr for the accelerator structure, the consumption cost of accelerator structure is M $ 32.8 /year for BNL cost estimation.

As discussed in the introduction, the accelerator incinerator does not require a high-power accelerator. A 15 - 30 MW power accelerator might be sufficient to incinerate minor actinides which is produced from 10 LWR . In the cost estimated by LANL, BNL and Chalk River, the capital cost of accelerator structure is 20-25 % of the total capital cost of the accelerator. In the case of ATP accelerator the accelerator structure is about half of the total cost. This cost can be reduced by lowering the proton energy, but a low energy proton gives a small neutron yield. Since the cost of accelerator structure can not be greatly reduced, even when the beam currents is small, in the order of 15 - 30 mA. It has been suggested that the segmented cyclotron accelerator is used instead of linac. Because the accelerator structure of the linear accelerator is rather expensive, when we use the linear accelerator to incinerate minor actinides, the high power accelerator is more economical. The 300 MW beam power can incinerate all the minor actinides produced in 200 LWR when the multiplication factor of the target is k=0.95. However the beam must be segmented to irradiate a reasonable sized target, and it is not expected that there will be a large inventory of minor actinides in order of 120 ton in the near future.

8.4 Cost analysis of Segmented Cyclotron

Using a cyclotron type accelerator, the cost of the accelerator structure can be reduced substantially, because the proton is accelerated many times in an

Linac	Chalk River		LANL		BNL	
Current (mA)	300.	15.	300.	15.	300.	15.
Energy (GeV)	1.0		1.0		1.0	
Year M$	1981		1979		1979	
Accellerator Structure	95.	47.5	54.	30.	75.	37.5
RF	261.	13.	160.	8.	350.	17.5
Total	356.	60.	214.	38.	425.	55.

Table 3.1 The cost Estimation of linac in various Laboratory.

accelerator structure D. But the cost of the magnet which used to circulate the particle has to be added. The cost of RF parts must be proportional to the beam power, so that there is no difference between the cyclotron and the linac.

Figure 3 & 4 in section 2 shows the segmented cyclotron system which was proposed for incinerating the minor actinides produced in 10 LWR. This system is composed of three RFQ, three 4 segmented cyclotron, and one 12 segmented cyclotron.

Recently aother 1.5 GeV and 10 mA proton cyclotron was studied by Odera[Od,90]. This accelerator system is composed of RFQ which accelerate proton from 30 KeV to 3 Mev, followed by 3 stage-segmented cyclotrons accelerate protons from 3 to 50 Mev ,50 to 500 MeV, and 500 to 1,5 GeV.

As an injector, this uses a radio frequency quadrupole accelerator(RFQ) with RF frequency of 100 MHz and power of 300 kW.

The first segmented cyclotron is a 4 sectors magnet, with a weight of 80 ton/magnet (Total weight 320 ton) ,4.5×10^4 AT Magnetic field of 5.2-5.6 kG and the maximum gap of magnetic poles 10 cm. Two RF cavities with RF frequency of 100 MHz and power of 400 kW are used to accelerate the proton.

A second stage cyclotron uses an 8 sector magnet which weight is 724 ton / magnet (total weight 5800 ton), 4.5×10^4 AT magnetic field of 7.4-10 kG and the gap length of the magnetic poles is 8-5.5 cm. The protons are accelerated in the 6 RF cavities, using 1 MW RF power with a frequency of 100 MHz and each with power of 1MW.

The third stage cyclotron is composed of a 16 sector magnet where each magnet weighs 726 ton (Total weight 11600 ton), 7.2×10^4 AT magnetic field of 10.0-15.4 kG.and its gap length is 8 cm-5.0 cm. RF parts are composed of 12 cavities and their RF frequency is 100 MHz and the RF power is 1 MW.

This cyclotron is designed so that beam loss is almost negligible for proton energy above 3 Mev. To satisfy this requirement, the magnetic field should be small, and this results in an increase of the circular radius of proton trajectory; the gap length of circular motion at the maximum radius is above 3 cm, so that the efficiency of the beam leaving the cyclotron is 100%.

This cyclotron was estimated conservatively, and the cost of each components are shown in table 4.1 in 1990 10^8¥.

	Ion Source	RFQ	Cycro-1	Cycro-2	Cycro-3	total
Source	2.					2.
Magnet			4	40.	60.	104.
accel.Cav.		1.5	5	18	36	60.5
RF(incl.DC)		2.0	6	18	36	62.
Vacuum.	2.	1.0	2.	4.	8.	17.
others	1. (Dev.)	1.5	1.	3.	5.	11.5
sum	5.	6.	18.	83.	145.	257.

Cost of the other components are:

Beam transport system (Between accelerator. achromatic system between accelerator and target system) 25.

Diagnostic of beam and Safety system (Non) 15.

Control and Operation system (Incl. remote control maintenance apparatus) 30.

Cooling system (Ion, removal apparatus) 15.

sum 85.

Total sum 342

Costs are given in 1990 10^8 ¥

Table 4.1 Cost of segmented cyclotron (1.5GeV,10mA)

This table does not include the target and treatment process of radioactive material, the electric power used, and the building.

8.5 Comparison between linac and segmentted cyclotron.

To make rough comparison between the cost of the linac and the cyclotron with small beam power, the following assumptions are made. The cost of the RF generator is propotional to the beam power and the cost of the accelerator structure is propotional to α power (α = 0.2) of the beam currents. The cost of the 15 mA, 1GeV proton linac which was calculated using the above assumptions from the cost estimated at various laboratories are shown in the table 3.1. The cost estimated from the LANL data is too low by comparison with the ones calculated from the data of BNL and Chalk River. The cost of the accelerator structure for 1 GeV and 15 mA is 40-50 M$ (1980) and cost of a RF generator is in the order of 13-18 M$. That is, the cost of the acceleraotor structure is about three times that of a RF generator for a 15mA accelerator. This ratio can be reduced by increasing the beam currents.

In the table 5.1, the cost of cyclotron is compared with the cost of the small beam power linac (1GeV, 15 -30 mA), which is calculated from the data from the ATP accelerator[AT,90], using the same assumptions as the above. Because of the high cost of the accelerator structure in ATP, the cost of accelertaor of accelerator structure is more than 10 times of the cost of RF generator for 15 mA beam current.

The cost in US M $ (conversion ratio of 150 ¥ to 1 $) of the segmented cyclotron is shown in the column (a). The cost of accelerator structure includes the cost of the magnet which is almost twice of the accelerator structure. In the column (b), the cost calculated by normalizing the cost of RF generator to that of the ATP (15mA accelerator) is shown.

8.6 Cost of small accelerator for incinerationr

When we use the cost data of the ATP, a substantial part of the cost of the accelerator incinerator comes from the accelerator portion even for a small beam power. However this incinerator produces a large excess of electric power, and also of the fissile material, Pu or U-233, by providing a blanket of fertile materials: this reduces the cost of incineration. When the high power accelerator is used for incineration, this system earns more momey by selling the excess electricity and fissile material.

For the incinerator in which 900 MW thermal heat generated by fissoning the minor actinide, the electric power generated is 300 MW. By subtracting from this value the electric power for running the accelerator of 15-30 MW beam power for

a target which has k=0.95-0.9, we get an excess production of electric power of 270- 285 MW.

At present, the electricity generated by a coal burning power plant is roughly 60 mil / KWH; thus, this excess electric power corresponds to 114 M$. At least 100 kg of the fissile material of Pu or U-233 is produced (which can be easily increased by optimizing the reactor design.) Earning from this production of the order of 5 M $, at price of 50$/gr of fissile material.

If we use the accelerator power of 300 MW beam, we can incinerate 20 times that of the previous case when we use the target with k=0.95; the earnings from selling the electric power becomes 2.3 B $ /year and the earnings from the production of fissile material becomes 100 M $/year. These amounts are far more than the costs of the accelerator and target.

	Accelerator of ATP			Cyclotron	
Current (ma)	15	30	250	10	
Energy (GeV)	1.0	1.0	1.6	1.5	
YearM$		1989		1989	
Accelerator Structure	320	368.	991.	(a) 165	(b) 73.45
RF	27.6	55.2	738.8	62.	27.6
Total	348.	423.3	1729.7	227.	101.

Table 5.1 The Cost Estimation of ATP linac [At,90] and Segmented Cyclotron

9. Problem of Radiation hazard [Ia,88],[Mc,83]

In this chapter we discuss the problem of radiation hazard associated to the accelerator facility, which is somewhat different from that in conventional nuclear reactor plants. The target side may be similar to the nuclear reactor; however, the shielding problem in the direction of the high energy proton beam is unique , and does not correspond to the shielding of the nuclear reactor, so that we give a rather detailed description of this.

9.1 Proton energy vs shielding

Particle accelerators pose unique problems for health physics. The primary particle beam can produce radiation at enormous dose rates over small experimental areas. Moreover, the secondary radiation (bremsstrahlung, neutrons, scattered electrons and so forth) can create very high dose rates over large areas of the working area. Especially hazardous is the beam spill of the accelerator which is very important in maintaining the accelerator. When the beam spill is large, some remote control device might be required to reduce the area contaminated by beam spill. Some designs have been proposed to put the beam scrapper in the small area so that only in this region will the radiation level be high, compared to other areas.

Let us briefly describe the proton nucleus interaction relevant to the radiation hazard of the proton accelerator.

1) Elastic interaction region.

In this domain, protons of energy less than 6 - 8 MeV interact only by elastic scattering. The range of proton is quite limited; it is less than 1mm in most solid material and less than 1m in air. Only direct exposure to the primary beams must be prevented.

2) Inelastic interaction region above the neutron threshold energy.

If the incident particle has enough energy above 8 MeV to penetrate the coulomb barrier, the dominant inelastic process is the isotropic emission of neutron from the target nucleus up to about 100 MeV. The dose rate produced by evaporation neutron can be quite high. The need to attenuate, therefore, dominates the shielding requirements in this energy range.

3) Particle production region

In addition of evaporated neutrons, neutrons and protons will also be emitted in the forward direction at an energy which can be a significant fraction of the incident particle energy. In these collision processes, energy is transferred to or lost from the target material. If the incident particle energy is high enough, the emission of the cascade particle will peak more and more in the forward direction. When the energy of the incident proton exceeds about 140 MeV, pion and other particles can be produced which must also be managed.

Because so many particles are produced in the forward direction, shielding must be more extensive along the direction of beam. For example,muons produced by the decay of pions in flight are very penetrating especially at energies greater than a few GeV.

9.2 LAMPF facility

Before discussing the detailes of the shielding problem, we present a example of LAMPF facility, because this facility is close to our accelerator incinerator.

The Clinton P. Anderson Linear Accelerator Meson Physiscs Facility, (LAMPF) is operated by the Los Alamos National Laboratory. (fig.2.1 is overview of the facility). The main facility (Fig.2.2) is a high intensity linear accelerator (linac) producing proton beams of energy 800 MeV at an average current of up to 1 mA, variable energy (300 to 800 MeV) H^- beams at up to 10 m A average current, or variable energy polarized H^- beams up to 10 nA average current. The

accelerator is pulsed at a repetition rate of 120 Hz, with a duty factor of from 6% to 9%.

LAMPF consists of three stages. The first stage comprises three accelerator systems, an injector that produces high intensity H+ and low intensity H- or polarized H- beams. Two beams are accelerated on alternate half cycles of the RF field in the subsequent second and third stages of the accelerator.

The second stage is a drift-tube-type linac, 62 m long that accelerates the beam to 100 MeV.

The third stage is a side coupled waveguide type accelerator that accelerates the proton beam up to 800 MeV: its length is about 685 m. Poured concrete, compacted earth and/or steel and concrete slabs and blocks are used as radiation shielding for the accelerator, beam switch yard, target, beam stop, and the experimental area. Drift tube linac channel is shielded by concrete walls and by a roof varying in thickness from 0.6 m at the low energy end, to 1.5 m at the 100 MeV end. The side-coupled waveguide section and the beam switchyard are in a tunnel about 9 m underground. Access to the beam channel is controlled by locked and interlocked doors, and by gates.

* Induced radioactivity.

The intense primary proton beams, secondary pion and neutron beams, and scattered particles induce radioactivity in the accelerator and target components, shielding and nearby equipment. Surface contamination is not as serious as the induced activity. Because the major part of the activity is within solid materials, careful surveillance and control is required during maintenance activities. Also, the cooling water system and the air surrounding the targets and beam stops have considerable amounts of induced activity. The activity in the cooling water systems is controlled by passing part of the circulating water through the deionization columns. This process removes most radio-nuclides except tritium, which can be removed from the system by evaporation. In case of leaks, a drain system is provided that is connected to two 2500 gallon underground storage tanks. The liquid in the tanks can be pumped out and disposed of. This process depends on an analysis of the radio-activity of the liquid. Radio-activity in the air consists primarily of C-11, N-13, O-15 and a little Ar-41,which have a relatively short half-life. These activities are exhausted to the atmosphere through a ventilation stack. The gaseous and particulate effluent are continuously monitored.

9.3 Rutherford Appleton Laboratory (RAL) high intensity spallation neutron source.

Another facility close in design to the accelerator incinerator is RAL the 800 MeV proton synchrotron facility. The main feature of the spallation neutron source is a high intensity 800 MeV rapid cycling proton synchrotron, which delivers high energy protons on to a depleted uranium target. The main parameters of this neutron source are given in Table 3.1 [Bo,85]

Fig 3.1 is a general view of the facility, consisting of three accelerators, beam transport systems, and a target station. Important aspects of radiation protection are the shielding of the accelerator and the target station, personnel protection, the radioactivity induced in the accelerator, beam transport components and target, and the environmental impact.

Shielding the 800 MeV synchrotron is largely achieved by using an existing building formerly designed to house a 7 GeV weak focusing proton synchrotron (Nimod).

Additional local shielding is added beam scrappers, which are regions of controlled localized beam loss. Fig. 3.2 shows a schematic view of the target, and Fig.3.3 shows the configuration of shielding. Along the 800 MeV proton beam transport line, The approximate steel equivalent shield thickness varies from 2.2 m to about 5.5 m in a the forward direction.

Calculations show that dose equivalent rates of induced radioactivity are to be expected are 0.01- 0.1 $Sv.h^{-1}$ (1-10 rem h^{-1}) at a regions of localized beam loss around the accelerator . Remote handling systems for accelerator maintenance are required at these levels.

Table 3.1 . MAIN DESIGN PARAMETERS OF SNS

Final proton energy	800 MeV
Proton pulse repetition rate	50 Hz
Injection energy	70.44 MeV (H^- ions)
Proton intensity per pulse	2.3×10^{13}
Extracted proton pulse duration	0.4 μs
Average neutron production rate	$3 \times 10^{16}\ s^{-1}$

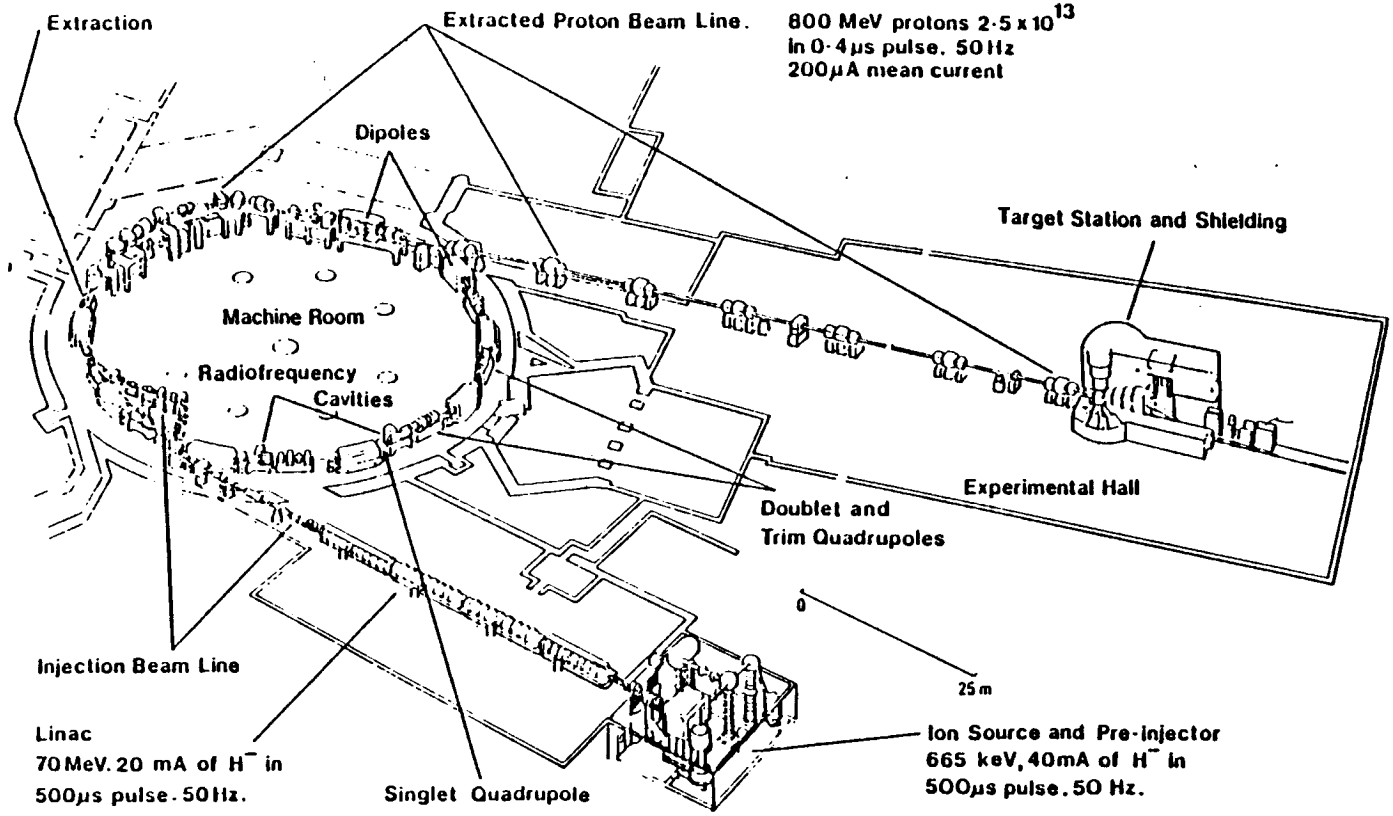

Figure 3.1 *General view of the synchrotron facility at the Rutherford Appleton Laboratory; major parameters of the three accelerators are also shown.*

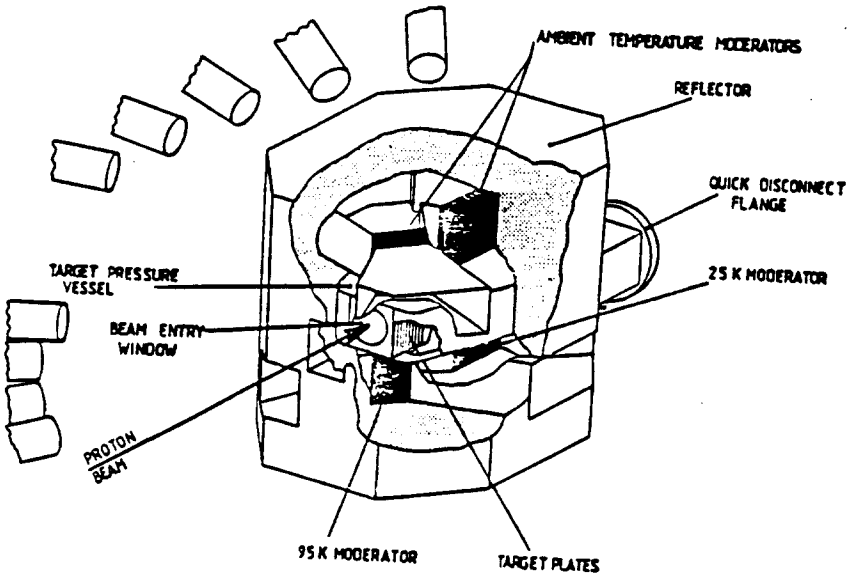

Figure 3.2 *Target assembly with four wing moderators.*

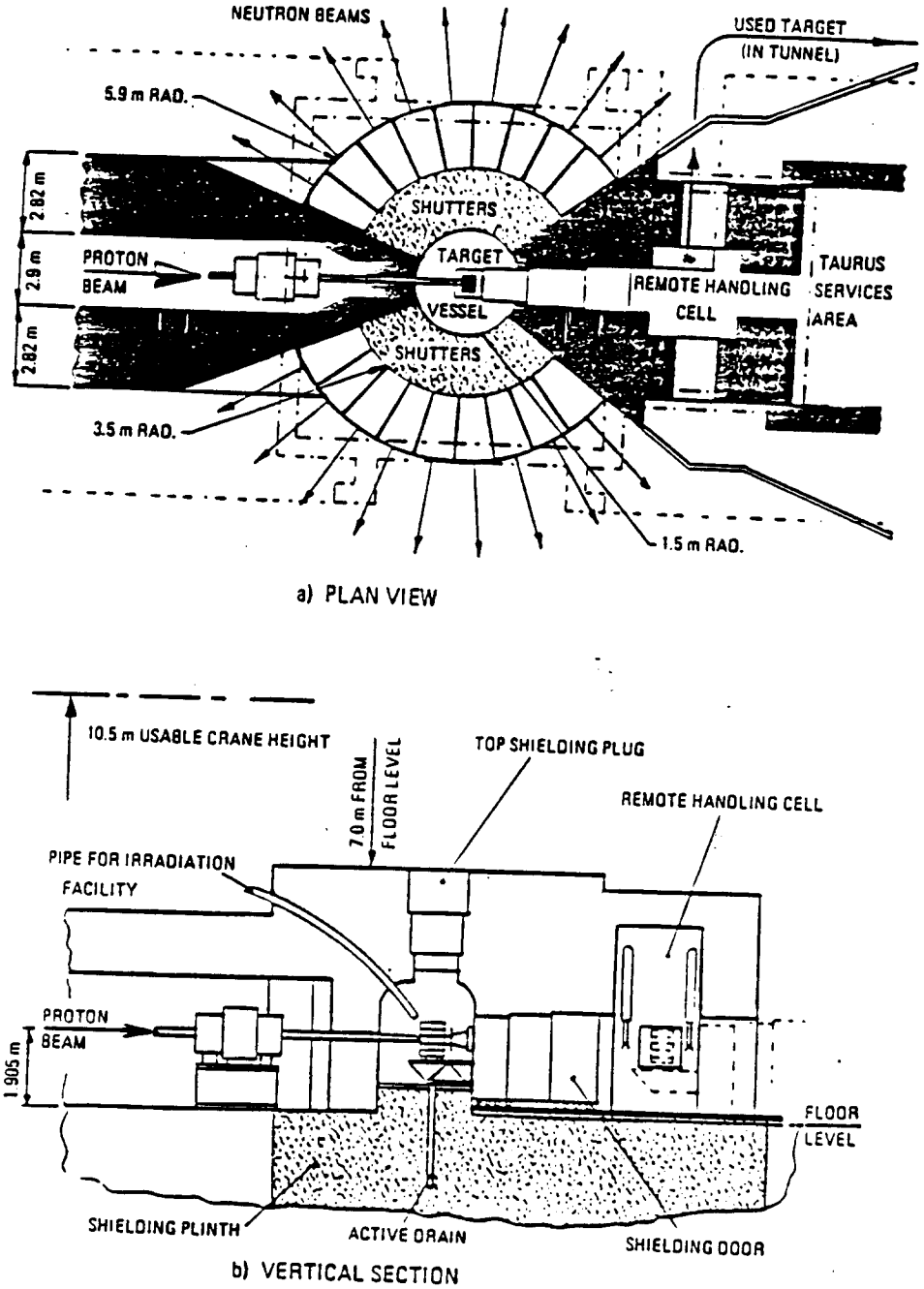

Figure 3.3 *Target station block shield schematics (SNS).*

After six months irradiation by the 200 μ A proton beam, the U-238 target has a total saturated inventory of activity of the order of 7x 10^{15} Bq (200 KCi); one day after shutdown, the targets will contain 1 x 10^{14} Bq (3 k Ci) of I-131. Remote handling equipment will be needed to work with the irradiated target, surrounding hardware, and shielding.

9.4 Shieldiing

Efficient accelerator shielding designs can be achieved by:
(1) Determination of the source term.
(2) Specification of the required dose equivalent levels outside the shielding (dose equivalent limitations).
(3) Design of a shield with adequate attenuation to achieve the required dose equivalent limits.

Operational considerations may impose an upper limit to the source strength. For example, accelerator elements are destroyed or damaged when the incident protons are an high intensity. In some cases, such damage becomes "catastrophic", for example, an accelerator using a super-conducting magnet that is quenched as a result of excessive power input during the beam loss, or in the case of the physical destruction of a target, or the piercing of the vacuum chamber. There are also 'chronic beam losses' that degrade the magnet's insulation by radiation damage. This results in down-time for the necessary repaire to the accelerator.

The radiation environments outside accelerator shield are usually dominated by the radiation from particles which have no electrical charge or which interact weakly with nuclear matter- photons, muons and neutrons. It is often necessary to consider the production and transport of many other radiations such as kaons, pions, and protons, because they also contribute to production of photons, muons and neutrons outside the shield.

The number of particles increases as the energy of the accelerated particles is increased. Below about 500 MeV, it is sufficient to take into account the production of neutron and photons by the first interaction of the charged particle and the transmission of both components through the shield.

At energies above 500 MeV, the development of the hadronic cascade becomes increasingly complex and the production of pions (and even kaons) must be taken in account.

At energies above 10 GeV, muons become of increasing concern until in the 100 GeV region they can dominate some radiation environments Because of the increasing complexity of the hadronic cascade as energy increases,it is necessary to have sophisticated computational method for studing the shielding.

4.1 Shielding at proton energies energy less than 3 GeV

The principal concern in shielding proton accelerators of less than about 3 GeV in energy is the neutrons produced by the high energy proton. Most of the published experimental and theoretical data in this energy range concerns neutrons whose energy is less than 400 MeV . Consequently our principal consideration will be given to proton accelerator shielding below that energy level.

It is difficult to treat theoretically the energy region between 400 MeV and 3 GeV because the hadron cascade process has not then stabilized. Experimental data are scarce,so we have to resort to interpolation from data between 400 MeV and the ' high energy limit' achieved at proton energies several GeV.

At proton energies above 3 GeV, the lateral shielding and to some extent, the longitudinal shielding may be dominated by simple models. At these higher energies (above 3 GeV) simplification is possible because the attenuation length of high-energy neutrons is independent of neutron energy above 100 MeV, and the yield of high energy neutrons is roughly proportional to the primary proton energy E_p. Below 1 GeV neither of these simplifications may be made: hadron cross-sections change rapidly with energy and particle yields and no longer even are approximately proportional to E_p.

* Particle yields from the proton-nucleus interaction

Tesch[Te,85] reviewed the published information on the total number of neutrons produced per proton interacting in various target materials (C, Al, Cu, Fe, Sn, Ta and Pb) over the energy range from 10 MeV to 1.45 GeV [Te,85]. His summary is given in Table 4.1 , together with references to the original sources. These data suggest that, with sufficient accuracy, the ratios of the neutron yields from different target materials are independent of E_p in the range 20 MeV to 1 Gev and are given by:

C:Al: Cu-Fe: Sn: Ta-Pb

= (0.3±0.1): (0.6±0.2): (1.0): (1.5±0.4): (1.7±0.2)

For a detailed calculation of accelerator shielding more information is required than the total number of neutrons produced : in particular, the energy and angular distribution of the neutrons must be known. Two nuclear process are of importance in determining the yield following the proton- nucleus interactions namingly, nuclear evaporation, and intranuclear cascades.

* Transport of the mono-energetic neutron through shielding

Below 400 MeV, neutron transport in the shielding can be treated by the standard method of solving the Boltzman transport equation, especially by the method of spherical harmonics, the method of discrete ordinates, and the Monte Carlo method. Studies by O' Brien and Alsmiller et al. have shown that these methods give essentially equivalent results [OB,70, Al,69a].

Discrete ordinate calculations of the penetration of neutrons in broad beam geometry through concrete in the energy range from 50 to 400 MeV were reported by Alsmiller et al [Al,69b], and from 1 to 100 MeV by Wyckoff and Chilton [WY,73]. Comparison of these two sets shows agreement; both sets also agree with the calculation of O'Brien, using the spherical harmonic method[OB,70].

These three sets of calculations may be parametarized using an simple exponential function of the form:

$$H(z) = k_0 \exp(-x/\lambda) \qquad (4.1)$$

where H(z) is the dose equivalent at depth x in the shield,

λ is the attenuation length, and

k_0 is the extrapolation dose equivalent at zero depth.

Figs.4.1 and 4.2 show the parameters λ and k_0 as function of neutron energy.

There are surprisingly few published data on the attenuation of neutron in the forward direction at beam energies below 1 GeV. Paterson described some early shielding studies for 90 MeV neutrons[Pa,57], suggesting that the attenuation length λ was approximately given by the well-known relation [Pa,73].

$$\lambda = 1 \,/\, N\, \sigma_{inel} \qquad (4.2)$$

where σ_{inel} is inelastic cross- section of the shield material.

Theoretical studies suggested that , at least for high energies, the effective attenuation length λ_{eff} would, in fact, be somewhat greater than that predicted by Eq.(4.2). The experience of Sychev et al. [Sy,66a,b] at Dubna suggested that for broad beam geometry in the energy range between 350 MeV and 660 MeV the attenuation length was given by :

$$\lambda_{att} = (1.3\pm0.1)\ \lambda_{inel}. \qquad (4.3)$$

The results of thin- and thick-copper target calculations for a concrete (ρ= 2.4 g cm^{-1}) shield are summarized in Figs. 4.3 and 4.4.

4.2.* Shielding of proton accelerators at energies greater than 3 GeV.

At proton energies about 3 GeV, calculation of the hadronic cascade is important to determine the shield thickness of the proton accelerator, while above 10 GeV, the production of muons must be taken into account for specifying

Table 4.1 NUMBER OF NEUTRONS PRODUCED PER PROTON FOR DIFFERENT TARGET MATERIALS
(some values have been slightly adjusted by interpolation) (from Tesch [Te 85])

	Neutrons per incident proton				
E_p (MeV)	C	Al	Cu, Fe	Sn	Ta, Pb
10			1.2×10^{-3}	1×10^{-3}	2×10^{-4}
20	1.1×10^{-3}	2×10^{-3}	4×10^{-3}	1.3×10^{-2}	2.4×10^{-3}
30	1.1×10^{-3}		1.1×10^{-2}		2×10^{-2}
			1×10^{-2}		1.7×10^{-2}
40	6×10^{-3}	1.5×10^{-2}	4.3×10^{-2}	4×10^{-2}	
50	7.6×10^{-3}	2×10^{-2}	2.2×10^{-2}		3×10^{-2}
			3.3×10^{-2}		6.6×10^{-2}
60	1.6×10^{-2}	3×10^{-2}	8×10^{-2}	9×10^{-2}	1.2×10^{-1}
70			5.5×10^{-2}		
100	3.6×10^{-2}	1.0×10^{-1}	1.8×10^{-1}	2.3×10^{-1}	2.1×10^{-1}
	3×10^{-2}	1.1×10^{-1}	1.6×10^{-1}		3×10^{-1}
					3.4×10^{-1}
200	1.9×10^{-1}	4×10^{-1}	1.0	1.2	1.2
	2×10^{-1}	4×10^{-1}	6.5×10^{-1}		1.2
					1.5

250					2.3
					2.5
300					3.0
400					6.0
500	1.0	1.6	2.7		4.7
					7.0
					8.5
550		1.8			10
					7.4
700				7.5	14
					11
800		3.1			16
					14
					13
1000	2.0	3.2	6	11	11
		3.1			20
					17
1450				17	32

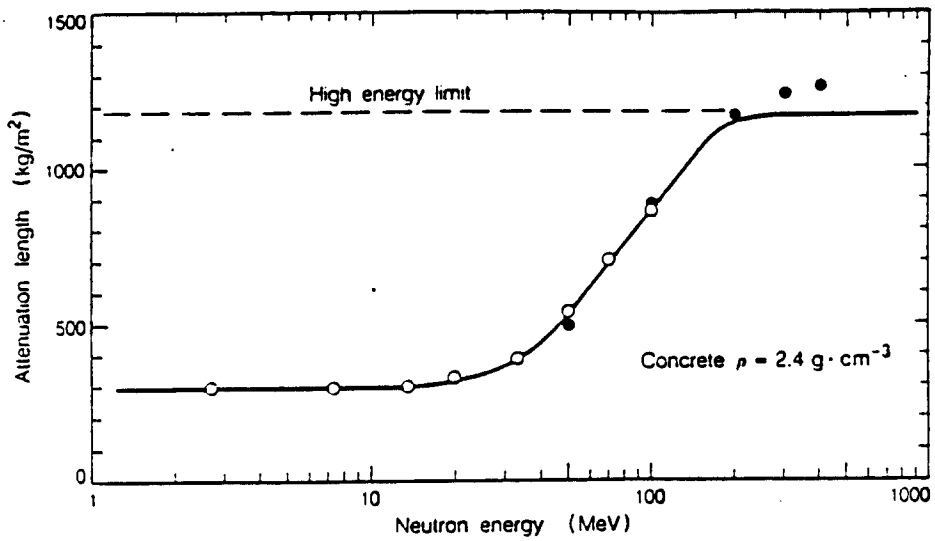

Figure 4.1 *The variation of the attenuation length λ for monoenergetic neutrons in concrete as a function of neutron energy. Full circles indicate the data of Alsmiller et al., , open circles those of Wyckoff and Chilton, . The solid line shows recommended values of λ and the dashed line shows the high energy limiting value of 1170 kg·m⁻².*

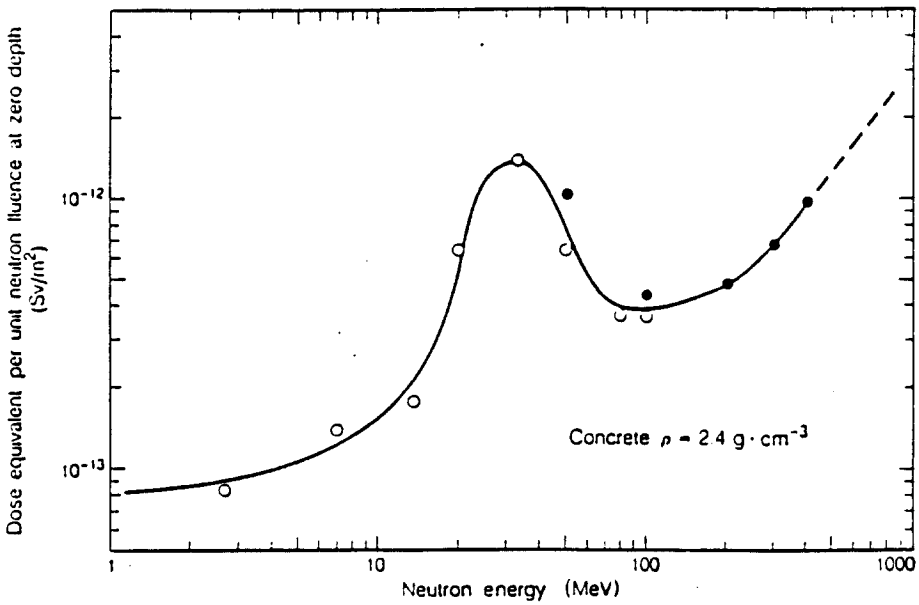

Figure 4.2 *The variaton of the parameter k_0 as a function of monoenergetic neutron energy; k_0 is the value of the dose equivalent per unit neutron fluence extrapolated from deep in the shield back to zero depth. Full circles indicate values calculated by Alsmiller et al. open circles indicate values calculated by Wyckoff and Chilton. The solid line indicates recommended values of k_0.*

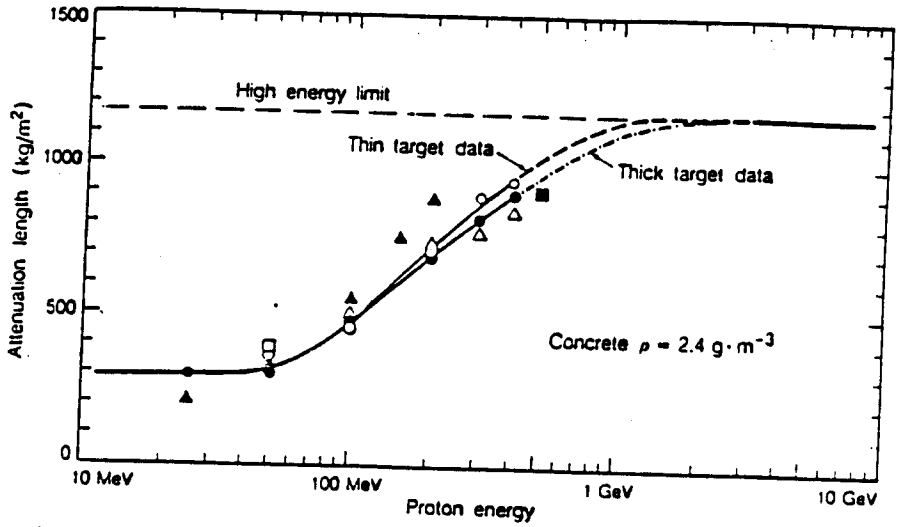

Figure 4.3 *Effective attenuation length in concrete as a function of proton energy. Open circles are the thin target data, closed circles are the thick target data, Δ — data of Ban et al., □ — data of Allen and Futterer reported by Patterson and Thomas*

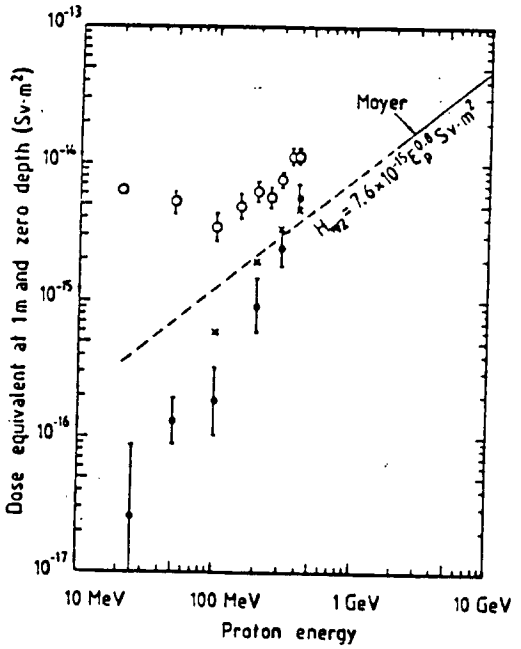

Figure 4.4 *The parameter $H_{+/2}$ as a function of proton energy. Open circles are the thin target data, closed circles are the thick target data. The solid line above 3 GeV indicates the high energy Moyer parameter. The dashed line, where the Moyer model is no longer valid, is indicated merely to guide the eye.*

shielding in the forward direction. Fairly detailed reviews of the early shielding studies in the GeV energy region are given in the references of [Li,61, Pa,71, Pa,73, Ri,73].

Design of beam stop (E > 3 GeV)

In the specifications for shielding the end stop, two separate contributions must be taken into account. The first is that from the hadron cascade itself; this process is always dominant at proton energies less than 10 GeV. The second is the contribution from muons generated by the decay of pions and kaons in the cascade and from the processes of direct production in proton-nucleus interactions. Lindenbaum [Li,61] explained the early experiments in terms of neutron inelastic cross-sections and showed that for narrow-beam geometries, the attenuation length is identical to the inelastic mean free path.

The simple analytical one-dimensional description of Lindenbaum [Li,61] provides a qualitative but instructive analytical treatment of the hadron cascade in the shield.

Figs.4.5 and 4.6 show the variation of dose equivalent along the proton beam axis calculated using the Monte carlo codes of CASIM [VB,71],[VG,71], FLUKA82 [AA,84],[Ra,85] and TRANKA [Ra,67] for which short summaries are described in section 9.10. Data are presented on concrete and steel for proton momenta from 1 GeV/c to 1 TeV/c. For concrete , there appears to be reasonable agreement between the data calculated by the FLUKA 82 and CASIM codes at the depth where there is overlap of about 5 m, and moderate agreement between the CASIM and TRANKA data to within about a factor of four at depth of 14 m. However, for steel a serious discrepancy is observed. The CASIM data are a factor of four higher than those from FLUKA82 and the CASIM and TRANKA data differ by more than three orders of magnitude. Similar discrepancies between the results of the calculations are also observed in the case of transverse shielding.

Figs.4.7 and 4.8 show the dose equivalents corresponding to the longitudinal maxima of the star density contours of Van Ginnenken and Aweschalom, multiplied by the square of the radius, as a function of radius for iron and concrete shields respectively.

9.5 Skyshine

A common weak point in accelerator design has been thin " roof " shielding. As a result, skyshine (air scattered) neutrons commonly contribute significantly to the radiation dose in uncontrolled areas. Measurements have verified that mathematical models used to calculate doses of neutron skyshine are in good agreement up to about 200 ft. However, at distance of half a mile or more, the various model may disagree by at least an order of magnitude. At large distances, dose rates are simply too low to measure any degree of accuracy.

A summary of the skyshine phenomenon around the accelerators was discussed by Rindi and Thomas, who reviewed experiences up to 1975. Neutrons are the dominant component of skyshine, and Fig 5.1 shows measurements of neutron flux density versus distance taken at several accelerators. It can be concluded from the data that the empirical relation of

$$\phi(r) = q \exp(-r/\lambda)/ 4\pi r^2 \qquad (5.1)$$

is a simple but adequate expression for skyshine intensity around most accelerators, where r is the distance from the accelerator enclosure, q is an effective source strength of neutrons emitted from the shield surface, and λ is an effective absorption length.

In practice, the value of λ observed between 267 m and 990 m .

9.6 Total radioactivity

The total quantities of radioactivity produced in an accelerator structure may be related to the total number of inelastic interactions produced by a proton in the materials of interest.

A simple, approximate relationship between the total saturated activity

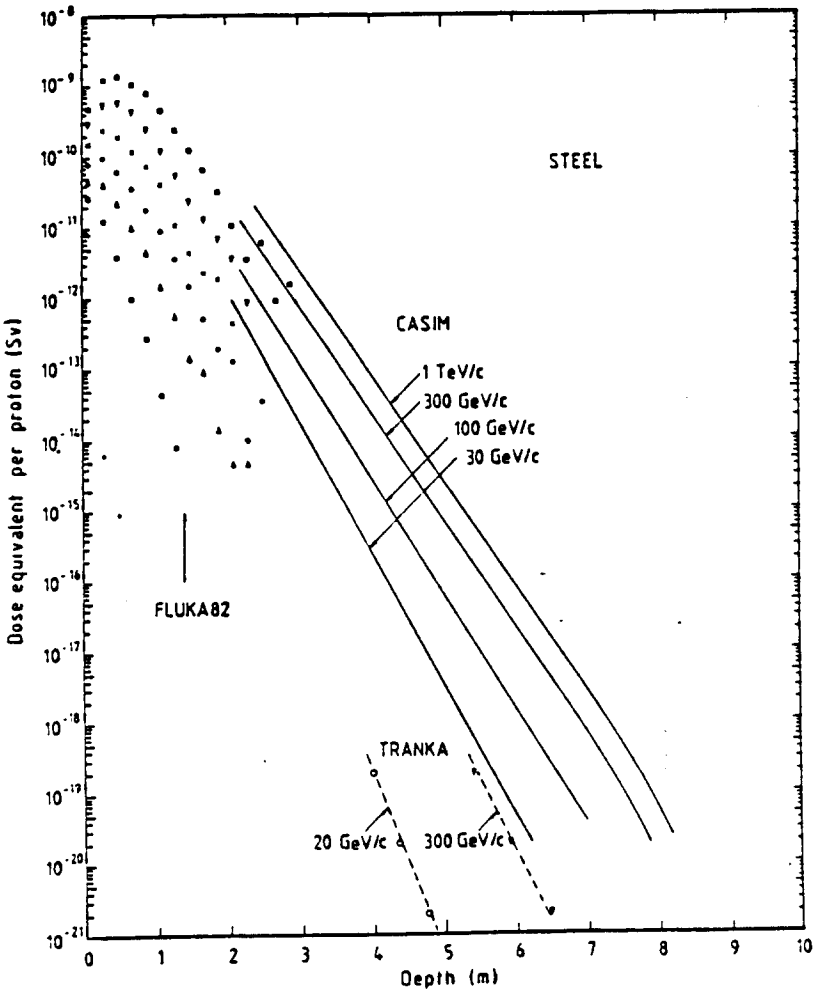

Figure 4.5 *Variation of the dose equivalent on the longitudinal axis as a function of depth in the shield for proton induced cascades in steel of density 7.88 g·cm^{-3}. The FLUKA82 calculations are for incident proton momenta of 1 GeV/c (+), 3 GeV/c (solid square), 10 GeV/c (open triangle), 30 GeV/c (solid circle), 100 GeV/c (×), 300 GeV/c (solid inverted triangle) and 1 TeV/c (open square). The solid lines correspond to the results of CASIM calculations at the marked proton momenta. The dashed lines are fits by eye through the TRANKA points for proton momenta of 20 GeV/c (o) and 300 GeV/c (open inverted triangle).*

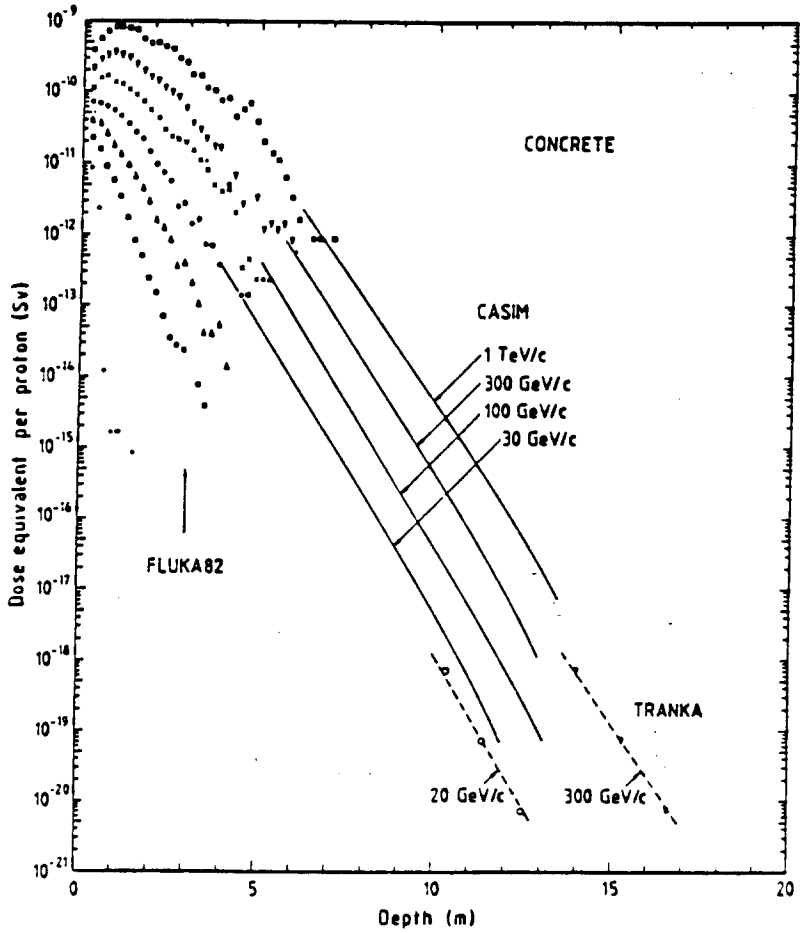

Figure 4.6 *Variation of the dose equivalent on the longitudinal axis as a function of depth in the shield for proton induced cascades in concrete of density 2.4 g·cm^{-3}. The FLUKA82 calculations are for incident proton momenta of 1 GeV/c (+), 3 GeV/c (solid square), 10 GeV/c (open triangle), 30 GeV/c (solid circle), 100 GeV/c (×), 300 GeV/c (inverted solid triangle) and 1 TeV/c (open square). The solid lines correspond to the results of CASIM calculations at the marked proton momenta. The dashed lines are fits by eye through the TRANKA points for proton momenta of 20 GeV/c (o) and 300 GeV/c (inverted open triangle).*

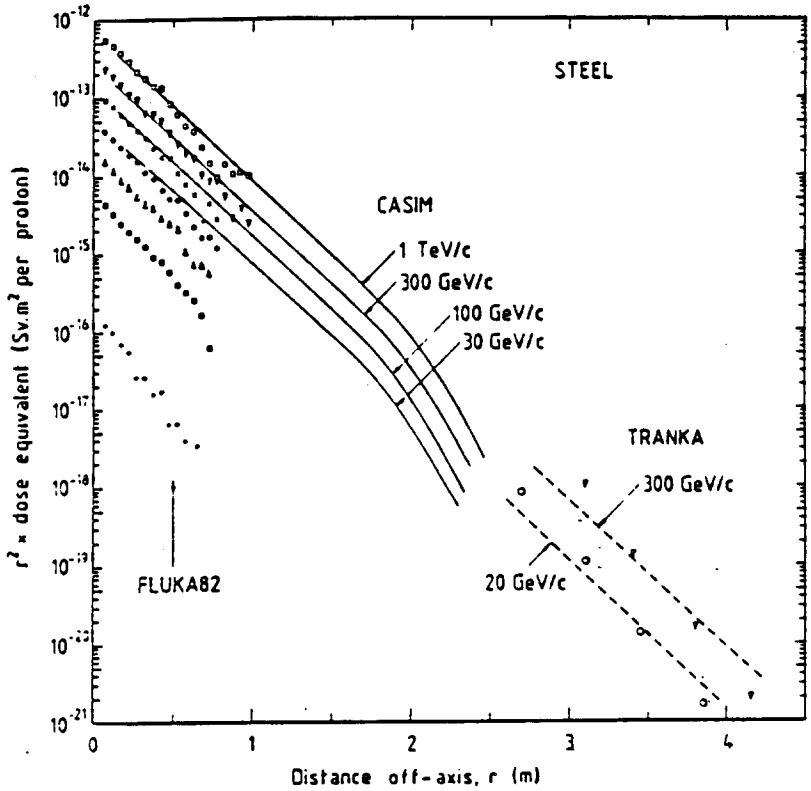

Figure 4.7 *Variation of the dose equivalent at the position of the longitudinal maximum multiplied by the square of the radius as a function of radius off-axis for proton induced cascades in steel of density 7.88 g·cm^{-3}. The FLUKA82 calculations are for incident proton momenta of 1 GeV/c (+), 3 GeV/c (solid square), 10 GeV/c (open triangle), 30 GeV/c (solid circle), 100 GeV/c (×), 300 GeV/c (inverted solid triangle) and 1 TeV (open square). The solid lines correspond to the results of CASIM calculations at the marked proton momenta. The dashed lines are the extensions of the CASIM lines of 30 GeV/c and 300 GeV/c through the TRANKA points for proton momenta of 20 GeV/c (o) and 300 GeV/c (open inverted triangle).*

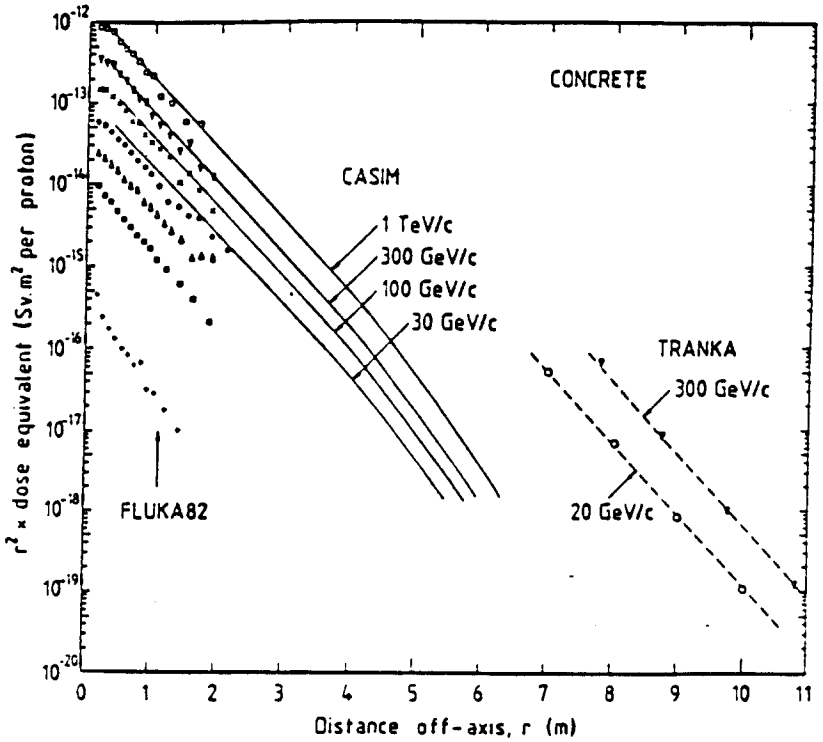

Figure 4.8 *Variation of the dose equivalent at the position of the longitudinal maximum multiplied by the square of the radius as a function of radius off-axis for proton induced cascades in concrete of density 2.4 g·cm^{-3}. The FLUKA82 calculations are for incident proton momenta of 1 GeV/c (+), 3 GeV/c (solid square), 10 GeV/c (open inverted triangle), 30 GeV/c (solid circle), 100 GeV/c (×), 300 GeV/c (inverted solid triangle) and 1 TeV (open square). The solid lines correspond to the results of CASIM calculations at the marked proton momenta. The dashed lines are best fits by eye using an effective absorption mean free path of 1170 kg·m^{-2} through the TRANKA points for proton momenta of 20 GeV/c (o) and 300 GeV/c (open inverted triangle).*

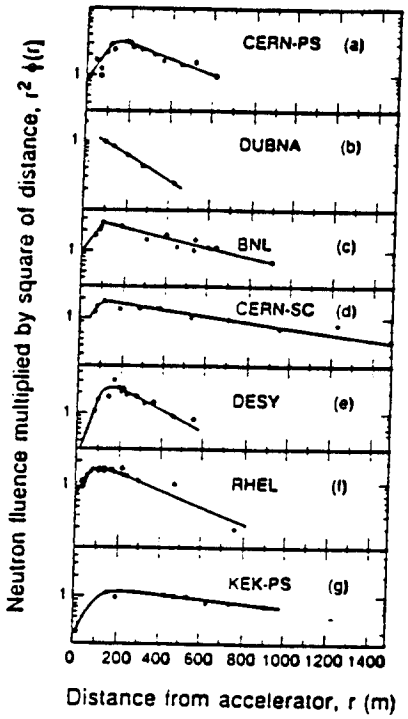

Figure 5.1 *Measurements performed around various accelerators. On the abscissa is the distance from the accelerator in metres; on the ordinate is the product of the measured neutron flux density and the square of the distance. In these co-ordinates, a $1/r^2$ variation is represented by a horizontal line. (a) Measurements of fast neutron flux density performed at the CERN 28 GeV proton synchrotron (b) measurements of fast neutron flux density performed at the Dubna 10 GeV proton synchrophasotron (c) measurements of dose equivalent rate performed at the Brookhaven 30 GeV proton AGS (d) measurements of the fast neutron flux density performed at the CERN 600 MeV proton synchrocyclotron (e) fast neutron flux density measurements performed at the DESY 7.5 GeV electron synchrotron (f) fast neutron flux density measurements performed at the Rutherford Laboratory proton linear accelerator (g) measurements made at the 12 GeV proton synchrotron at KEK*

(A_{sat}) and the value of inelastic interactions per second, N is expressed as:

$$A_{sat} = k\ N \qquad (6.1)$$

where k is a constant to be determined.

The number of inelastic interactions in various materials may be studied as a function of proton energy using Monte Carlo simulations of the hadron cascade induced by the protons in the semi-infinite medium. Table 6.1 gives the results using the program FLUKA82 [AA,84] for protons of different energies incident on shields of oxygen and copper. The data show that the total number of inelastic interactions (stars) produced is not greatly dependent on the target material, but is approximately proportional to the incident proton energy. The mean number of stars per GeV will be taken to be 2.9.

Equation (6.1) may be modified to :

$$A_{sat} = 2.9\ k\ E \qquad (6.2)$$

with E in GeV.

9.7 Radioactivity in earth and water

The radionucleides that can be produced by hadron-induced spallation interactions in the oxygen of the cooling water are given in Table 7.1 [Ch 78] together with half -lives and estimated production cross sections.

9.8 Beam loss problem

Earlier, we discussed the health physics problem associated with accelerator, the one of most imortant problem is the beam loss. This problem was discussed by D. Young [Yo,79] taking the example of the 300 ma in the Fermi lab 200 Mev linac.

He concluded that " I maintain that beam loss problems are serious concern in a high intensity, high-energy linac, but that it should be possible to limit beam loss so that " hands on " maintenance and repair of accelerator components can be performed".

R.A. Jameson [Ja,90] also studied the beam loss problem in the LAMPF and TPA accelerators. BY analyzing the experimental data of LAMPF accelerator (see Fig.8.1) ,he concluded that the hands-on maintenance can be retained by lowering the fractional loss /m in the case of ATP. (FIG.8.2).

The TPA LINAC is composed of two 350 MHZ,125 mA RFQs up to 2.5 MeV, with 350 MHz DTLs following them up to 20 MeV, and then funneling into a 700 MHZ, 250 mA coupled-cavity-linac (CCL) for acceleration to final energy of 1.6 GeV

Recently Russian group designed the linear accelerator for incineration reactor. According to their study, they concluded that it is possible to make a 300 mA 1.5 GeV proton linear accelerator which does not requires manipulator for their maintenance from the following reason.

A linear accelerator is considered to be radiation free if the induced γ-activity does not 28 μGy / hour. The corresponding level of beam losses amounts to

$$Wq = 1\ \text{GeV nA / m} \qquad (8.1)$$

Under this condition and with specific acceleration of 1 MeV / m in the second part of accelerator (i.e. 0.1- 1.5 GeV) the total permissible beam current loses amount to 3 μA. With the beam current of the 300 mA it leads to the permissible relative losses of about 10^{-5}. Radiation free can be achieved by using the methods of beam phase volume filtering, suppression of coherent longitudinal and transverse oscillations, contact-less beam parameter measurement, beam diagnostics through the beam loss measurement, and residual gas limitation in the H^- beam channel.

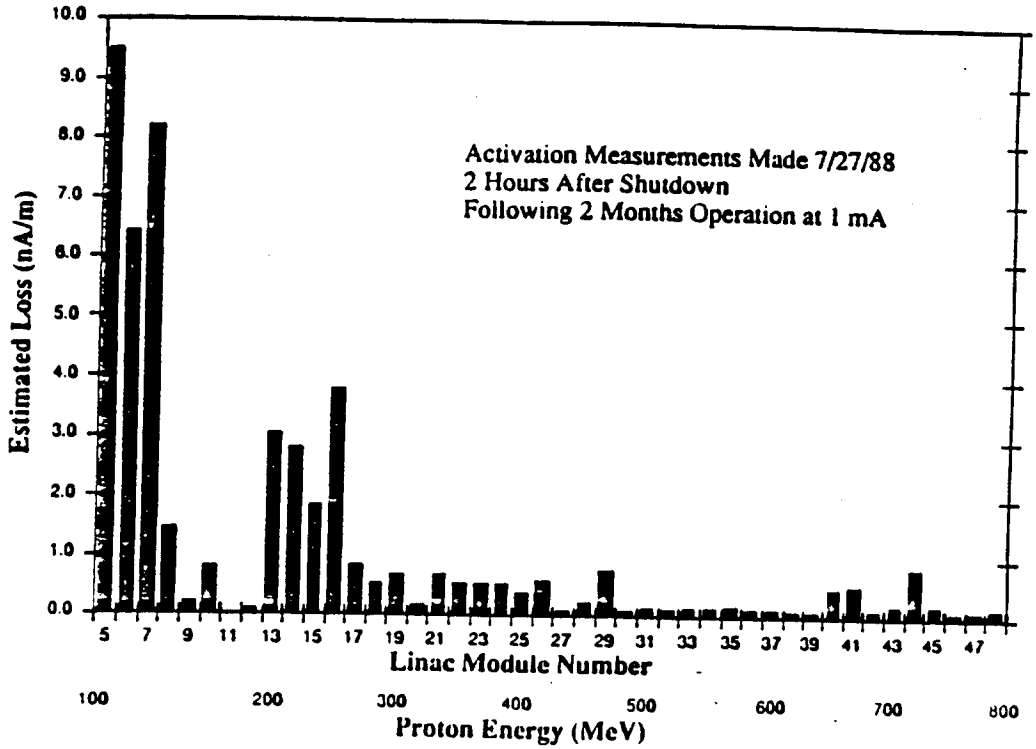

Figure 8.1 Estimated beam loss in LAMPF CCL for 1 mA average current operation.

	LAMPF	APT
Activation (mRem/h)	4*	100
Beam loss (nA/m)	0.2	5
Fractional loss /m	2×10^{-7}	2×10^{-8}
Aperture/beam RMS	6.3	20

* Except for a few hot spots

APT needs 10 times lower fractional loss /m than LAMPF to retain hands-on maintenance. A factor of 100 should be achievable.

* APT has factor of 2 to 3 advantage because it is not a pulsed machine.
* Need additional factor of 5 to 3 from large aperture/beam-RMS ratios. We believe that much larger factors will be attainable.

Figure 8.2 Actual beam losses, activation levels, and aperture/beam ratio for LAMPF, with estimate for APT linac.

Table 6.1 STAR PRODUCTION IN VARIOUS MATERIALS

Kinetic energy	Material			Stars/GeV
	Oxygen	Copper	Mean	
300 MeV	0.57	0.52	0.55	1.8
1 GeV	3.8	3.1	3.5	3.5
3 GeV	11.6	9.1	10.4	3.8
30 GeV	93	78	86	2.9
300 GeV	780	660	720	2.4

Table 7.1 SPALLATION PRODUCTS FROM ^{16}O

Isotope	Half-life $T_{1/2}$ (s)	Production cross-section σ (mb)	Ratio of atoms per star σ/σ_{inel} (%)	Beta decay	Gamma energies (MeV)	Gamma emission probability
^{10}C	19.1	4	1.4	100% β^+	0.717	1
					1.023	0.017
^{14}O	71.1	9	3.1	100% β^+	2.312	0.99
^{15}O	124	28	9.6	100% β^+	none	
^{13}N	600	5	1.7	100% β^+	none	
^{11}C	1220	10	3.4	100% β^+	none	
^{7}Be	4.60×10^{6}	9.3	3.2	100% EC	0.477	0.103
^{3}H	3.89×10^{8}	33	11.3	100% β^-	none	
^{14}C	1.81×10^{11}	1.9	0.65	100% β^-	none	
^{10}Be	5.05×10^{13}	0.9	0.31	100% β^-	none	

9.9 Other radiation sources

While the accelerator is the most obvious source of radiation at a facility, there can be others such as klystrons, experimental devices in other buildings, or RF tests. Other sources can be much harder to control because the health physicist may not know they exist, the way that the radiation is produced may not be understood or the experimenter or user may not recognize that a device produces radiation.

In general, whenever there is high voltage or RF power in a vacuum, x-rays can produced. This statement is true, even through there is no heated filament or some other obvious source of electrons.

9.10 Codes used for radiation shielding calculation due to high energy particle.

A) Nucleon Meson Transport code (NMTC) and High energy transport code (HETC)

These codes was described in detail in the previous section. For many years NMTC and HETC have been a benchmark for hadron code used in radiation physics and radiation protection. These codes are described in detail in the above sections. They originate from the Neutron Physics Group of the Oak Ridge National Laboratory. Descriptions of the code have been given by Armstrong and Gabriel[Ga,85], and operating instructions by Chandler and Armstrong [Ch,72].

The main feature of NMTC and HETC are their use of an intranuclear cascade plus evaporation model to determine the products (energy and angular distributions, and multiplicities) from non-elastic collisions. The earliest version of HETC was developed by Coleman [Co,68] ; the code, referred to at that time as NMTC, was essentially limited to the calculation of cascade induced by proton energies less than 3 GeV. Below 15-20 Mev , charged particle interactions were neglected and neutrons were transported using the O5R Monte Carlo program of Irving et al. [Ir,65]

HETC revised and extented this limitation of NMTC to beyond 3 GeV using an extrapolation model by Gabriel et al.[Ga,70, Ga,71a,b]. The earlier intranuclear cascade code of Bertini was replaced by his newer MECC-7 code[BE,69] and the evaporation part was replaced by the EVAP-4 code of Guthie [Gu,70].

Although an extremely powerful and flexible code, there is one major weakness and operational inconvenience in HETC, namely its treatment of collisions above 3 GeV by an extrapolation model. It would be preferable to incorporate a fundamental treatment of such high energy interactions.

B) Hadron cascade code (FLUKA)[AA,85],[Ra,85]

The FLUKA series of the hadron cascade code are based on the work of J. Ranft of CERN and the University of Leipzig. The first code became operational in 1965. These codes do not treat the intranuclear cascade and evaporation stages of the inelastic hadron-nucleus interaction as separate entities. Because the intranuclear cascade mostly contains particles below 1 GeV, it does not significantly affect the growth of the extranuclear hadron cascade for high energy incident particles. Additionally, particles below a cut-off energy of 50 MeV are not transported. Macroscopic physical quantities, such as the density of inelastic interactions or the density of deposited energy as a function of position in the cascade are available as standard output options. Other physical quantities are available through user written subroutines. The earliest versions of the program were restricted to single medium problems in cylindrical geometry. The latest versions allow multimedia and a variety of geometry options.

In the earliest version, called TRANKA [Ra,67], the products of the inelastic hadron-nucleus interactions were generated from the Trilling representation of the inclusive production cross-sections [Tr,66]: Kaon production in these interactions was ignored . In addition, particle splitting was introduced in an attempt to improve the statistical accuracy of deep penetration problems.

In recent years, FLUKA has been completely rewritten but with most of the physics characteristic being maintained [AA,84,Ra,85].

The new program is called FLUKA 82. This program works with multiregion, multimaterial geometry. Cylindrical, cartesian, spherical and combinatorial geometry options are available. The old inelastic event generator from the earlier programs has been maintained as an option (EVENTI), but a new event generator (EVENTQ) is now the standard default option. This new generator is based on measured exclusive particle production cross-sections below 5 GeV and on a dual multi-string fragmentation model for particle production above 5 GeV to about 10 TeV .

C) Cascade simulation program (CASIM)[VB,71],[VG,71]

The Monte Carlo program CASIM was developed by Van Ginneken at the Fermi National Accelerator Laboratory. CASIM simulates the average behavior of cascades developed by high-energy hadrons (10-1000 GeV) in targets of large dimensions. It is a weighted Monte Carlo program: only one high energy secondary is generated per collision, but this carries with it a weight related to its probability of production. Path length stretching and particle splitting have also been used.

High energy secondary particle production uses the Hagedon Ranft thermodynamical model [Ra,70], and the production of intranuclear cascade particles is based on the same equations as those used in FLUKA82 [Ra,85]. The macroscopic physical quantities available as standard output from the program include inelastic interaction (star) density and energy density as a function of position in the cascade. Particle fluxes, etc., can also easily be made available by the program.

10. Conclusion and Recommendation

In this paper, we described the several theoretical models which have been used for studying the accelerator breeder. The accelerator MA incinerator using the fast neutron is similar to the accelerator breeder.

At present, almost no nuclear data available for minor actinide, To study the accelerator actinide incinerator, the theoretical model used for studying the accelerator breeder with the U-238 target was used. However, the nuclear data for U-238 are also scarce and considerable uncertainty exist in the wide spread of experimental data for neutron yield and a fission cross section as discussed above.

It is highly recommended to make measurement of the neutron yield and neutron spectrum measurement for both uranium or plutonium thick and thin target, and to make the highly reliable theoretical model to simulate medium energy proton reaction for actinde materials.

The activity to measure the neutron yield from the depleted uranium target by Vasilkov's group are going on at Dubna, They are measuring the detailed neutron spectrum for various injecting energies of p, d, t and He particles. The theoretical models which has been used for this study can be certainly improved together with the more microscopic data analyzing this experimental data.

For the shielding problem of the target, the bump observed in the neutron spectrum should be studied to make a more predictable theoretical model.

At present, the neutron yield caused by injecting the medium energy of proton into minor actinide can be estimated in the error range of ±20 %. Thus we can make an approximate evaluation of the concept of an accelerator minor actinide incinerator.

As discussed in the section of the cost analysis, the linear accelerator is more economical for high power accelerator of 300- 400 MW. The high power accelerator has too much excessive power to incinerate the actinide with the target which is near critical. By using the beam of H^- instead of proton, the beam can be easily segmented into many small beams before injecting the incinerator targets by using the foil or gas target. Thus this high power accelerator can economically run many subcritical actinide targets.

Recently a metal fuel fast reactor has been studied extensively at ANL. This has many interesting feature such as small reactivity change from initial phase to final phase in one burn up cycle. Because of this small reactivity change, the sub-criticality of the target can be maintained close to near criticality, and it makes a proton beam current small and can alleviate a radiation damage problem associated with medium energy proton. Furthermore it makes the power distribution flat and can reduce the power peaking factor. By providing a external neutron created by small intensity proton beam to the subcritical fast reactor, it can be operated more safely and makes more flexible choice of structural and fuel materials to get higher breeding gain.

We described the code relevant to design and simulation of transmutation of actineide by spallation. Since this concept is rather new, only the preliminary design has been carried out, thus the code for engineering has not been published yet. Thus, instead of describing this engineering design code, the cost estimation of accelerator for incineration and the problem of radiation hazard are added.

Finally, we would like to emphasiz that this alternative approach to solve the disposal problem of high level waste is still infancy stage, and it is required to detailed study of not only incinerate the MA nuclei and also transmuting the long lived fission products such as Sr-90, Tc-99 and Cs-137.

Ackowlegement

The author would like to thank Drs. F.Atchison, G.J.Russel, F.S. Alsmiller, R.G.Alsmiller, T.Mukaiyama, Y.Nakahara, T.Nishida, R.E.Prael, H.Takano, G.H.Stevens, Umezawa for providing him the valuable informations for writing this report.

References

[AA,68] T.W. Armstrong and R.G. Alsmiller, Jr.: Nucl. Sci. Eng. 33, 291 (1968).

[AA,69] T.W. Armstrong and R.G. Alsmiller, Jr.: Nucl. Sci. Eng. 38, 53 (1969).

[AA,71] R.G. Alsmiller, Jr., T.W. Armstrong, and B.L. Bishop: Nucl. Sci. Eng. 43, 257 (1971).

[AA,84] P.A.Aarnio J.Ranft,G.R.Stevenson:" A long write-up of the FLUKA82 Program', Rep. TIS-RP/106-Rev,CERN,Geneva (1984).

[AC,72] T.W. Armstrong and K.C. Chandler: "HETC, Monte Carlo High Energy Nucleon Meson Transport Code," ORNL-4744 (1972).Nucl. Sci. and Engr. 49, 110 (1972).

[AF,81] T.W.Armstron and D.Filges " A comparison of high energy fission models for the HETC transport code ,ICANS-V. (1981)

[Ai,84] J. Aichelin, and J.Huelfner Phys. Lett. 136B 15 (1984))

[Al,69a] Alsmiller. Jr., et al. " High energy (< 400 MeV) neutron transport using the method of discrete ordinate . Nucl. Sci. Eng. 36 251, (1969)

[Al,69b] Alsmiller. Jr., et al. " Shielding against neutrons in the energy range 50 to 400 MeV, Nucl. Instrum. Methods 72 , 213 (1969).

[Al,81a] R.G. Alsmiller, Jr., et al.: "Neutron Production by Medium Energy (~1.5 GeV) Protons in Thick Uranium Targets", Oak Ridge National Laboratory, ORNL-TM-7527, January 1981.

[Al,81b] F.S. Alsmiller, et al.: "A Phenomenological Model for ParticleProduction from the Collision of Nucleons and Pions with Fissile Elements at Medium Energies," ORNL-TM-7528 (1981).

[AM,86] E.D. Arthur, D.G. Madland and D.M. McClellan: "Bibliographic Survey of Medium Energy Inclusive Reaction Data," LA-10699-MS (1986).

[AN,67] ANISN Multigroup one dimensional discrete ordinate transport code with anisotropic scattering, Westinghouse Astronomical Lab.(1967) CCC-255/ ANISN.

[Ar,83] T.W. Armstrong, et al.: "An Investigation of Fission Models for High Energy Radiation Transport Calculations, Jül-1859 (1983).

[At,79] F. Atchison: "Spallation and Fission in Heavy Metal Nuclei under Medium Energy Proton Bombardment", Meeting on Targets for Neutron Beam Spallation Sources, G. Bauer (Editor), KFA-Jülich, FRG, 11-12 June 1979, Jül-conf-34, January 1980.

[At,80] F. Atchison: "Spallation and Fission in Heavy Metal Nuclei under Medium Energy Proton Bombardment," Jül-Conf-34 (1980).

[At,81] F. Atchinson:"A Theoletical study of a target reflector and moderator assembly for SNS", RL-81-006 (1981)

[AT,90] "Accelerator Production of Tritium (ATP), " report to the U.S.Department of Energy, DOE/S-0074, Energy Advisory Board (Feb .1990)

[Ba,68] V.S. Barashenkov, et al.: "Computational Scheme of Intranuclear Cascade", JINR R2-4065 (1968).

[Ba,78] V.S. Barashenkov " Breeding nuclear fuel with Accelerator: The electronuclear method. Nuclear physics aspects. Sov. J.Part. Nucl. 9,452, (1978)

[BB,72] V.S. Barashenkov, H.W. Bertini, K. Chen, G. Friedlander, G.D. Harp, A.S. Iljinov, J.M. Miller, and V.D. Toneev: Nucl. Phys. A187, 531 (1972).

[Be,63] H.W. Bertini: "Monte Carlo Calculation on Intranuclear Cascade," ORNL-3383 (1963).

[Be,69] H.W. Bertini: Phys. Rev. 188, 1711 (1969).

[Be,72] H.W. Bertini:"Calculation of Spallation - Fission competition in the Reactions of Protons with Heavy Elements at Eneries ≥ 3 GeV. Phys. Rev. C-6 660 (1972).

[Be,73] M.J. Bell: "Origin - The ORNL Isotope Generation and Depletion Code," ORNL-7628, Oak Ridge National Laboratory (1973).

[BG,68] V.S. Baraschenkov, K.K. Guduma, and V.D. Toneev: "Computational

Scheme of Intranuclear Cascase," JINR-R2-4065 (1968).
[BG,71] H.W. Bertini and M.P. Guthrie: Nucl. Phys. A169, 670 (1971).
[BG,73] V.S. Barashenkov, F.G. Gereghi, A.S. Iljinov, and V.D. Toneev: Nucl. Phys. A206, 131 (1973).
[BG,74] V.S. Barashenkov, F.G. Gereghi, A.S. Iljinov, and V.D. Toneev: Nucl. Phys. A222, 204 (1974).
[BI,73] V.S. Barashenkov, A.S. Iljinov, N.M. Sobolevsky, and V.D. Toneev: Usp. Sov. Phys. 109, 91 (1973).
[BI,74] V.S. Barashenkov, A.S. Iljinov, N.M. Sobolevskii, and V.D. Toneev: Sov. Phys. Usp., 16, 31 (1974).
[Bl,75] M. Blann: Ann. Rev. Nucl. Sci. 25, 123 (1975).
[Bl,89] M. Blann: "Precompound Decay Models for Medium Energy Nuclear Reactions," UCRL-101262 (1989).
[BM,65] V.S. Barashenkov, V.M. Mal'tsev, and V.D. Toneev: "Interaction of Fast Protons with Heavy Nuclei", JINR-R-1969, Dubna (1965).
[BM,65] V.S. Barashenkov, V.M. Mal'tsev, and V.D. Toneev: "Calculation of Gast Particle Induced Fission", Dubna Report JINR P-1970, 1965.
[Bo,90] C.D.Bowman," Data Need for Construction of Application of Accelerator based Intense Neutron Source" Proc of 2nd Int. Symp. in Advanced Nucl. Energy Research. p.77, Mito, JAERI Jan. 24-26, 1990
[BM,90,b] G.I.Batskiku, B.P. Murin, et.al. Linear accelerator for Burner-reactor. Linear accelerator conference, alberquaqui, Sept, 1990.
[Br,86] J.F. Briesmeister, editor: "MCNP - A General Monte Carlo Code for Neutron and Photon Transport", LA-7396-M Revision 2, Los Alamos National Laboratory (September 1986).
[BR,87] P. Bonnaue, H. Rief, P. Mandrillon, and H. Takahashi: "Actinide Transmutation by Spallation in the Light of Recent Cyclotron Development"; NEACRP-A-910, Session B.1.2 (1987). (European American) Reactor Physics Committee Report.
[BR,88] J.F. Briesmeister: "MCNP3B Newsletter", Los Alamos National Laboratory memorandum X-6:JFB-88-292, July 18, 1988.
[BT,66] G.A. Bartholomew and P.R. Tunnicliffe, Eds.: "The AECL Study for an Intense Neutron Generator", Atomic Energy of Canada Limited, Report No. AECL-2600, Ch. VII, p. 12 (1966).
[BW,39] N. Bohr and J.A. Wheeler: Phys. Rev. 56, 426 (1939).
[BW,52] J.M. Blatt and V.F. Weisskopf: Theoretical Nuclear Physics, John Wiley, New York 1952).
[Ca,84] X. Campi, J.D. Desbois, E.Lipparini (nucl. phys. A428 (1984) 327c-344c.)
[Ca,57] A.G.W.Cameron, Canad.J.Phys.,35,1021,(1957]
[CA,70a] W.A. Coleman and T.W. Armstrong: "NMTC Monte Carlo Nucleon Meson Transport Code System," ORNL-4606 (1970) (also RSIC CCC-161).
[CA,70b] W.A. Coleman and T.W. Armstrong: "The Nucleon-Meson Transport Code NMTC," ORNL-4606, Oak Ridge National Laboratory (1970).
[CA,72] K.C. Chandler and T.W. Armstrong: "Operating Instructions for the High-Energy Nucleon-Meson Transport Code HETC," ORNL-4744, Oak Ridge National Laboratory (1972).
[CCC,328] 3DB " A three-dimensional multigroup diffusion theory code for fast reactor criticality and barn-up analysis" Battelle Pasific Northwest Laboratory.BNWL-1264 (UC-32)
[CCC,428] One dimensional, multi-group, diffusion accelerated, neutral particle code.
[CCC,456] Two dimensional, diffusion accelerated discrete ordinate transport code system, LA,10049-M.
[CA,71] W.A. Coleman and T.W. Armstrong: "NMTC - A Nucleon-Meson Transport Code," Nucl. Sci. and Engr. 43, 353 (1971).
[CD,82] M.R. Clover, R.M. DeVries, N.J. DiGiacomo, and Y. Yariv: Phys. Rev. C, 26, 2138 (1982).
[CFF,68] K. Chen, Z. Fraenkel, G. Friedlander, J.R. Grover, J.M. Miller, and Y. Shimamoto: Phys. Rev. 166, 949 (1968).
[CFM,68] K. Chen, G. Friedlander, and J.M. Miller: Phys. Rev. 176, 1208 (1968).

[CE,81] S.S. Cierjacks, et al.: "High Energy Particle Spectra from Spallation Targets", in Ref. (5), ICANS-V, Jül-Conf-45 (1981).
[Ch,68] K. Chen, et al.: Phys. Rev., 166, 949 (1968).
[Ci,82] S. Cierjacks, et al.: "Differential Neutron Production Cross Sections for 590 MeV Protons", Int. Conf. Nucl. Data for Sci. and Technol., Antwerp, 1982.
[Ci,87] S. Cierjacks, et al.: Phys. Rev. C36, 1976 (1987).
[Cl,82] M.C. Claiborne: "Neutral Induced Transmutation of High Level Radioactive Wastes." ORNL-TM-3964, Oak Ridge National Laboratory (Dec. 1972).
[Cl,83] P. Cloth, et al.: The KFA-Version of the High-Energy Transport Code HETC and the generalized Evaluation Code SIMPEL," Jül-Spez-196 (1983).
[Co,65] R.R. Coveyou, et al.: "O5R, A General Purpose Monte Carlo Neutron Transport Code", ORNL-3622 (1965).
[CO,70] W.A. Coleman, and T.W. Armstrong: "The Nucleon-Meson Transport Code NMTC", ORNL-4606 (1970), RSIC CCC-161.
[Cr,82] A.G.Croff: "ORIGIN2: A versatile computor code for calculating the Nucleide compositions and characteristics of nuclear materials." Nucl. Tech. 62,335 (1983).
[CS,63] S.Cohen and W.J.Swiatecki: Ann. Phys.,22,406 (1963).
[DR,58] I. Dostrovsky, P. Rabinowitz, and R. Bivins: "Monte Carlo Calculations of High-Energy Nuclear Interactions. I Systematics of Nuclear Evaporation", Phys. Rev. 111, 1659 (1958).
[Dr,62] L. Dresner: "EVAP - A Fortran Program for Calculating the Evaporation of Various Particles from Excited Compound Nuclei", ORNL-TM-196, Oak Ridge National Laboratory (April 1962).
[Do,58] I. Dostrovsky: Phys. Rev. 111, 1659 (1958).
[En,67] W.W. Engle, Jr.: "A Users Manual for ANISN, a One-Dimensional Discrete Ordinates Transport Code with Anisotropic Scattering," K-1693, Oak Ridge Gaseous Diffusion (1967).
[Fo,69] P. Fong: "Statistical Theory of Nuclear Fission, Gordon and Beach Science Publishers, New York, 1969.
[Fr,75] J.S. Fraser et al., Physi. in Canada,21, 17 (1975)
[Fr,80] J.S.Fraser et al., Proc. Symp. Neutron cross sections from 10 to 50 Mev Upton, New York, May 12-14, 1980, Conf-800551, p.155, BNL-NCS-5124, Brookhaven National Laboratory (1980)
[FT,80] K. Furukawa, K. Tsukada, Y. Nakahara: "Molten-Falt Target and Blanket Concept, Inter-collaboration on Advanced Neutron Source, ICAN-S-N, Oct. 20-24, 1980; KEK, Tsukuba.
[Fu,81] K. Furukawa, K. Tsukada, and Y. Nakahara: Nucl. Sci. Technol. 18 (1), 79 (1981). Russian trans., Atomic Tech. Abroad, 1982 (7) 35; JAERI-M83-050 (1983).
[GA,70] T.A. Gabriel, R.G. Alsmiller, Jr., and M.P. Guthrie: "An Extrapolation Method for Predicting Nucleon and Pion Differential Production Cross Sections from High-Energy (> 3 GeV) Nucleon-Nucleus Collisions," ORNL-4542, Oak Ridge National Laboratory (1970).
[Ga,79] P. Garvey: "Neutron Production by Spallation in Heavy Metal Target-Experiments and Calculations", in Jül-Conf-34 (1979).
[GC,65] A. Gilbert and A.G.W. Cameron: Can. Journ. of Phys. 43, 1446 (1965).
[GK,78] P. Grand, H. Kouts, J. Powell, M. Steinberg, and H. Takahashi: "Conceptual Design and Economical Analysis of Light Water Reactor Fuel Enrichment/Regenerator", BNL 50838, (UC-80, TID-4500) (1978).
[GM,83] K.K. Gudima, S.G. Mashnik and V.D. Toneev: Nucl. Phys., A401, 329 (1983).
[GO,75] K.K. Gudima, G.A. Ososkov, and V.D. Toneev: Yad. Fiz. 21, 260 (1975).
[Gr,56] R.A.Grass et al. : Phys. Rev. 104, 404, (1956)
[Gr,66] J.J. Griffin: Phys. Rev. Lett., 17, 4 (1966).
[GR,81] P. Grand: private communication (March 1981).
[GRR,88] J.S.Gilmore, G.J.Russel, H.Robinson, R.E,Prael: "Fertile-to fissile

and Fission Measurements for Uranium and Thorium Bombarding by 800 MeV Protons",Nucl.Sci. Eng. 99,44 (1988)

[GU,70] M.P. Guthrie: "EVAP-4: Another Modification of a Code to Calculate Particle Evaporation from Excited Compound Nuclei", ORNL-TM-3119 (1970).

[GX,81] Group X-6, "MCNP - A General Monte Carlo Code for Neutron and Photon Transport", LA-7396-M Revised, Los Alamos National Laboratory (April 1981).

[HB,72] R.L. Hahn and H.W. Bertini: "Calculations of Spallation-Fission Competition in the Reaction of Protons with Heavy Elements at Energies <3 GeV", Phys. Rev. C6, 660 (1972).

[HM,72] J.R. Huizenga, and L.G. Moretto: Ann. Rev. of Nucl. Sci. 22, 427 (1972).

[He,58] W.N.Hess: Rev.Mod.Phys.,30,368 (1958)

[Ho,56] R.Hofstadter:Rev. Mod.Phys. 28,214 (1956)

[Ho,89] P.E.Hodgson: "Pre-equilibrium Processes in Nuclear Reaction," Heavy Ion Collisions, pp. 220-247, Springer (1984).

[HK,69] J. Hudis and S. Katcoff: Phys. Rev. 180, 1122 (1969).

[Hu,55] J.R. Huizenga: Physica, 21, 410 (1955).

[HY,64] The Nuclear properties of the Heavy Elements Vol III, page 176, prentice-Hall 1964).

[IA,88] "Radiological Safty aspects of the operation of proton accelerators" IAEA, Tech. Rep.283 (1988]

[IC,77] A.S. Iljinov and E.A. Cherepanov: INR Preprint P-0064, Moscow (1977).

[IC,78] A.S.Iljinov,E.A. Cherpanov, and S.E. Chirinov," An Analysis of Nuclear Fissibility for Intermediate- Energy Proton Induced Reactions" Zeit. fur Physik A 287,37-43 (1978)

[IC,80] A.S. Iljinov, E.A. Cherpanov and S.E. Chirginov: Sov. J. Nucl. Phys., 32, 166 (1980).

[IR,65] D.C. Irving, et al.: "O5R, a General Purpose Monte Carlo Neutron Transport Code," ORNL-3622, Oak Ridge National Laboratory (1965).

[IS,75] A.V. Ignatyuk, G.N. Smirenkin, and A.S. Tishin: Yad. Fiz. 21, 485 (1975).

[IS,90] K. Ishibashi, et al.: "Improvement of the Spallation-Reaction Simulation Code by Considering both the High-momentum Intranuclear Nucleons and the Preequilibrium Process," Proc. the 2nd International Symp. Adv. Nucl. Energ. Res. - Evolution by Accelerators -, (Jan., 1990, Mito, Japan).

[Iv,89] D.I.Ivanov et al.: "Measurement of the U-238 and Np-237 photo-fission cross section using tagged photons in the energy range 60-240 MeV." Int.Conf. fiftieth anniversary of fission Leningrad, USSR, Oct 16-20, 1989)

[Ja,79] R.A. Jameson: "High-Intensity Deuteron Linear Accelerator (FMIT)", IEEE Trans. Nucl. Sci., NS-26 (3), 2186 (1979).

[Ka,81] C. Kalbach: Phys. Rev. C23, 124 (1981) and C24 819 (1981).

[Ka,85] C. Kalbach: "PRECO-D2: Program for Calculating Preequilibrium and Direct Reaction Double Differential Cross Sections," LA-10248 (MS) (1985).

[Kn,77] E.Knapp " Accelerator Costs and Efficiency" Proc. of Inf. Meeting on Accelerator- Breeding, held BNL ,Upton New york, 11973 Jan.18-19, (1977).

[KNS,79] H.J.Krapp,J.R.Nix and A.J.Sierk.: Phys.Rev. C20,992 (1979)

[KN,77] E. Knapp: "Accelerator Cost and Efficiency", Proc. Information Meeting on Accelerator Breeding, CONF-770107 (BNL 1977) p. 294.

[Ko,77] Proc. of Inf. Meeting on Accelerator- Breeding, held BNL ,Upton New york, 11973 Jan.18-19, (1977)

[KS,77] H. Kouts and M. Steinberg (ed): Proc. Inform Meeting, Accelerator-Breeding, Jan. 1977. BNL, Report Conf. 770107 (1977).

[Ku,80] V.M. Kupriyanov, et al.: Sov. J. Nucl. Phys., 32, 184 (1980).

[Ku,89] S.Kurosawa "Catalogue of High Energy accelerator" XIV Int. Conf. on High Energy Accel. Aug 22-26,1989 Tsukuba,KEK, Japan (1989)

[LB,73] K.D.Larthrop and F.W.Brinkley:"Twotran-II:An Interfaced Exportable Version of the TWOTRAN code for Two-Dimensional Transport Los Alamos report LA-4848-MS (1973)

[LC,50] K.J. LeCouteur: Proc. Phys. Soc. (London), A63, 259 (1950).

[Le,52] W.B. Lewis: "The Significance of the Yield of Neutrons from Heavy Elements Excited to High Energies", Atomic Energy of Canada Limited, Report No. AECL-968 (1952).

[Le,53] W. Lewis: Atomic Energy of Canada Ltd., Rapport AECL-969 (1953).

[Le,68] W. Lewis: Atomic Energy of Canada Ltd., Rapport AECL-3190 (1968).

[LH,69] W.W.Little, Jr. and R.W. Hardie: "2DB user's manual revision 1", Battelle Memorial Institute, Pacific Northwest Laboratories Report BNWL-831 Rev1 (1969).

[Li,61] S.J.Lindenbaum: The Shielding of high-eneergy accelerators, Ann.Rev. Nucl. Sci. 11, 213 (1961).

[LV,77] K.D. Larthrop and J.C. Vigil: Ref. 6, P. 177.

[Ma,77] F.R. Maynatt: Ref. 6, P. 85.

[MB,58] N. Metropolis, R. Bivins, M. Storm, A. Turkevich, J.M. Miller, and G. Friedlander: Phys. Rev. 110, 185 (1958).

[Mc,88] R.C.McCall et al. " Health Physics Manual of Good Practices for Accelerator Facilities" SLAC- Report-327 April, (1988).

[Me,58] M. Metropolis: Phys. Rev., 110, 185 (1958).

[Mo,85] E.Moller, M.C.Nemes & D.H.E. Gross Nucl. Phys. a-433, 671-690 (1985)

[MS,66] W.D. Myers and W.J. Swiatecki: Nucl. Phys., 81, 1 (1966).

[MS,67] W.D. Myers and W.J. Swiatecki: Ark. Fys., 36, 343 (1967).

[MT,88] T. Mukaiyama, H. Takano, T. Takizuka, T. Ogawa, and M. Osakabe: "Conceptual Study of Actinide Burner Reactor", Proc. 1988, Int. Reactor Physics Conference (Jackson Hole, 1988).

[My,77] F.R. Mynott et al.: "Preliminary Report on the Promise of Accelerator Breeding and Converter Reactor Symbiosis as an Alternative Energy System", ORNL/TM-5750 (February 1977).

[Na,80] Y. Nakahara, "Studies on High-Energy Spallation and Fission Reactions:, Proc. of 4th Meeting of International Collaboration on Advanced Neutron Sources (ICANS-IV), KEK National Laboratory for High-Energy Physics, Tsukuba, Japan, 20-24 October 1980.

[NF,63] E.F. Neuzil and A.W. Fairhall: Phys. Rev., 129, 2705 (1963).

[NI,69] J.R. Nix: Nucl. Phys., A130, 241 (1969).

[NN,86] Y. Nakahara and T. Nishida: "Monte Carlo Algorithms for Simulating Particle Emissions from Preequilibrium States during Nuclear Spallation Reaction," JAERI-M 86-074 (1986).

[NT,79] Y. Nakahara and H. Takahashi: Atomnaya Energina, 47, 83 (1979).

[NT,82] Y. Nakahara and T. Tsutsui: JAERI Memorandum M82-198 (1982).

[NT,89] T. Nishida, H. Takada, I. Kanno, and Y. Nakahara: Computer Process & Nuclear Data Needs for the Analysis of Actinide Transmutation by a Particle Accelerator, Report on OECD NEA Data Bank Meeting (12-13 Dec. 1988).

[NTT,81] Y.Nakahara, Tsutsui, Taji: "ACCEL", JAERI memo 9502 (1981).

[OB,69] K. O'Brien: Nucl. Instr. Meth. 72, 93 (1969).

[OB,70] K.O'Brien " Shielding calculations for Broad neutron beams normally incident on slabs of concrete", Report HASL-21, USAEC Health and Safty Lab. (1970)

[OB,71] K. O'Brien " Neutron spectra in the side shielding oa a large particle accelerator", Rep. HASL-240, USAEC Health and Safty Lab. (1971)

[Od,90] M.Odera private Communication (1990)

[Pa, 57] H.W.Patterson " The university of California Syncro-Cyclotron" Conf. on Shielding High- Eneergy Accelerator New York 11-13, April 1957, Rep. TID-7545, USAEC (1957)

[Pa,71] H.W.Patterson , R.H.Thomas " Experimental shielding studies -A Review, Part. Accel. 2, 77 (1971)

[Pa,73] H.W. Patterson R.H.Thomas, Accelerator Health Physics. Academic Press., New york (1973)

[PB,88] R.E. Prael and M. Bozoian: "Adaptation of the Multistage Preequilibrium Model for the Monte Carlo Method (I)", LA-UR-88-3238, Los Alamos National Laboratory (September 1988). R.E. Prael and M. Bozoian: "Adaptation of the Multistage Preequilibrium Model for the Monte Carlo Method (II)", Los Alamos National Laboratory (to be published).

[PL,73] H.C. Pauli and T.Lederberger: Proc. 3rd IAEA Symp. Phys. Chem. of Fission, SM-174/206, vol1,(1973).

[Pr,89] R.Prael and H.Lichtenstein LA-UR-89-3014 (1989)

[PS,76] G.A.Pik-pichak and V.M.Strutinskii "Physics of Nuclear Fission" (ed) N.A.Perfilov and V.S.Eismond, Israel Program for Scientific Translation, Jerusalem (1964)

[PSR,115] SUPERTOG-Jr A code for generating transport group constants, energy deposision coefficient and atomic displacement constant with ENDF/B. JAERI-M 6935.

[PSR,118] NJOY " A code system for producing pointwise and multi-group neutron and photon cross sections from ENDF/B-IV and V evaluated nuclear data. LA-7584-M;ENDF-272.

[Ra,67] J. Ranft: "Improved Monte Carlo calculation of the nucleon-meson cascade in shielding material,I and II". Nucl. Instr. Meth. 48, 133, and 261 (1967).

[Ra,70] J.Ranft: "Secondary particle spectra according to the thermodynamical model'. ,Rep. TUL-36, Karl Marx Univesity, Leipzig (1970).

[Ra,72] J.Ranft et al. Part. Accel. 4,101 (1972).

[Ra,85] J.Ranft et al. FLUKA82, CERN Divisional Report TIS-RP/156/ CF, (1985)

[RC,82] W.A.Rhodes,R.L.Childs, An updated version of the DOT4 one and two dimensional neutron / photon transport code ORNL report 5851 (1982)

[Ri,65] R.J.Riddell,Jr. 'High energy nuclear cascades in matter'. Rep. UCRL-11989, Lawrence Radiation Lab. Berkley, CA, (1965)

[Ri,73] A.Rindi, and R.H.Thomas:" The radiation enviroment of high-energy accelerators', Ann. Rev. Nucl. Sci. 23 ,315 (1973)

[RS,77] Radiation Shielding Information Center, "HETC Monte Carlo High-Energy Nucleon-Meson Transport Code", Report CCC-178, Oak Ridge National Laboratory (August 1977).

[Ru,80] G.J. Russel et al Proc. Symp. Neutron cross sections from 10 to 50 Mev Upton, New York, May 12-14, 1980, Conf-800551, p.169, BNL-NCS-5124, Brookhaven National Laboratory (1980)

[Ru,81] G.J. Russell, et al.: "Fertile-to-Fissile and Fission Measurements for Depleted Uranium Bombarded by 800 MeV Protons", in Ref. (5), ICANS-V, Jül-Conf-45 (1981).

[Sc,79] S.O. Schriber: "High-beta Linac Structure", Proc. 1979 Linear Accelerator Conf. (Montauk, Sept. 1979) BNL 51134, p. 164.

[Sc,82] S.O. Schriever: "Canadian Accelerator Breeder System Development", Rapport AECL-7840 (1982).

[Se,47] R. Serber: Phys. Rev. 72, 1114 (1947).

[SF,61] D.P.Sathus, H.P.Flatt," Sizzel" North American Aviation Program Describe (1961)

[SG,68] T. Sikkeland, A. Ghiorso, and M.J. Nurmia: Phys. Rev. 172, 1232 (1968).

[SL,57,58,61] R.M. Sternheimer and S.J. Lindenbaum: Phys. Rev. 105, 1874 (1957); Phys. Rev. 109, 1723 (1958); Phys. Rev. 123, 333 (1961).

[SM,68] T. Sikkeland, J. Maly, and D.F. Lebeck: Phys. Rev. 169, 1000 (1968).

[SS,70] E.A. Straker, P.N. Stevens, D.C. Irving, and V.R. Cain: "The MORSE Code - A Multigroup Neutron and Gamma-Ray Monte Carlo Transport Code", ORNL-4585 (September 1970).

[St,67] V.M.Strutinski: Nucl.Phys. A95, 420 (1967).

[ST,73] R. Silberberg and G. Tsao: "Partial Cross-Sections in High-Energy Nuclear Reaction, and Astrophysical Applications," Astrophys. J.

Suppl. Series., No. 220 (1973).

[Ta,80a] H. Takahashi: "Fission Reaction in High-Energy Cascade", to be published in Proc. of Symp. on Neutron Cross Sections 10-50 MeV, Brookhaven National Laboratory 12-14, May 1980,BNL-NCS-51245

[Ta,80b] K. Tasaka: "DCHAIN2: A Computer Code for Calculation of Transmutation of Nuclides," JAERI-M 8727 (1980).

[Ta,80c] H. Takahashi, et al.: "Nuclear Fuel Breeding by Using Spallation and Muon Catalyzed Fusion Reaction; Atomkernenergie, Kerntechnik; 36, 195 (1980).

[Ta,84] H. Takahashi:"Fission Reaction in High Energy Cascade," BNL-NCS-51245 (1984).

[Ta,85] H.Takahashi," Actinide Transmutation by the Spallation Process," presented at Workshop on the Feasibility of Research Program in Actinide Transmutation by Spallation Process, Euratom, Ispra,Varese, Italy , June 18-21, 1985.

[Ta,90] H.Takahashi " The role of accelerator technology in Nuclear fuel Cycle" Proc of 2nd Int. Symp. in Advanced Nucl. Energy Research. p.77, Mito, JAERI Jan. 24-26, 1990

[Te,85] A. Tesch " A simple estimation of the lateral shielding for proton accelerators in the energy range 50 to 1000 MeV, Radat. Prot. Dosim. 11 . 3, 165,(1985)

[TK,89] T. Takizuka, I. Kanno, H. Takado, T. Ogawa, T. Nishida, and Y. Kaneko: "A Study on Incineration Target System"; International Conference on Emerging Nuclear Energy"; held at Kalrsruhe, July 3-7 (1989).

[TM,80] H. Takahashi, N. Mizoo, and M. Steinberg: "Use of the Linear Accelerator for Incinerating the Fission Produce of CS^{137} and Sr^{90}"; International Conference on Nuclear Waste Transmutation, July 22-24, 1980. The University of Texas at Austin.

[TM,89] H. Takano and T. Mukaiyama: "Nuclear Characteristics Analysis of Tru Burner Reactors," JAERI-M 89-072 (1989) (in Japanese).

[Tr,66] G.H.Trilling :" Pion and proton flux from high energy proton collisions", Rep. UCRL-16830, Lawrence Berkley, CA (1966)

[TT,90] H. Takada ,T.Takizuka et al " A Conceptual Study of Actinide Thermal System with Proton Accelerator" Proc of 2nd Int. Symp. in Advanced Nucl. Energy Research. p.375, P.381, Mito, JAERI Jan. 24-26, 1990.

[TN,84] K. Tsukada and Y. Nakahara: Atomkernenergie Kerntech., 44, 186 (1984).

[TP,84] H. Takahashi, J. Powerll, and H. Kouts: "Accelerator Breeder with Uranium and Thorium Target", Atomkernenergie - Kerntechnik, 44, 181 (1984).

[UY,81] M. Uno and M. Yamada: Prog. Theoret. Phys., 65, 1322 (1981).

[VA,68] R.G. Vasil'kov et al.: "Mean Number of Secondary Neutron by High Energy Proton" Yadern. Fiz. 7, 88 (1968), Trans: Sov. J. Nucl. Phys. 7, 64 (1968).

[VA,77] C. Van Atta: Lawrence Livermore Laboratory, UCRL-79151 (1977).

[Va,78] R.G. Vasil'kov, et al.: Atomnaya Energiya 44, 329 (1978).

[VB,71] A. VanGinnekin and T. Borak: IEEE Trans. Nucl. Sci. Vol. NS-18, No. 3, 746 (1971).

[VG,71] A. VanGinnekin: National Accelerator Laboratory, private communication (1971).

[VG,78] R.G. Vasil'kov, V.I. Goldanskii, et al.: Atomnaya Energiya 48, 329 (1978).

[VH,58] R. Vandenbosch and J.R. Huizenga: In Proceedings of the Second United Nations International Conference on the Peaceful Uses of Atomic Energy (United Nations, Geneva, 1958), Vol. 15.

[VH,73] R. Vandenbosch and J.R. Huizenga:"Nuclear Fission" Academic Press (1973)

[VL,76] C. Van Atta, J. Lee, and W. Heckrott. Larence Livermore Laboratory, UCRL-52144 (1976).

[VT,90] G.Van Tuyle, M.Todoso, H.Takahashi, G.Slvik, and A.Aronson "Proposed

Transmutation of Long-Lived Radioactive Waste to produce Electric Power" Tran.Amer, Nucl. Soc. 100 (1990)

[We,37] V. Weiskopf: Phys. Rev. 52, 295 (1937).

[WG,69] R.Q.Write, N.M.Green, et al. "SUPERTOG: A program to generate fine group constants and Pn scatteering matrices from ENDF/B" (1969)

[Wy,73] J.M.Wyckoff, A.G.Chilton,: "Dose due to practical neutron energy distributions incident on concrete shielding walls" Proc. 3rd Int.Cong. IRPA (W.S.Snyder Ed) Rep. CONF-730907-P1 694 (1973)

[YF,79] Y. Yariv and Z. Fraenkel: Phys. Rev. C., 20, 2227 (1979).

[YF,81] Y. Yariv and Z. Fraenkel: Phys. Rev. C., 24, 488 (1981).

[Yo,77] D.Young, " Beam Loss problems and Accelerator Currents of 300 mA in the Fermilab 200 MeV Linear Accelerator" Proc. of Inf. Meeting on Accelerator- Breeding, held BNL ,Upton New york, 11973 Jan.18-19, (1977)